8-27-2012 12:00 AM

A Telerobotic Drilling Control System with Haptic Feedback

Faraz Shah
The University of Western Ontario

Supervisor
Dr. Ilia G. Polushin
The University of Western Ontario

Graduate Program in Electrical and Computer Engineering
A thesis submitted in partial fulfillment of the requirements for the degree in Master of Engineering Science

A TELEROBOTIC DRILLING CONTROL SYSTEM WITH HAPTIC FEEDBACK

(Spine title: A Telerobotic Drilling Control System with Haptic Feedback)
(Thesis format: Monograph)

by

Faraz Shah

Graduate Program in Electrical and Computer Engineering

A thesis submitted in partial fulfillment
of the requirements for the degree of
Master of Engineering Science

The School of Graduate and Postdoctoral Studies
The University of Western Ontario
London, Ontario, Canada

THE UNIVERSITY OF WESTERN ONTARIO
School of Graduate and Postdoctoral Studies

CERTIFICATE OF EXAMINATION

Examiners:

Supervisor:

. . . . . .
Dr. J. Jiang

. . . . . .
Dr. I. Polushin

. . . . . .
Dr. M. R. Kermani

Supervisory Committee:

. . . . . .
Dr. O. R. Tutunea-Fatan

The thesis by

Faraz Shah

entitled:

A Telerobotic Drilling Control System with Haptic Feedback

is accepted in partial fulfilment of the
requirements for the degree of
Master of Engineering Science

. . . . . .
Date

. . . . . .
Chair of the Thesis Examination Board

Abstract

Drilling a borehole is a common method for extracting oil, gas, and natural resources from beneath the surface of the earth. The main topic of this Thesis is the design of control algorithms for virtual reality based telerobotic system with haptic feedback that allows for the remote control of the vertical drilling operation. The human operator controls the vertical penetration velocity using PHANTOM Omni haptic device while simultaneously receiving the haptic feedback from the locally implemented virtual environment. The virtual environment is rendered as a virtual spring with stiffness updated based on the estimate of the the stiffness of the rock currently being cut. Based on the existing mathematical models of drill-string/drive systems and rock cutting/penetration process, a robust servo controller is designed that guarantees tracking of the reference vertical penetration velocity of the drill bit. A scheme for online estimation of the rock stiffness is implemented. Simulations of the proposed control and parameter estimation algorithms have been conducted using MATLAB; consequently, the overall telerobotic drilling system with a human operator controlling the process using PHANTOM Omni haptic device is tested experimentally where the drilling process is simulated in real time using Open Haptics toolkit.

Keywords: Teleoperation, Drilling Systems, Haptic Feedback, Controller Design

Acknowledgement

First and foremost, I would like to offer my utmost gratitude to my supervisor Dr. Ilia G. Polushin, Assistant Professor, Department of Electrical and Computer Engineering, Western University, whose gracious support, ever-present guidance, encouragement and invaluable assistance paved my way to culminate this dissertation. I am highly thankful to Dr. Polushin for providing me the opportunity to work in the area of Telerobotic Drilling.

I acknowledge the support of Mr. Amir Takhmar, PhD student, Department of Electrical and Computer Engineering, Western University, and highly appreciate his technical assistance with PHANTOM Omni Haptic Device. Also, I am extremely grateful for the help of Mr. Mir Zayed Hasen, MESc, Department of Electrical and Computer Engineering, Western University for his valuable support during programming. Furthermore, I would like to thank Amir Takhmar, Zayed Hasan, Farshad Anoushapour and Nojan Madinehi for their great support as colleagues and providing me a wonderful working experience.

I would like to thank Dr. Rajni Patel, Distinguished University Professor and Tier-1 Canada Research Chair, Department of Electrical and Computer Engineering, Western University and Dr. Mehrdad R. Kermani Assistant Professor, Department of Electrical and Computer Engineering, Western University, for building my foundations in the fields of Robotics and Advanced Control Systems, respectively.

Last but not the least, I would like to express my gratitude to my parents back home. They were always supportive and encouraging throughout the time.

Contents

List of Figures

List of Tables

List of Acronyms

API: American Petroleum Institute
BHA: Bottom Hole Assembly
BOP: Blowout Preventer
DC: Direct Current
HWDP: Heavy Weight Drill Pipes
IADC: International Association of Drilling Controllers
JAR: Jammers
PC: Personal Computer
PDC: Polycrystalline Diamond
SHOC: Shock Absorbers
STAB: Stabilizer
TOB: Torque on Bit
WOB: Weight on Bit
XO: Crossover Sub

Chapter 1

Introduction

1.1 Teleoperation and Drilling

Teleoperation is a general term that describes different technologies that allow human operators to execute tasks in remote or hazardous environments. The word *tele* has Greek origins and means *at a distance*; thus, as the name suggest, teleoperation provides the capability to operate at a remote location. The main components of a teleoperator system are the master manipulator together with its local master controller, the communication channel, and the slave manipulator with its local slave controller. The master manipulator (occasionally comprising of a joystick or a stylus attached to the telerobotic device) is operated by the human, and the slave manipulator interacts with the environment [8, 9]. Using the master manipulator, the human operator generates a trajectory which is consequently executed by the slave. In force reflecting teleoperator systems, the interaction forces between the slave and the remote environment are reflected back to the motors of the master device; the purpose of such a force reflection is to create a feeling of direct contact between the human operator hand and the remote task.

The goal of this research is to design a telerobotic system for the drilling process. By drilling a borehole, the natural resources such as oil, gas, gold and other minerals are extracted from beneath the surface of earth. Drilling is conducted by crushing the rocks with

the help of a drill bit. The bit is used as a cutter which is attached through drillpipes and scrapes the rock surface, while the drillstring assembly, which comprises of drillpipes and the Bottom Hole Assembly (BHA), is rotated from the top. Conventional drilling has some limitations. For instance, there is always a danger of oil spill followed by an explosion on the drilling rig. Most of the time the drilling crew faces extreme temperatures and environment that may be detrimental for their health. Also, in order to facilitate the drilling process, significant man power must be deployed on the drilling site. This contributes to huge expenses carried for the safety and service of the people living and working on both onshore and offshore drilling sites.

Telerobotics for drilling well is a relatively novel idea, and it is a substantial endeavour to automate one of the fundamental processes in the extraction of energy and resources. As telerobotics is integrated with drilling, it can greatly decrease the number of people working and monitoring operation on the site. This, in particular, can reduce the work site hazards. Also, telerobotics can bring actual analysis of in-situ conditions (underground drilling environment) in real time to the human operator that works remotely, where (s)he will be able to determine the current drilling conditions and, in particular, promptly enforce the change in vertical speed of penetration for drill bit in the oil well. Real-time control and optimization of the drilling speed is crucial for today's drilling industry, as it can reduce time and immense cost associated with the drilling an oil well.

This research presented in this Thesis is an effort to transform a conventional mechanical drilling system into a semi-automated and teleoperated system which can be operated remotely. Although relatively simple, the analysis presented here provides substantial steps and techniques that could be implemented in a drilling system. The theory is established by combining together the mathematical models of drill-string/drive system and rock cutting/penetration. Then, a robust servo controller is designed to eliminate the external disturbances and track the desired (reference) trajectory for the vertical penetration velocity of drill bit. The desired vertical velocity is generated using the PHANTOM Omni Haptic

device, where the vertical position of the stylus is translated into the magnitude of the reference vertical velocity for the drill bit. On the other hand, the haptic device interacts with a virtual spring with stiffness updated based on the current estimate of the actual stiffness of the rock. This allows the human operator to haptically feel the stiffness of the rock during the drilling process. To obtain an estimate of the rock stiffness, an on-line estimator is also designed.

The results obtained from this project may also potentially lead to applications to the remote directional drilling. The potential applications of this research can further be expanded to seafloor drilling/mining and extraterrestrial drilling.

1.2 Motivation and Relevant Applications

The motivation for the research work presented in this Thesis is gathered from numerous projects and research articles in the literature on telerobotics as well as on drilling systems. Conventional oil well drilling has made significant progress, and currently it is one of the most automated processes in oil and gas industry. However, there are still some fundamental challenges associated with the drilling. One of the challenges is the choice of vertical penetration velocity of the drillbit. For efficient drilling operation, this velocity must depend upon the type of rock beds drilled. In particular, the velocity must be adjusted when mechanical characteristics of a rock strata change. If the drilling operator haptically perceives the changing rock stiffness in real time, this would allow for a quick adjustment of the vertical drilling velocity. Directional drilling is another area which would benefit from introduction of haptic feedback into the drilling operation. Often the borehole should make a curve to reach oil reservoirs. In this type of drilling, it may be difficult to estimate the actual position of the drillbit in real time, since the actual path of the borehole may vary from its prescribed path. Therefore, it may be hard to predict the mechanical characteristics of the rock formations. Again, introduction of haptic feedback would allow for the human operator to feel the changes in mechanical characteristics of the rock and adjust the vertical

velocity of penetration accordingly.

The potential application domain of this research is not limited to onshore/ offshore oil well drilling, but the same principles can be applied, in particular, to differrent types of mining robots. In the case of mineral excavation at significant depths, it is very difficult to conduct the operations with human workforce. Mining robots provide a substitute for human hand tools effort, in an attempt to drill small holes to put TNT for rock blasting. However, until recent years, no technology has been implemented to excavate mines for up to 10 Km deep. At these depths, the human support to monitor and control mining robots diminishes due to extreme mountain rock pressure and temperatures, which makes it relevant to apply the principles of teleoperation to the remote rock cutting and drilling [10].

Another developing area within the mining world is the seafloor mining. This has been an area of great interest for many companies and researchers. Since the natural resources are depleting fast on the land, new methods for building robots with tele-autonomy for dredging and mining ocean are currently under development [11, 12]. The concepts of the design of submersible seafloor dredging and mining robotic vehicles are described in [12, 13, 14]. These mobile robots are connected to the umbilical which serves as the link to the surface platform. In this case, teleoperation can be performed over electrical and electronic cables connected in parallel to umbilical cord. Thus, the time delay could be reduced through wired communication medium. It is noteworthy here, that the design of these cutters is similar to PDC drill bit cutter design for oil well drilling. Hence the core concept of telerobotic drilling could be expended for these Aqua-mobile robots by importing their models for cutting and implementing similar algorithm as used in this research.

Another relevant application of the telerobotic drilling is *tele-surgery*. The dynamical models of dental surgical instruments are similar to those for rock cutting. The five degree of freedom end-effector is adequate for conducting high speed drilling for cortical layer gimleting and teleoperated insertions of screw in the vertebrae [15]. To further elaborate this task, the surgeon performing the operation can control and position and orientation of surgical instrument and can apply force to drill or screw and receiving the tissue or bone

stiffness, as feedback, in real time. The similar approach could be formulated for dental surgery, where the drilling is required to extract cavities from teeth and to crush unnecessary tooth bone parts when it is required extract and/or install a new tooth.

Finally, the interplanetary exploration may also greatly benefit from development of telerobotic drilling systems. Drilling the extraterrestrial terrain to discover and research the minerals and composition beneath, is one of the basic tasks in space exploration [16]. This could be made possible through the development of telerobotic and teleoperated drilling systems [14, 16]. Using teleoperated mining systems, the cost and risk associated with human deployment can be avoided.

1.3 Objectives of the Thesis

The main objectives of this work are as follows:

1) Design a control algorithm that guarantees the convergence of the vertical penetration velocity of the drilling systems to its reference value. Since drilling action comprises of two processes, which are rotational motion of the drillstring and the vertical penetration of the drill bit, a robust servo controller should be designed to track desired vertical velocity by controlling the rotational velocity of drill bit and rejecting the torque-on-bit that is produced during the cutting action.

2) Design and evaluate an on-line parameter estimation algorithm for the unknown parameter of the rock intrinsic specific energy, as well as the corresponding adaptive control system.

3) Design and experimentally evaluate a telerobotic drilling system with virtual environment-based haptic feedback that allows the human operator to feel the stiffness of the rock in contact with the drill bit.

1.4 Contribution of the Thesis

The contribution of this Thesis can be summarized as follows:

1) A feedforward robust servo control law is designed that guarantees the fast convergence of the drill bit rotational velocity to its reference value while rejecting the measured disturbance of the torque-on-bit.

2) A cascaded control law is designed that guarantees the convergence of the vertical penetration velocity to its reference value.

3) An on-line parameter estimation algorithm is designed that estimates the stiffness (intrinsic specific energy) of the rock in contact with the drill bit. The corresponding adaptive control system, where the parameter of actual intrinsic specific energy is replaced with its estimate, is designed and simulated.

4) A teleoperated drilling system with haptic feedback is designed and evaluated, where the drilling process is controlled by the human operator in real time using the PHANTOM Omni Haptic device. The stiffness (intrinsic specific energy) of the rock in contact with the drill bit is reflected to the human operator hand using virtual spring with stiffness updated according to the current estimate of the actual rock stiffness (intrinsic specific energy). Experimental results are presented that demonstrate feasibility of the proposed approach.

1.5 Outline of the Thesis

The Thesis is organized as follows. Chapter 2 presents an introductory discussion of the conventional drilling systems. It provides an overviews of the drilling structure, the rig, and describes its basic components and assembly, such as the derrick, hoisting system, rotational system, bottom hole assembly, *etc*. It also describes the types of drill bits and associated assembly. Chapter 3 presents the mathematical models of the cutting and drilling

processes. A literature survey of different models of drill string and drive system is given, and the mathematical models of the drilling process are derived and subsequently used for control design. Chapter 4 deals with the design of control algorithms for rotational and translational motion of the drilling systems. The control algorithms designed allow to achieve a desired rate of the vertical penetration, and extensive simulation results are presented. Chapter 5 is devoted to the design and simulations of an on-line parameter estimator of the intrinsic specific energy which is a parameter that describes the hardness of the rock. Simulation results are presented in this Chapter in support of the theoretical developments. In Chapter 6, the structure of a telerobotic drilling system is described and the corresponding experimental results are presented. Finally, in Chapter 7, some conclusions are given and possible future directions are formulated.

1.6 Conclusions

This Chapter presents a brief introduction to telerobotics and a conventional oil well drilling system. A general idea of how the drilling operation can be controlled using a teleoperator with haptic feedback is described. The motivation for this research along with relevant applications are discussed. Objectives of this Thesis are formulated, and the contribution is described.

Chapter 2

Drilling Rig: Mechanics and Operation

In this Chapter, the physical drilling system is described, including its major components, sections and sub-sections. The history of drilling oil wells and refining dates back to the 9th century, when Arab and Persian chemists not just drilled oil but also set up distillation laboratories. In the last few centuries, oil wells were drilled in different parts of the world. The first commercial oil drilling in Ontario started in 1958 at Oil Springs. Over the years, technology and methods have enhanced with the progress of science and modern systems facilitated the drilling, and operational procedures were developed to bring more precision to the drilling process.

Most of the modern day drilling technology is based on the rotary drilling [1]. Although percussion hammer drilling is also used to drill first few meters of the bore-hole, however, the rest of the operation is typically performed by rotary mechanics. In this chapter, we will highlight some important features of the physical drilling plant starting from the top of drilling rig and going down to the bottom of the bore-hole covering all the essential aspects of it. Figure 2.1 shows the conventional oil well drilling rig with its major components.

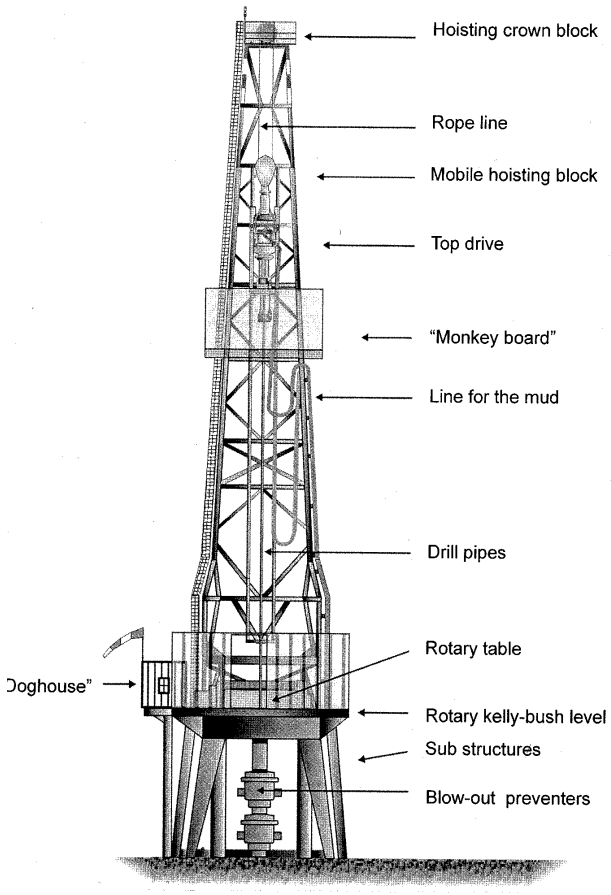

Figure 2.1: Layout of a drilling rig and its main components taken from [1]

2.1 Drilling well structure

The four legged structure directly above the well is called derrick. It is typically made up of steel columns coupled with grits and braces for strengthening. Derricks are rugged structures that can withstand high winds and can easily lift heavy loads (drill pipes). Derricks are typically 24.5 to 57 meter tall, with the loading capability ranging from 39,000 to 631,000 Kg [2]. Derricks are used to support the hoisting system. The hoisting system plays a crucial role in drilling. One of the key actions in drilling is to lift and drop the drillstring/ BHA load, down on the rock. This is needed in order to replace drill bit and/or bottom hole assembly (BHA), add another drill pipe, or for the maintenance of drillstring. This lifting and dropping action is performed using the hoisting assembly. Figure 2.2 shows the linkage of rotary components of the drilling rig.

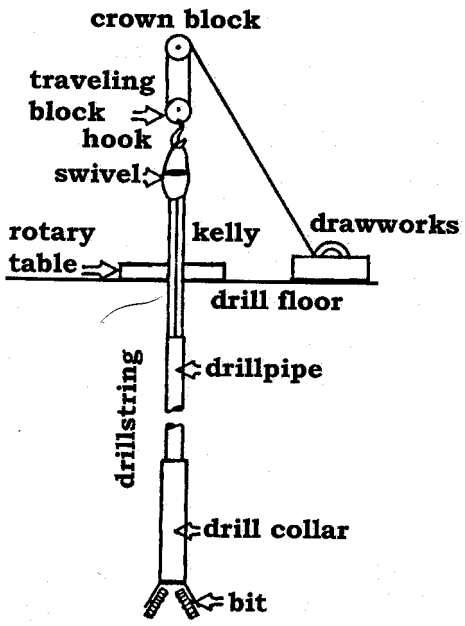

Figure 2.2: Drilling rig complete rotating system taken from [2]

2.2 Hoisting System

Hoisting system consists of crown block, traveling block, hook (swivel and kelly), hoisting line and draw works. The crown block is mounted on the top of derrick and it supports the pulley that is responsible for vertically moving the traveling block. Crown block is basically a pulley with the drive element being the hoisting line that runs over pulley through the groove. The hoisting line or drilling line is a multi-strand braided steel wire, wounded around fiber or steel core about 1 inch in diameter [2]. The hoisting line carries all the weight of rotational assembly. On the other side, it is spooled around a revolving reel called the draw works. The draw works consists of a steel frame and it is located on the drilling floor. The draw works are controlled by the driller through a control pedal; they are driven by the prime movers. Prime movers are DC-electrical or diesel engines that supply power to the draw works.

Suspended below the crown block through the hoisting line is traveling block. It is also called mobile hoisting block. Traveling block connects the hoisting system to the rotating system which consists of swivel and kelly and goes down to rotary table and extends up to the drill pipes. The hoisting system is shown in Figure 2.3.

2.3 Rotational System

The traveling block is connected with a hook which is also called the crane block [1]. Beneath the hook, there is swivel which is suspended by the bail of hook. While the load of the drill pipes is held by the crown block and traveling block, the swivel allows the drill pipes to rotate through their bearings. Underneath the swivel, there lies the most important component of rotating system, which is the kelly. The kelly is attached to the rotary table. It has four to six sides which enable it to get a firm grip with the rotary table and helps it to rotate as the rotary table moves [2]. The rotary table is a fixed circular platform which is located on the derrick floor. Rotary table is subjected to clockwise motion with the help of

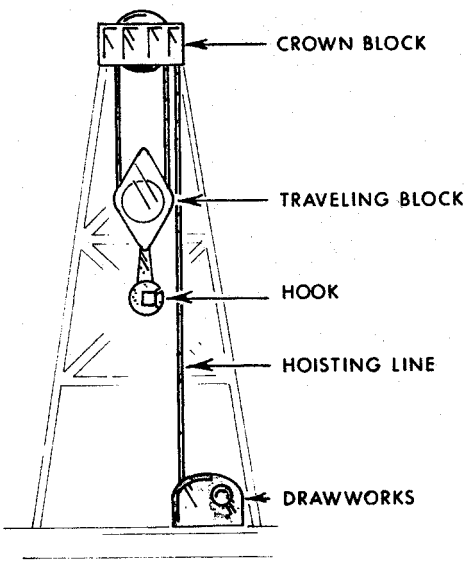

Figure 2.3: Hoisting System taken from [2]

prime movers.

Kelly is a heavy duty molybdenum steel pipe about 12 to 16 m long [2]. The kelly is connected to the rotary table with the help of two different sets of bushings. The inner bushing is called the kelly bushing. The kelly bushing makes a linkage with rotary table through master bushings. Master bushings are attached directly to the rotary table. Thus, the whole assembly of the kelly, the kelly bushing, the master bushing, and the rotary table rotates as a single unit. The unit rotates in the clockwise direction if looked down from the top of the derrick floor; thus, the whole drilling string moves in the same clockwise direction. The kelly bushing also has rollers which allow for the vertical motion of the kelly. Therefore, the hoisting system can lift and/or drop kelly/ drill pipes as the well is bored. The smooth motion of kelly through kelly bushing also permits easy connection of the drill pipes with the kelly. Figure 2.4 shows the rotary table along with the swivel and the kelly.

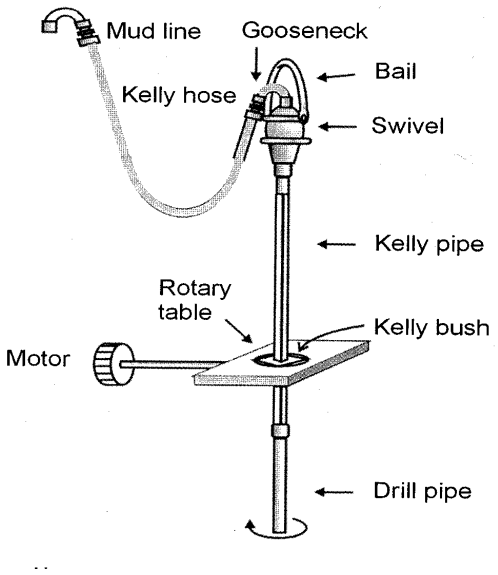

Figure 2.4: Rotary-table system with kelly and swivel taken from [1]

2.4 Drill Pipes

Kelly is always mounted on the top side of a drill string. The drill pipes typically have length of about 10 meters. Thus, after every 10 meters of well bore drilled, another drill pipe is attached to the kelly. American Petroleum Institute (API) describes three lengths and five grades of strength for drill pipes. The drill pipes typically have outer diameter of 7 to 14 cm. Each pipe has tool joint connector side, which is thicker and bulkier, to connect with the other pipes. The drill pipes are robust and resilient to wear and typically capable of lasting for more than one drilling. Abrasion by formation is one of the common factor which causes wear in pipes; it happens due to the mud flow through the pipes and pipe-chemical interaction. Drill pipe wear produces drillstring waves which may contribute to the slip-stick oscillations of the drillstring.

2.5 Drillstring

The drillstring is the rudimentary part of the rotary system. Drillstring is the assembly of rotating pipes which are responsible for transmitting rotation and weight to the bit and bridge up a connection between the bottom hole tools. The brief discussion about bottom hole tools will be presented below. The drillstring comprises of two main sections: the drill pipes and the bottom hole assembly [1]. The drill pipes were described above. The bottom hole assembly (BHA), on the other hand, is a combination of heavy weight pipes called drill collars along with the mechanical and electrical accessories associated with them. The components of a drillstring along with drill-pipes and BHA are shown in Figure 2.5.

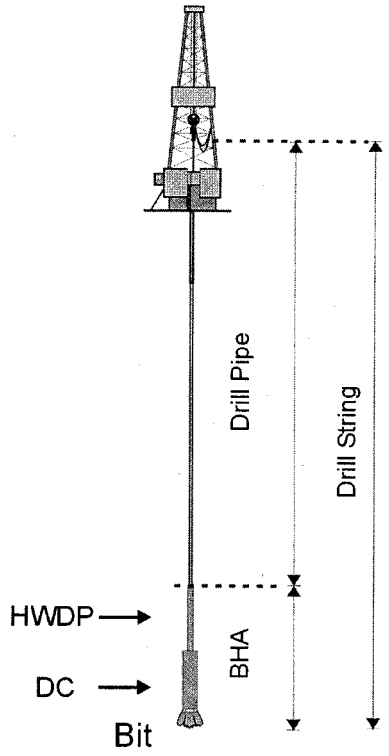

Figure 2.5: Drillstring components taken from [1]

2.6 Bottom Hole Assembly (BHA)

The main function of BHA is to apply weight on the drill bit. This weight is termed as the weight on bit (WOB). The BHA is assembled with massive thick walled and strong pipes called drill collars made up of heat treated alloy steel [2]. Drill collars put all the weight of the drill string on the bottom, which allows to maintain steady vertical drilling. Furthermore, breaking and kinking action should be avoided since they are detrimental for the drill string. Drill pipes are linked with the drill collars through heavy-weight drill pipes (HWDP). They have intermediate strength and weight, and are used to reduce the stress between the drill pipes and the drill collars.

2.6.1 Bottom Hole Assembly Elements

Here, we briefly mention the function of mechanical devices and instruments installed within BHA, as each of these elements performs a certain task while drilling a bore-well. The *stabilizer* or (*STAB*) is used to to keep the drill string in the center of the bore-hole. It is a pipe like element with blades that make a contact with the walls of the well. It also has grooves to circulate the mud [2, 1]. In order to suppress the high amplitude axial vibrations developed inside the drill string, the *vibration dampener* or *shock absorber* (*SHOC*) are used, which utilize rubber, spring, or compressed gas to absorb vibrations. Mechanical instrumented tools called *subs* are used between the drill collars as well as at the junction of the drill bit and the drill collars. For instance, a *bit sub* is placed between the bit and the drill collar, while *crossover sub* (*XO*) is used to make a connection between different collars and also between the pipe and the collar. During the drilling process, it often occurs that the drill bit sticks in the rock. In order to overcome this, the *jammers* (*JAR*) are used that initiate hammer percussions to set the bit free. Also, the *reamers* or the *hole openers* are the tools that use roller cones to enlarge or straighten the bore hole. Finally, the electronic and magnetic equipments installed at the BHA are separated from each other and from the external disturbances through *non-magnetic collars* (*monel*) which are used as jackets for

these devices.

2.7 The Drill Bit

At the very end of drillstring lies the drill bit. The drill bit is responsible for cutting of rocks. The cutting action is created by simultaneous actions of the weight on bit (WOB) which is applied on the top of the bit through drill collars and of the torque which transmitted from rotary table through drillstring. A small portion of the drilling energy may be also radiated in form of seismic waves [1]. Different types of drill bits are available for various kind of well drilling. Bits can be classified into several types and characteristics. International Association of Drilling Contractors (AIDC) characterizes bits with three numbers, where the first number describes the cutting face structure, the second designates the strength of bit relating to the hardness of the formation to be drilled, and the third number describes the unique mechanical design of the bit. The most commonly used types are *roller-cone* or *tricone* bits and *polycrystalline diamond compact (PDC)* bits. Each of these types has several sub classes with unique characteristics that allow to achieve certain parameters of drilling. In general, they can be selected for different drilling jobs depending upon the expected drilling rate performance, cost per unit depth, the bit life, *etc* [1]. The main features and performance characteristics of the roller-cone and the polycrystalline diamond compact bits are briefly described below.

2.7.1 Roller-Cone Bits

The roller-cone bit, also called tricone bit, has three rotating cones with chisel-like teeth (supported by three legs made of heat treated steel alloy). It is designed to break the rocks by indentions and gouging [1]. Roller-cone bits that are built for medium to harder rock formations have teeth coated with tungsten carbide. The three cones rotate on sealed and lubricated bearings [2]. The rock chips, which are produced while cutting and crushing the rock, can be removed from the jets of mud derived from nozzles located between the cones.

The mud circulation and cleansing of the crushed rock chunks is briefly described below. The bit is provided with threads so that it can be connected upwards to the drill collar. The roller-cone bits are usually used in exploration wells as these bits do not completely crush and pulverize rock particles like PDC bits. The rock chunks yielded by roller-cone bit can later be used for rock formation analysis [1].

2.7.2 Polycrystalline Diamond Compact (PDC) Bits

Polycristalline diamond compact (PDC) bits are also called *fixed cutter* bits as they are formed with solid metal body without any moving parts. The PDC bit is equipped with chisels that are sintered diamond cutters, and they are attached to tungsten carbide cylinder. The use of diamond increases sharpness of the cutters, while tungsten carbide is resilient to impacts and has high strength. The working temperatures for PDC bits are up to 350° C [1]. The PDC bits are more expensive than other types of bits, however, they are also more durable, which makes them more economical overall.

The PDC bits have several other advantages over other bits. First, they have a relatively simple cutting action which can therefore be modeled easily. The weight on bit (WOB) of PDC bits is about 20-40 kN, which is smaller in comparison with other bits. The smaller WOB decreases the vibrations of the drillstring. Because of fixed cutters and due to its durability, the PDC bits drill faster than any other bits. Also, as there are no moving parts, the chances of failure for the bit are reduced. Another big advantage of the PDC bits is that less power is required for cutting and shearing action in comparison with the roller-cone bits. The PDC bits are also lighter in comparison with the tricone bits, which allows for easier deviation control in directional drilling well. The PDC bits, however, have some shortcomings. For instance, PDC bits are not designed to withstand highly abrasive and hard formations. When used for cutting harder formation, the life of PDC bits decreases although fast penetration rates can still be achieved. Another feature of the PDC bits is their "cutting and grinding" action, which demolishes all the rock pieces into sand. As a result,

no rock samples could be obtained, which makes it difficult for the geologists to analyze the rock bed formation. Still, PDC bits are by far the most widely used bits in the industry.

2.8 Circulating System

In order to clear away the rock cuttings produced by the bit cutting action, mud water is circulated through the hole. This mud water or drilling mud is kept in tanks placed on the drilling site, and it is pumped to circulate through the bore hole [2]. These pumps used for mud water circulation are called *mud hogs*; they are driven by prime movers. The mud flow is then sent to swivel through a rubber tube called mud hose. From the swivel, the mud water flows down through drill pipes and drill collars and is subsequently ejected out through the drill bit nozzles. In case of roller-cone bits, the nozzles are placed between the cones. For PDC bits, the mud is ejected through the small holes called water-courses located on the face of the bit. This mud when ejected with high pressure through the face of the bit, takes away all the cutting chunks and rock formations from the bit whole cavity and cleans up the hole. This results in smooth cutting of rock as there is no layer of crushed rock particles or sand between the bit blades and the rock surface.

This mud water then flows back through the annular space between the well casing and the rotating drillstring, after which it flows out through blowout preventer (BOP) and goes to the mud return line [2]. As the mud flows on the return line, it goes through vibrating nets made up of woven cloth and located in steel frames. These are called *shale shakers*. The shale shakers act as filters to drilling mud separating the residual solids and coarse sand particles from the mud water. After this filtration, the mud water is sent back to the mud tanks where it is accumulated for another flow cycle.

The mud circulation has many advantages. In particular, the mud circulation reduces the friction between the drill string and the well walls (well casings). The mud particles

separated through shale shakers can provide valuable information about rock formations to geologists. The drilling mud also acts as a cooling agent. The mud flows down to the bottom and absorbs all the heat from drill collars, drill bit, and the bit rock cutting cavity. Another significant role of the mud water is to prevent the collapse of the well. The mud water flows through annular region between drillstring and well casings, and thus provides a cushion to drill string. This avoids any bent in drill strings and also suppress casings outward to obviate casing collapse. Finally, the pressure of the mud flow provides power to the downhole motor, steerable systems (for directional drilling) and turbines located in the bottom hole assembly.

2.9 Well Casing

In order to protect the walls of the well, metallic tubulars are inserted in the bore hole. These tubulars are called *casings*; they are cemented from outer side with the walls of well. Casings come with different diameter sizes and lengths. The outer or upper casings have larger diameter, however, it becomes smaller as one moves down the well-bore. Thus, the casings size is also reduced. The advantage of the casing is that the annular space between casings and drill-pipes provide the clear way for mud water to go up. The top most casings also support the weight of well head and the blow out preventers.

2.10 Conclusions

In this Chapter, the main components of the drilling system are described, and the purpose of each component is explained. The next Chapter deals with the derivation of a mathematical model of the drilling system.

Chapter 3

Mathematical Models of Drilling and Cutting

In this Chapter, different mathematical models of drilling rig structures described in the literature are presented, and the drilling response of drag bits is investigated. The Chapter is organized as follows. In Section 3.1, the mathematical models of the cutting process, including the models of a blunt cutter and a drag bit are described. In Section 3.2, different mathematical models of drillstrings and drive systems are presented. Finally, the equations of vertical penetration for the drill bit are explained in Section 3.3.

3.1 The Cutting Process

Cutting and penetration through a solid media is one of the fundamental processes involved in drilling. For this purpose, crushing the rocks with the help of drill bits is the most common and widely used method for creating a bore hole through various rock strata. Out of many types of bits, the most extensively used type in drilling industry is called drag bit. In drilling, the term ”drag bit” is defined as a bit consisting of fixed cutter blades mounted on the surface of the body of bit [3, 4, 17, 18, 19, 20]. In 1970s, the development of synthetic polycrystalline diamond compact (PDC) bits embarked a new era for the design of

different drag bit geometries. The PDC bits, which were described in some detail in the previous chapter, are composed of thin layer of polycrystalline diamond material bonded on tungsten carbide substrate. This composition gives PDC strenuous resistance against wear during cutting and efficient shear strength for crushing the rocks [4].

The mathematical model of the drilling response for PDC bits was first described explicitly by Detournay *et. al.* [3]. The four quantities associated with the drilling action, which are torque-on-bit T (with units of $N \cdot m$), weight-on-bit W (N), rate of vertical penetration v ($\frac{m}{s}$) , and the drill bit angular velocity ω ($\frac{rad}{s}$), were related with the set of equations in [3] and later revised in [4]. Detournay and Deforny in [3] interpreted the series of experiments conducted by Glowka [17] on a single cutter at Sandia National Laboratories. One of the significant conclusions made by Detounay and Deforny in [3] was that "the bit rock interaction is characterized by the coexistence of two processes: cutting of rock and frictional contact underneath the cutters." This was suggested previously by Fairhurst and Lacabanne in [21] and was later also mentioned in [17, 18, 19]. Thus, the model of a drag bit is constructed by developing the model of a single cutter through experiments and consequent integration of several cutters into the model for a drag bit.

Most of the theory presented here is taken from the papers of Detournay and coauthors [3], [4]. At first, some of the basic formulae for cutting are defined. Later on, based on these fundamental equations, a complete model for the drilling response of drag bits is established.

3.1.1 The Model of A Blunt Cutter

A drag bit typically consists of several cutters. In this Section, the model of a single cutter is examined. Later in Section 3.1.2, this single-cutter model is used to establish the model of a drag bit by integrating the contributions of all the cutters. The equations for a blunt cutter were established based on the results and observations obtained from the single cutter

experiments conducted by Glowka [17]. The prominent observations made by Glowka are that "*the two processes cutting and friction underneath the cutter, generally coexist during motion of a cutter*" and "*the cutting process is characterized by two constants ϵ and ζ, and friction process by one parameter μ concludes that a linear constraint exists between the drilling specific energy λ and drilling strength Σ for single cutter.*"

According to the above observations, only the cutting force acts on a perfectly sharp cutter; this force is defined by F^c. This cutting force has two components: surface (horizontal) F^c_s and normal (vertical) F^c_n, they are defined as follows

$$F^c_s := \epsilon A, \tag{3.1}$$

$$F^c_n := \zeta \epsilon A = \zeta F^c_s. \tag{3.2}$$

In equations (3.1) and (3.2), $\epsilon > 0$ is a parameter called the intrinsic specific energy with units of (Pa), which represents the amount of energy required to cut a unit volume of rock with a perfectly sharp bit. This parameter essentially determines the stiffness of the rock. Also, $\zeta > 0$ is the ratio of the vertical force to the horizontal force between rock and cutter contact surfaces. Typical values of ζ are in the range of [0.5-0.8] [4]. Also, A is the cross-sectional area of the cut; more specifically, it is the cross-sectional area of the groove traced by the cutter. It is described by Detournay in [3] that "*the horizontal and vertical forces on the cutter averaged over a distance which is large with respect to the depth of cut, and are proportional to the cross-sectional area A, of the cut*".

In the case of a blunt cutter, it was shown experimentally by Glowka [17] that, during the cutting process, wear flat of the cutter is in contact with rock. This produces additional frictional force F^f [3]. Similar to the cutting force, the frictional force F^f has also two components F^f_s and F^f_n, which act along the surface and in the normal direction, respectively. The horizontal (surface) F^f_s and the vertical (normal) F^f_n components of the frictional forces are related according to the following equation:

$$F^f_s = \mu F^f_n, \tag{3.3}$$

where $\mu > 0$ is a coefficient of friction. The frictional coefficient can also be scaled according to the formula $\mu = \tan\phi$, as defined in [3, 4, 17], where ϕ is the internal frictional angle. The model of a blunt cutter with different components of the cutting and friction forces is illustrated in Figure 3.1 which is borrowed from [3].

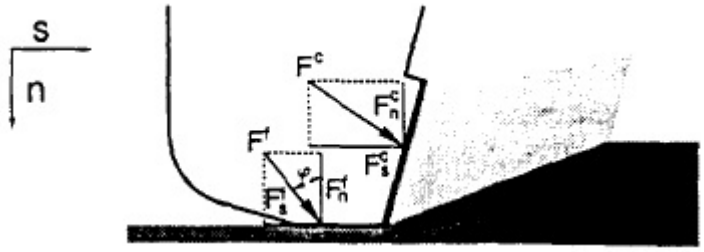

Figure 3.1: Model of the blunt cutter as defined by Detournay in [3]

The total forces applied to the blunt cutter is the sum of the cutting forces F^c and the frictional forces F^f. Combining equations (3.1), (3.2), (3.3), one can derive the following relation between the horizontal (surface) $F_s = F_s^c + F_s^f$ and the vertical (normal) $F_n = F_n^c + F_n^f$ forces,

$$F_s = (1 - \mu\zeta)\epsilon A + \mu F_n. \tag{3.4}$$

The expressions for drilling specific energy Λ and drilling strength Σ for the single cutter are defined as follows,

$$\Lambda := \frac{F_s}{A}, \tag{3.5}$$

$$\Sigma := \frac{F_n}{A}, \tag{3.6}$$

where, as before, F_s are the horizontal (surface) forces, F_n are the vertical (normal) forces, and A is the cross-sectional area of the cutter. The drilling specific energy Λ and drilling strength σ are not independent of each other; specifically, using the above equation (3.4), one can show that the relation between Λ and σ for the case of blunt cutter is expressed by the following equation,

$$\Lambda = \Lambda_0 + \mu\Sigma, \tag{3.7}$$

where $\Lambda_0 = (1 - \mu\zeta)\epsilon$. Overall, the model of a blunt cutter is characterized by the cutting and frictional forces that act on the cutting blade and wear flat of the cutter, respectively.

In the next subsection, the model of drag bit (PDC drill bit) is described. It is based on the model of a single cutter described above, however, it is more complicated and depends on a few extra parameters.

3.1.2 Drilling Action of a Drag Bit

A standard drill bit usually exhibits two kinds of motions: rotational along its axis of rotation and vertical motion while penetrating through the rocks. As described in [4], in the normal mode of operation of the drill bit, the bit rotational velocity ω is parallel to its axis of rotation, and the penetration velocity v is directed vertically straight through the rocks. Similarly, the weight-on-bit W acts in the vertical direction and the torque-on-bit T is applied in parallel to the direction of rotation of drill bit. The weight and torque acting on a PDC bit are illustrated in Figire 3.2 taken from [4]. The variables v and ω are regarded as kinematic variables, while the variables T & W are as dynamic variables in [4]. As mentioned above, the processes of cutting and friction occur simultaneously while drilling; consequently, the weight-on-bit W and the torque-on-bit T are decomposed into cutting and frictional components, as follows

$$T = T^c + T^f, \tag{3.8}$$

$$W = W^c + W^f. \tag{3.9}$$

The decomposition of torque-on-bit T and weight-on-bit W into cutting and frictional components is shown in Figure 3.3 which is also borrowed from [4]. The direction of weight-on-bit components W^c and W^f is always vertically downwards, parallel to the direction of motion of the drill bit; whereas the direction of torque components T^c and T^f is considered parallel to the tangent of rotational motion of drill bit.

The cutting components of the weight-on-bit and torque-on-bit depend on the radius of PDC drill bit a, intrinsic specific energy ϵ , the parameter ζ, and the depth of cut d. The

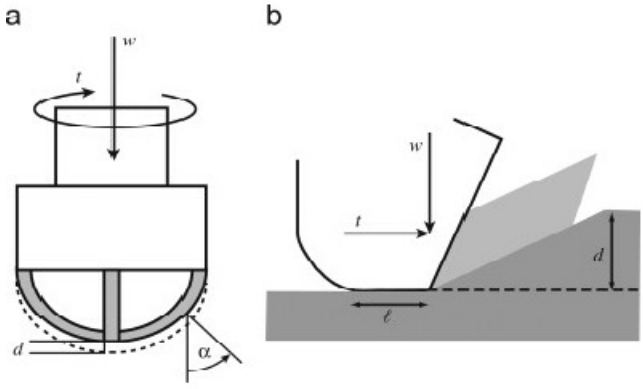

Figure 3.2: Sketch of a drag bit (a) and equivalent two dimensional cutter showing two forces torque and weight along with depth of cut *d* described by Detournay in [4]

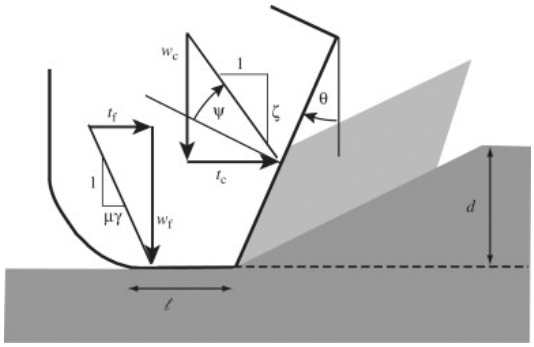

Figure 3.3: Decomposition of torque and weight described by Detournay in [4]

first three parameters are already defined in the previous section. The new parameter here is the depth of cut d with units in m; however, typical values of d is within range of several millimeters (mm). The depth of cut d plays significant role in the equations to follow that describe the cutting components of torque-on-bit T and weight-on-bit W. The equations for these two cutting components are as follows [4],

$$T^c = \frac{1}{2}a^2\epsilon d, \tag{3.10}$$

$$W^c = a\zeta\epsilon d. \tag{3.11}$$

The frictional components of torque-on-bit T and weight-on-bit W are proportional to each other; more specifically, they are related according to the formula

$$\gamma = \frac{2T^f}{\mu a W^f}, \tag{3.12}$$

where γ is a constant called bit constant. The bit constant γ depends on the dimensions of the cutting blades and the arrangement of cutters on a bit. The value of γ is typically greater than 1 [3, 4].

By rearranging equations (3.9), (3.11), (3.12), the expression for T^f can be obtained as follows

$$T^f = \frac{1}{2}a\mu\gamma W - \frac{1}{2}a^2\mu\gamma\zeta\epsilon d. \tag{3.13}$$

Equation (3.13) can in turn be rewritten in terms of W, T and d. This can be done by first using equation (3.10) to obtain value for T^c, and then using (3.8). This results in the formula

$$\frac{2T}{a} = (1 - \mu\gamma\zeta)\epsilon da + \mu\gamma W. \tag{3.14}$$

Equation (3.14) describes the drilling response model of a drag bit. It is reminiscent of the equation (3.4) which describes the response of PDC drag bit with a single cutter. In [3] and later in [4], the above model (3.14) is also rewritten in terms of two other variables, which are drilling specific energy E and drilling strength S. These variables are defined as follows,

$$E := \frac{2T}{a^2 d}, \tag{3.15}$$

$$S := \frac{W}{ad}. \tag{3.16}$$

Thus, the drilling specific energy E is a function of torque-on-bit T, while the drilling strength S is a function of weight-on-bit W. Both E and S are inversely proportional to the depth of cut d. Substituting E and S back in equation (3.14) yields the following equation,

$$E = E_0 + \mu\zeta S, \tag{3.17}$$

where $E_0 := (1-\beta)\epsilon$, and $\beta := \gamma\mu\zeta$. Formula (3.17) can be interpreted as a linear equation $y = mx + c$, where E is on vertical axis and S is on horizontal axis. The point E_0 represents the intercept of line with S whereas $\mu\gamma$ represent the slope of line. This is illustrated in Figure 3.4.

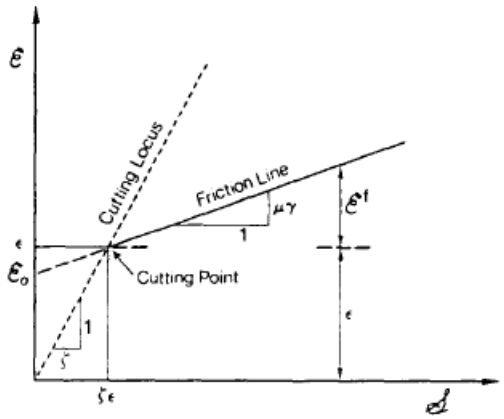

Figure 3.4: Schematic diagram of drilling specific energy E and drilling strength S by Detournay in [3]

The drilling system's efficiency is specified with parameter η which is defined as the ratio between the intrinsic specific energy and the drilling specific energy [3],

$$\eta := \frac{\epsilon}{E}. \tag{3.18}$$

Another way to describe the drilling efficiency is by using the ratio of E and S [3],

$$\chi := \frac{E}{S}, \tag{3.19}$$

The relationship between parameter χ and the drilling efficiency is described by the formula

$$\eta = \frac{\chi - \mu\gamma}{(1-\beta)\chi}. \tag{3.20}$$

By contemplating the $E - S$ plot, a few other details are worth mentioning here. In Figure 3.4, the dotted line (cutting locus) represents the response of a perfectly sharp bit without any frictional force components. The S-intercept of the friction line is given by E_0. This means that, if $\beta < 1$ (which is a general case according to [3, 4]), then E_0 is positive on E axis. Since the dimentionless parameter ζ accounts for the cutting action, the line with gradient ζ^{-1} is referred to as the cutting locus in [3].

The cutting line and the friction line intersect at the point $(\zeta\epsilon, \epsilon)$. This point corresponds to an ideally sharp cutter where all the energy is dissipated into cutting action without any frictional loses as explained in [4]. In reality, all the states of drilling are located to the right of this point. Experiments with PDC bits in [3] showed that the drilling points (states) lie either on the friction line or just above it.

Another important point to note from Figure 3.4 is the magnitude of the intrinsic specific energy ϵ. In [4], it was again experimentally proved that the magnitude of specific drilling energy E is always greater than the intrinsic specific energy ϵ, which is why the efficiency $\eta = \frac{\epsilon}{E}$ is always less than 1. This loss in efficiency is due to the frictional losses during drilling.

3.2 Mathematical Models for Drilling Structure

So far, the cutting models of a PDC Drill bit have been briefly elaborated. Now, the rudimentary components of the complete drilling system will be described. In order to design a controller which could implement and achieve desired vertical speed for drilling, a mathematical model of the complete drilling system is required. In this Section, some mathematical models of drilling found in the literature will be presented.

3.2.1 Model of drillsting with drag bit by T. Richard, C. Germay, and E. Detournay

The model of Richard *et. al.* model [5, 22] describes the drillstring (along with the rotary mechanism at the top) with two degrees of freedom. Specifically, Richard *et. al.* [5, 22] describes the rudimentary drilling model by taking into consideration the axial and torsional motion of the drillstring (and the drill bit). This model describes the motion of the drill string and the bottom whole assembly while taking into account the bit-rock interaction model which comprises of frictional and cutting processes. Before going into the description of the equations of motions, the motion of drillstring and drill bit will be briefly explained. Any conventional drilling system has two basic motions, vertical and rotational. These two motions are generated when the bit makes contact with the rock and crushes the rock with a rotational motion, slicing the rocks through its blades or cutters. Also, the weight on bit applied from the top of drilling rig allows the bit to compress the surface of rock generating a vertical motion. The governing equation for the motion of a drillstring and drill bit presented in [5, 22] are as follows,

$$I\frac{d^2\phi}{dt^2} + C(\phi - \phi_0) = T_0 - T({}^t_0\phi, {}^t_0U), \tag{3.21}$$

$$M\frac{d^2U}{dt^2} = W_0 - W({}^t_0\phi, {}^t_0U). \tag{3.22}$$

The above differential equations describe the discrete model of drilling system characterized with two degree of freedom. In these equations, U and ϕ are the vertical and the rotational positions of the drill bit, T and W are the torque-on-bit and the weight-on-bit, respectively, M is equivalent point mass of drill string plus BHA bearing the units of (Kg), I represents the moment of inertia of drillstring and BHA with units $(kg \cdot m^2)$, and C represents the torsional stiffness of the structure with units $(\frac{Nm}{rad})$. The torque-on-bit T and the weight-on-bit W are functions of all the previous values U and ϕ, that is, they depend upon the history of ${}^t_0U$ and ${}^t_0\phi$. Furthermore, ϕ_0, T_0 and W_0 are the steady state values associated with the trivial solution found in [5, 22]. The parameters M, I, and C can be calculated

according to the formulas

$$M = \rho\pi(r_{bo}^2 - r_{bi}^2)L_b, \qquad I = \rho J_b L_b + \frac{1}{3}\rho J_p L_p, \qquad C = \frac{GJ_p}{L_p}, \tag{3.23}$$

$$J_p = \frac{\pi}{2}(r_{po}^4 - r_{pi}^4), \qquad J_b = \frac{\pi}{2}(r_{bo}^4 - r_{bi}^4), \tag{3.24}$$

where ρ is the density of the drill pipes and bottom hole assembly with the units of $(\frac{Kg}{m^3})$. $r_{pi}(r_{bi}), r_{po}(r_{bo}), L_p(L_b), J_p(J_b)$ denote the inner radius with units (*meter*), outer radius with units (*meter*), length with units in (*meter*) and polar moment of inertia with units in $(\frac{Nm^2}{rad})$ or $(kg.m^2)$ for drill pipes and (bottom hole assembly), respectively.

Assuming the friction effects are negligible, both variables T and W are proportional to the depth of cut d, according to equations (3.10), (3.11). As it is illustrated in Figure 3.5, the depth of cut d in [5, 22] is the thickness of rock ridge in front of the blade. It is assumed that the drill bit has n number of identical blades, and the difference of angular positions of these two successive blades is $(\frac{2\pi}{n})$. In this case, d is the combined depth of cut of all n blades in each revolution of drill bit, according to the formula

$$d := nd_n, \tag{3.25}$$

where d_n is the depth of cut of each blade. The depth of cut for each blade in turn is defined according to the formula

$$d_n(t) := U(t) - U(t - t_n), \tag{3.26}$$

where $U(t)$ and $U(t - t_n)$ are the vertical position of the drill bit at current time instant t and some previous instant $t - t_n$, respectively [5, 22]. The delay t_n in the above formula is exactly the time that is required for the drill bit to rotate by an angle $2\pi/n$ to achieve its current angular position $\phi_1(t)$; in other words, it also satisfies the following equation:

$$\phi(t) - \phi(t - t_n) = \frac{2\pi}{n}. \tag{3.27}$$

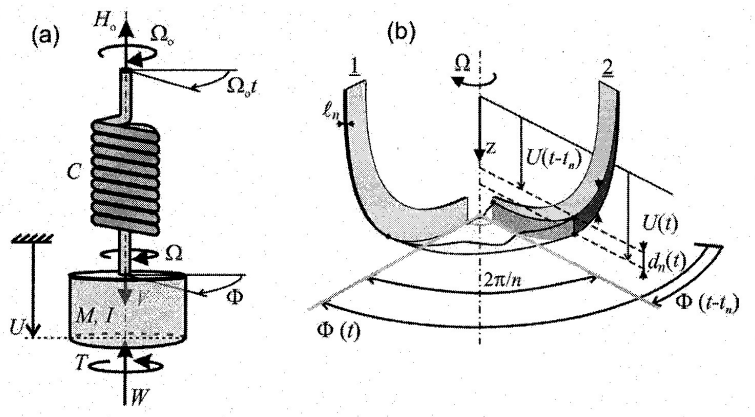

Figure 3.5: (a) A simplified model of drillstring; (b) Section of the bottom hole profile located between two successive blades; cited at [5]

3.2.2 Model of drillstring and drive system by M. Zamanian, S. Khadem and M. Ghazavi

Based on similar mathematical principles, Zamanian, Khadem and Ghazavi [6] presented a slightly modified model of drilling system. Specifically, the work [6] augments the model of [5, 22] by considering the effects of moment of inertia of the rotary table and an active damping system. The resulting model has two torsional degrees of freedom and one axial degree of freedom.

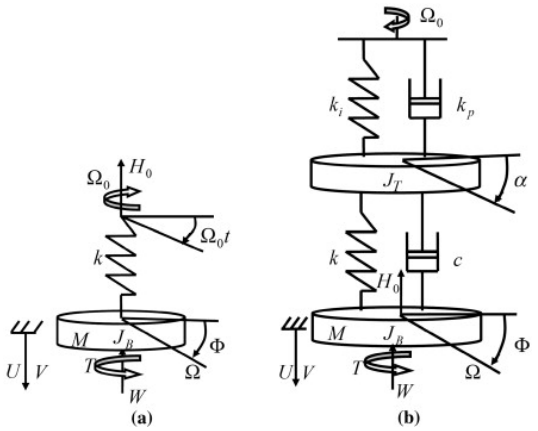

Figure 3.6: The model of drillstring and drive system presented in [6]

As it can be seen from the Figure 3.6 taken from [6], the model includes the rotary table at the top with one torsional degree of freedom as well as the body of drillstring (Bottom Hole Assembly) with one torsional and one axial degrees of freedom. At the top, this model is equipped with an active damping system, comprising of the rotational spring k_i and the rotational damper k_p. The active damping system is briefly described as "the electronic feedback system that modifies the energy flow through the motor" [6]. The governing equation of this model are given below,

$$J_T \frac{d^2\alpha}{dt^2} + k_p \left(\frac{d\alpha}{dt} - \Omega_o \right) + k_i \left(\alpha - \Omega_o t \right) + k \left(\alpha - \phi \right) + c \left(\frac{d\alpha}{dt} - \frac{d\phi}{dt} \right) = 0, \tag{3.28}$$

$$J_B \frac{d^2\phi}{dt^2} - k \left(\alpha - \phi \right) - c \left(\frac{d\alpha}{dt} - \frac{d\phi}{dt} \right) + T = 0, \tag{3.29}$$

$$M \frac{d^2U}{dt^2} = W_s - W - H_0. \tag{3.30}$$

In the above set of equations, the first two equations describe the torsional motion of the rotary table and the BHA, while the third equation exhibits the vertical motion of the drill bit. In (3.28)-(3.30), J_T is the equivalent moment of inertia of the rotary table and the motor with units ($\frac{N \cdot m^2}{rad}$) or ($kg \cdot m^2$), J_B is the moment of inertia of BHA ($kg \cdot m^2$), M is the mass of BHA (Kg), k is the torsional spring coefficient for BHA as described in Richard et. al. model, and c is damping coefficient for BHA (drillstring). In [6], c is calculated as $\frac{4L_p\bar{c}}{3}$, where $\bar{c}$ is the damping of mud per unit length. Also, T and W are applied torque-on-bit and weight-on-bit, H_0 is the constant weight applied from the top of the rig to drillstring with units (N), W_s is the submerged weight on the bit, α (rad) represents the angular position of rotary table, ϕ (rad) denote the angular position of BHA (also drill bit). The angular velocity of the rotary table is denoted by Ω_o, while the angular velocity of BHA and the drill bit is denoted by Ω; both have units of $\frac{rad}{s}$. Finally, U denotes the vertical position of the drill bit.

3.2.3 Mathematical model of drillstring and drive system by J. D. Jansen and V. D. Steen

A complete model of the drilling system with associated electric drive is presented in [7]. This model describes the drillstring as a simple torsional pendulum, where the drill pipes are represented as torsional springs and the BHA is described as a rigid body with inertia. Similarly to the previously discussed models, the drillbit is driven by an electric motor, where the torque is transmitted to the drillbit through drillstring. Figure 3.7 shows the structure of the drilling rig presented in [7]. Here, the drive system consists of electric motor with associated gearbox connected with the rotary table. The drill pipes are shown as tubular suspensions with BHA at the bottom.

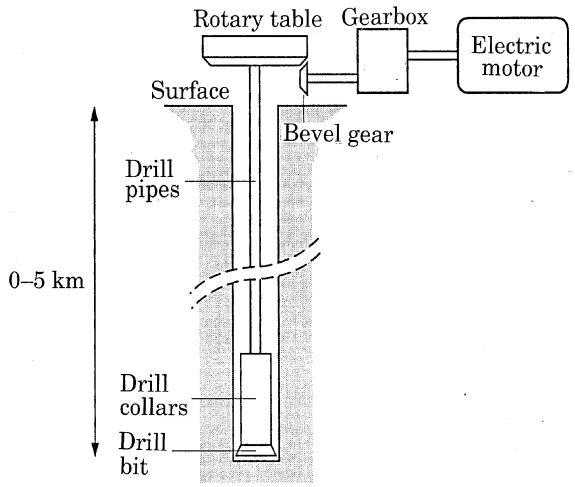

Figure 3.7: A simplified block diagram of oil well drillstring with surface mounted drive system [7]

The model developed in [7] is essentially based on the following simplifying assumptions.

1. The borehole assembly and drill bits behave like rigid bodies.

2. The moment of inertia of drill pipe is considered to be small in comparison with the moments of inertia of the borehole assembly and the rotary table and, therefore,

neglected.

3. The nonzero time propagation of the torsional force disturbances along the drill-string is neglected. The forces assume to propagate instantaneously along the drill-string.

Figure 3.8 shows the drive system and the drill string with equivalent electro-mechanical components. The DC motor is described by its equivalent inductance L with units (H) and an equivalent resistance R with units (Ω). Also, J_m is the moment of inertia of the motor with units ($\frac{N \cdot m \cdot s^2}{rad}$), while the moments of inertia of the rotary table and the BHA are denoted by J_r and J_1, respectively, with units $\frac{Nms^2}{rad}$. Also, c_2 is the damping coefficient of the rotary table, and c_1 is the equivalent damping associated with BHA and the drill pipes; both have units ($\frac{Nms}{rad}$). Coefficient k represents the equivalent torsional stiffness of the drill pipes ($\frac{Nm}{rad}$), ϕ_1 and ϕ_2 with units (rad) denote the angular positions of the drillbit (along with BHA) and the rotary table, respectively. Finally, T_b refers to torque with unit (Nm), and it represents the torque on bit plus the frictional forces acting between drill pipes and well bore.

Under the above described assumptions, the whole drill string drive system consists of three degrees of freedom and can be described by the following mathematical model. First, the motion of the drill string is described by following equation

$$J_1\ddot{\phi}_1 + c_1\dot{\phi}_1 + k(\phi_1 - \phi_2) - T_b = 0, \tag{3.31}$$

Here, ϕ_1 is the angular displacement of bit and drill collars (BHA), ϕ_2 is the angular displacement of the rotary table, J_1 is the equivalent moment of inertia of the collars (BHA) and the drill pipes, coefficient c_1 represents equivalent viscous damping, k is the equivalent torsional stiffness of the drill pipes, and T_b is a nonlinear function representing torque on bit (TOB) and other frictional forces. The dynamics of the rotary table and drive system is described by the following equation

$$J_2\ddot{\phi}_2 + c_2\dot{\phi}_2 - k(\phi_1 - \phi_2) - nT_m = 0, \tag{3.32}$$

where J_2 is combined moment of inertia of the rotary table and of the rotor of the electric motorcoupled together with a gearbox that has $1 : n$ gear ratio, c_2 is aggregated damping

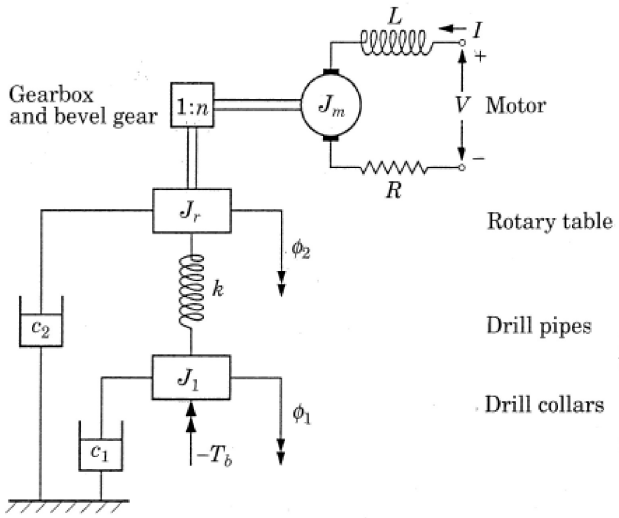

Figure 3.8: Representation of drillstring/drive system with mechanical and electrical components [7]

of all the components of the drive system, and T_m is the motor torque. Finally, the electric motor is described by the following equations

$$L\dot{I} + RI + V_b - V = 0, \qquad V_b = K\dot{\phi}_3 = Kn\dot{\phi}_2, \qquad T_m = KI \tag{3.33}$$

where I is the armature current, L is an equivalent armature inductance , R is an equivalent armature resistance, V_b is the back emf, V is the armature voltage, $\dot{\phi}_3$ is the rotor angular velocity, and K is a constant that depends upon the motor characteristics.

By combining all the above equations, the complete drillstring/drive system can be written in the following state space form,

$$\begin{bmatrix} \dot{\phi}_1 \\ \dot{\omega}_1 \\ \dot{\phi}_2 \\ \dot{\omega}_2 \\ \dot{I} \end{bmatrix} = \begin{bmatrix} 0 & 1 & 0 & 0 & 0 \\ \frac{-k}{J_1} & \frac{-c_1}{J_1} & \frac{k}{J_1} & 0 & 0 \\ 0 & 0 & 0 & 1 & 0 \\ \frac{k}{J_2} & 0 & \frac{-k}{J_2} & \frac{-c_2}{J_2} & \frac{Kn}{J_2} \\ 0 & 0 & 0 & \frac{-Kn}{L} & \frac{-R}{L} \end{bmatrix} \begin{bmatrix} \phi_1 \\ \omega_1 \\ \phi_2 \\ \omega_2 \\ I \end{bmatrix} + \begin{bmatrix} 0 \\ \frac{-T_b}{J_1} \\ 0 \\ 0 \\ \frac{V}{L} \end{bmatrix}. \tag{3.34}$$

Here, ω_1 and ω_2 are the angular velocities of the drill bit and the rotary table, respectively. Equation (3.34) is valid when the drill bit rotational velocity is greater than zero, that is $\omega_1 > 0$. In order to reduce the number of equations, a variable ϕ is introduced as the difference of ϕ_2 and ϕ_1. In this case, the original system can be rewritten in the following reduced state space form

$$\begin{bmatrix} \dot{\omega_1} \\ \dot{\phi} \\ \dot{\omega_2} \\ \dot{I} \end{bmatrix} = \begin{bmatrix} \frac{-c_1}{J_1} & \frac{k}{J_1} & 0 & 0 \\ -1 & 0 & 1 & 0 \\ 0 & \frac{-k}{J_2} & \frac{-c_2}{J_2} & \frac{Kn}{J_2} \\ 0 & 0 & \frac{-Kn}{L} & \frac{-R}{L} \end{bmatrix} \begin{bmatrix} \omega_1 \\ \phi \\ \omega_2 \\ I \end{bmatrix} + \begin{bmatrix} \frac{-T_b}{J_1} \\ 0 \\ 0 \\ \frac{V}{L} \end{bmatrix} \tag{3.35}$$

Equation (3.35) defines the reduced order model of the drillstring and drive system. The model (3.35) is used for control design in the subsequent chapters.

3.3 Rock Cutting and Vertical Penetration Equations

In this Section, we describe the equation for the vertical penetration and relevant assumptions we used to concatenate this vertical motion with the previously discussed drillstring/drive system. The the vertical motion of the drill bit is described by the following equation [6]

$$M\frac{dv}{dt} = W_s - W - H_0 - K_f v. \tag{3.36}$$

Here, v is the vertical velocity of the drill bit, H_0 is the constant upward force applied from the top of drilling rig, W_s is the submerged weight of the drill string and Bottom Hole Assembly (BHA). In this model we have assumed W_s and H_0 to be constants and defined their difference with another constant W_0 such that $W_0 = W_s - H_0$. Also, W is the applied weight on bit from the interaction of rock defined by equation (3.11), and $K_f > 0$ is the coefficient of viscous friction.

Formula (3.11) indicates that the applied weight on bit W is proportional to the depth of cut $d(t)$. Since a PDC bit has n blades, $d(t)$ actually corresponds to the combined depth

of cut of all n blades in each revolution of drill bit, according to the formula

$$d(t) := nd_n(t), \tag{3.37}$$

where $d_n(t)$ is the depth of cut of each blade which is defined by combination of formulas (3.26) and (3.27).

Using the equations (3.26) and (3.27) for calculating $d(t)$ would significantly complicate the control design. In this work, we simplify this problem by assuming that both the vertical and angular velocities change slowly; specifically, it is assumed that both $v(\tau) \equiv \dot{U}(\tau)$ and $\omega_1(\tau) \equiv \dot{\phi}_1(\tau)$ are approximately constant during each period $\tau \in [t - t_n, t]$. Using this assumptions, the equations (3.26), (3.27) can be rewritten as follows

$$d(t) \approx n \cdot v(t) \cdot t_n, \tag{3.38}$$

$$\omega_1(t) \cdot t_n \approx \frac{2\pi}{n}. \tag{3.39}$$

Combining (3.38), (3.39), and assuming $\omega_1(t) \neq 0$, one gets the following approximate expression for $d(t)$,

$$d(t) \approx \frac{2\pi \cdot t(t)}{\omega_1(t)}. \tag{3.40}$$

The above formula has a singularity at $\omega_1(t) = 0$. To remove this singularity, note that the drilling occurs when both $\omega_1(t) > 0$ and $v(t) > 0$. On the contrary, $\omega_1(t) \leq 0$, the drill bits do not cut the rock and therefore $d(t) \equiv 0$ in this case. Based on the above considerations, one can approximately define the depth of cut according to the formula

$$d(t) \approx \frac{2\pi \cdot v(t)}{\max\{\omega_1(t), \epsilon_0\}}, \tag{3.41}$$

where $\epsilon_0 > 0$ is sufficiently small positive constant. The formula (3.41) doesn't have singularity at $\omega_1(t) = 0$; it will be occasionally used for calculations of $d(t)$ instead of (3.40) in the cases where avoiding singularity is important (in simulations, *etc.*).

3.4 Conclusion

Necessary background has been covered in this chapter regarding the fundamentals of rock cutting, process of cutting through the drag bit, mathematical models of drillstring and drive

system, and finally the vertical penetration analysis of drag bit. The mathematical models used in this chapter constitute the foundation for our research and provide the necessary analysis of different models of drillstring presented in numerous articles. In next chapter these concepts are further analyzed to design controller to achieve desired vertical velocities for rock cutting.

Chapter 4

Controller Design for Drilling System

This Chapter deals with control design for drilling system. The structure of this Chapter is as follows. The general idea of the control approach used in this work is described in Section 4.1. Section 4.2 describes the control algorithm for stabilization of the vertical velocity, while Section 4.3 describes the robust servo controller that stabilizes the angular velocity in the presence of measured disturbances. Simulation results are presented in Section 4.4, and concluding remarks are given in Section 4.5.

4.1 Controller Design for Drillstring and Drive System

The block diagram of the overall drilling system is shown in Figure 4.1. As it can be seen from this figure, the block diagram has a complex structure and consists of several interconnected subsystems. Specifically, the vertical motion subsystem is described by equation (3.36); the output of this subsystem is the vertical velocity of penetration $v(t)$. The subsystem that represents the rotational motion is described by equations (3.35); this subsystem has one control input which is the armature voltage $V(t)$ and one output which is the angular velocity of the drill bits $\omega_1(t)$. Both $v(t)$ and $\omega_1(t)$ are the inputs of the nonlinear static block that represents the cutting process; this subsystem generates the depth of cut $d(t)$ according to equation (3.40). Both the torque-on-bit T and weight-on-bit W are

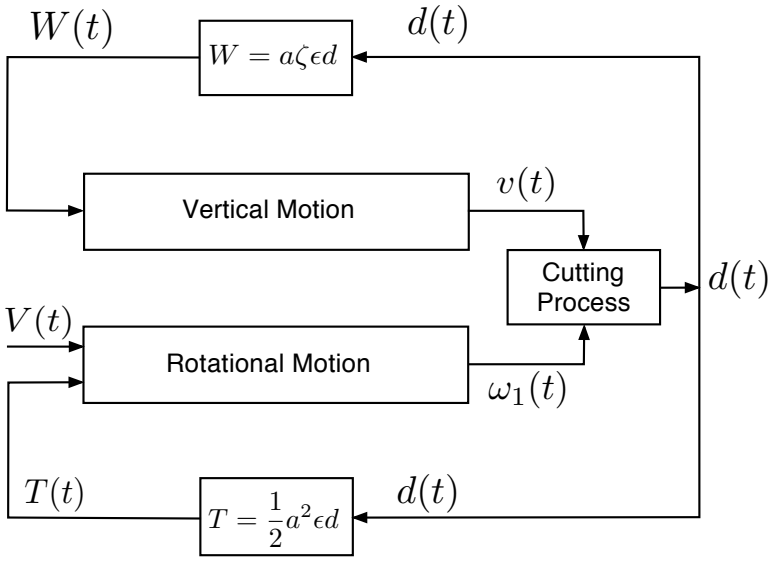

Figure 4.1: The block diagram of the drilling system

proportional to d; they are fed back to rotational motion and vertical motion subsystems, respectively.

Our goal is to design a control system that maintains a desired rate of drilling. Specifically, we are looking for the control algorithm for the armature voltage V that would guarantee that the velocity of the vertical penetration $v(t)$ tends asymptotically to an arbitrary positive desired value $v_{ref} > 0$. We start designing a control algorithm by considering the equation of vertical motion (3.36) in some detail.

4.2 Control of the Vertical Motion of a Drill Bit

The vertical motion of the drilling system is described by equation (3.36). For convenience, this equation is rewritten below in a slightly modified form, as follows

$$\dot{v} = -\frac{K_f}{M}\, v - \frac{(W_s - H_0)}{M} - \frac{W}{M}. \tag{4.1}$$

Here, v acts as the state of this first order differential equation. M is the combined mass of drill string and bottom hole assembly (BHA), W_s is the submerged weight of drill pipes and BHA (The weight when the hook on kelly drive has zero upward force or when the

complete load of drill string + BHA is resting on ground without upward pull), H_o is the upward force applied by the hook or kelly from the top of rig, and $K_f > 0$ is the coefficient of viscous friction. In this differential equation, the weight on bit W is the input to the system. It is dependent upon the depth of cut d, rock strength ϵ, ratio of drilling strength to drilling specific energy ζ and radius of drill bit a.

In the right-hand side of equation (4.1), the first term is linear with respect to v, the second term is constant which is defined by the parameters of the system, while the third term is proportional to the weight-on-bit W. The idea of the controller developed in this work is to somehow use the weight-on-bit W as the control input to the vertical motion subsystem. More specifically, combining formulas (3.11) and (3.40), one get the following expression for W,

$$W = a\zeta\epsilon\frac{2\pi}{\omega_1}v, \tag{4.2}$$

which essentially indicates that W is proportional to the vertical velocity $v(t)$ and inversely proportional to the angular velocity of the rotational motion $\omega_1(t)$. Substituting the last formula into (4.1), one gets

$$\dot{v} = \frac{W_s - H_0}{M} - \frac{1}{M}\left(a\zeta\epsilon\frac{2\pi}{\omega_1} + K_f\right)v. \tag{4.3}$$

The equation (4.3) is a linear differential equation with respect to v which, assuming $\omega_1 > 0$, has one stable equilibrium $v = v_0$ defined by the formula

$$\frac{W_s - H_0}{M} - \frac{1}{M}\left(a\zeta\epsilon\frac{2\pi}{\omega_1} + K_f\right)v_0 = 0. \tag{4.4}$$

Solving the above equation with respect to v_0, one gets

$$v_0 = \frac{W_s - H_0}{\left(a\zeta\epsilon\frac{2\pi}{\omega_1} + K_f\right)}. \tag{4.5}$$

The above equation (4.5) indicates that the location of the stable equilibrium $v = v_0$ of the vertical motion subsystem (4.1) can be controlled if one can control the rotational velocity ω_1. Specifically, equation (4.5) defines one-to-one correspondence between ω_1 from the range $(0, +\infty)$ and v_0 from the range $\left(0, (W_s - H_0)/K_f\right)$. In particular, for any given

$v_{ref} \in \big(0, (W_s - H_0)/K_f\big)$, there exists an unique $\omega_{ref} \in (0, +\infty)$ such that if the angular velocity satisfies $\omega_1(t) \equiv \omega_{ref}$, then v_{ref} is a globally exponentially stable equilibrium of the translational dynamics (4.1). For a given $v_{ref} \in \big(0, (W_s - H_0)/K_f\big)$, the corresponding ω_{ref} can be found using formula (4.5), as follows,

$$\omega_{ref} = \frac{2\pi a \zeta \epsilon}{\left(\frac{(W_s - H_0)}{v_{ref}}\right) - K_f}. \tag{4.6}$$

Therefore, the control goal of stabilization of the vertical penetration velocity $v(t) \to v_{ref}$ can be achieved by designing a controller for rotational motion that guarantees a sufficiently fast convergence of $\omega_1(t) \to \omega_{ref}$. The design of such a controlled is presented in the next section.

4.3 Stabilization of the angular velocity of the drilling system

The rotational dynamics of the drilling system together with the electric drive are described by equation (3.35), which is repeated below for convenience,

$$\begin{bmatrix} \dot{\omega}_1 \\ \dot{\phi} \\ \dot{\omega}_2 \\ \dot{I} \end{bmatrix} = \begin{bmatrix} \frac{-c_1}{J_1} & \frac{k}{J_1} & 0 & 0 \\ -1 & 0 & 1 & 0 \\ 0 & \frac{-k}{J_2} & \frac{-c_2}{J_2} & \frac{Kn}{J_2} \\ 0 & 0 & \frac{-Kn}{L} & \frac{-R}{L} \end{bmatrix} \begin{bmatrix} \omega_1 \\ \phi \\ \omega_2 \\ I \end{bmatrix} + \begin{bmatrix} 0 \\ 0 \\ 0 \\ \frac{1}{L} \end{bmatrix} V + \begin{bmatrix} \frac{-1}{J_1} \\ 0 \\ 0 \\ 0 \end{bmatrix} T_b \tag{4.7}$$

The above system has one control input which is the armature voltage of the electric drive V and one disturbance input which is torque on bit T_b. Our objective in this section is to design a control law for V which would track the reference angular velocity of the drill $\omega_1 \to \omega_{ref}$ while rejecting the disturbance T_b.

4.3.1 Feedforward robust servo control with disturbance rejection

To solve the control problem formulated above, one can use the approach to feedforward robust servo control problem presented in [23, 24]. Below, the above approach is presented

in a simplified way which, however, serves our purpose well. Consider a linear time invariant system of the form

$$\begin{aligned} \dot{x} &= Ax + Bu + Dw, \\ y &= Cx + Fu + Hw, \end{aligned} \tag{4.8}$$

where $x \in \mathbb{R}^n$ is the state, $u \in \mathbb{R}^m$ is the control input, $y \in \mathbb{R}^p$ is the output, $w \in \mathbb{R}^r$ are the disturbances, and A, B, C, D, F, and H are matrices of appropriate dimensions.

Consider a control problem described as follows. Suppose the disturbances $w(t)$ are measurable. Given a desired output signal $y_{ref}(t)$, design a control algorithm that guarantees $y(t) \to y_{ref}(t)$ as $t \to +\infty$. This problem was addressed in [23, 24] in a very general setting. In this work, a simple case is addressed where both y_{ref} and $w(t)$ are assumed to be constant signals, $y_{ref}(t) \equiv y_{ref}$ and $w(t) \equiv w_m$. In this case, the following conditions are necessary and sufficient for the existence of a linear time-invariant controller that solves the above described problem:

i) The pair (A, B) is stabilizable, which means that

$$\text{rank}\left[B, AB, A^2B, \ldots A^{n-1}B\right] = n; \tag{4.9}$$

ii)

$$\text{rank}\begin{bmatrix} A & B \\ C & F \end{bmatrix} = n + p. \tag{4.10}$$

If the above two conditions hold (and only in this case), the linear time-invariant controller that solves the above described problem is given according to the formula

$$u = Kx + \mathcal{G}^{\dagger} y_{ref} + \mathcal{G}^{*} w_m, \tag{4.11}$$

where $K \in \mathbb{R}^{n \times n}$ is the feedback gain matrix which is to be chosen such that $A - BK$ is stable and has the required dynamic properties,

$$\mathcal{G} = -C\left(A - BK\right)^{-1} B, \tag{4.12}$$

and

$$\mathcal{G}^{*} = \mathcal{G}^{\dagger} C\left(A - BK\right)^{-1} D, \tag{4.13}$$

where $\mathcal{G}^{\dagger}$ is the Moore-Penrose pseudoinverse of the matrix $\mathcal{G}$ in (4.12), defined by the formula

$$\mathcal{G}^{\dagger} = \mathcal{G}^{T}\left(\mathcal{G}\mathcal{G}^{T}\right)^{-1}. \tag{4.14}$$

4.3.2 Angular velocity stabilization

Here, the above described control approach is applied to the problem of stabilization of the angular velocity of drilling. The equations (4.7), which describe the rotational dynamics of a drilling system, can be rewritten in the form (4.8), where $x := \begin{bmatrix}\omega_1 & \phi & \omega_2 & I\end{bmatrix}^T \in \mathbb{R}^4$, $u := V \in \mathbb{R}^1$, $y := \omega_1 \in \mathbb{R}^1$, $w := T_{sl} \in \mathbb{R}^1$, and the corresponding matrices are

$$A := \begin{bmatrix} \frac{-c_1}{J_1} & \frac{k}{J_1} & 0 & 0 \\ -1 & 0 & 1 & 0 \\ 0 & \frac{-k}{J_2} & \frac{-c_2}{J_2} & \frac{Kn}{J_2} \\ 0 & 0 & \frac{-Kn}{L} & \frac{-R}{L} \end{bmatrix}, \quad B = \begin{bmatrix} 0 \\ 0 \\ 0 \\ \frac{1}{L} \end{bmatrix}, \quad D = \begin{bmatrix} \frac{-1}{J_1} \\ 0 \\ 0 \\ 0 \end{bmatrix}, \tag{4.15}$$

$$C = \begin{bmatrix} 1 & 0 & 0 & 0 \end{bmatrix}, \quad F = \begin{bmatrix} 0 \end{bmatrix}, \quad H = \begin{bmatrix} 0 \end{bmatrix}. \tag{4.16}$$

Our goal in this section is to design a controller that guarantees the convergence of the angular velocity of the drill bits $\omega_1(t)$ to a given constant reference value $\omega_{ref} > 0$ as $t \to +\infty$ while suppressing the disturbances represented by the torque $T_s l$. Below, we consider a drilling system that is described by the equations of the form (4.8) with matrices A, B, C, D, F, and H given by (4.15), (4.16), and with specific values of the parameters that are listed in Table 4.1. With these values, the matrices A, B, and D become

$$A := \begin{bmatrix} -0.1123 & 1.2647 & 0 & 0 \\ -1 & 0 & 1 & 0 \\ 0 & -0.2231 & -0.2005 & 0.0204 \\ 0 & 0 & -8640 & -2 \end{bmatrix}, \quad B = \begin{bmatrix} 0 \\ 0 \\ 0 \\ 200 \end{bmatrix}, \quad D = \begin{bmatrix} -0.0027 \\ 0 \\ 0 \\ 0 \end{bmatrix}, \tag{4.17}$$

while C, F, and H are described by (4.16).

Parameter	Description	Value	Unit
J_1	BHA + drill-string inertia	374	$[kgm^2]$
J_2	Rotary table + drive inertia	2120	$[kgm^2]$
c_1	BHA damping	42	$[\frac{Nms}{rad}]$
c_2	Rotary table damping	425	$[\frac{Nms}{rad}]$
k	Drill-string stiffness	473	$[\frac{Nm}{rad}]$
R	Motor armature resistance	0.010	$[\ \Omega]$
L	Motor armature inductance	0.005	$[H]$
K	Motor constant	6	$[Vs]$
n	Combined gear ratio for bevel and gear box	7.2	_
a	Drill bit radius	0.108	$[m]$
ζ	Ratio of drilling strength to drilling specific energy	0.7	_
ϵ	Intrinsic specific energy	60000	$[\frac{J}{cm^3}]$
M	Mass of Drill string(28120 Kg) + BHA(25080 Kg)	53000	$[kg]$
$W_s - H_0$	Submerged weight W_s − Applied Weight from top of the Rig H_0	100 or 1000	$[N]$
K_f	Viscous friction coefficient	20	$[\frac{Nm}{rad}]$

Table 4.1: Numerical Values for Drilling System Parameters

For the above described system, the necessary and sufficient conditions for stabilization (4.9), (4.10) are satisfied. Indeed, the stabilizability condition (4.9) is satisfied since

$$\text{rank}\left[B, AB, A^2B, \ldots A^{n-1}B\right] = \text{rank}\begin{bmatrix} 0 & 0 & 0 & 5.154273 \\ 0 & 0.000000 & 4.075472 & -8.968 \\ 0 & 4.075 & -8.968 & -700.339 \\ 200 & -400 & -34412 & 146307 \end{bmatrix} = 4. \tag{4.18}$$

On the other hand, the rank condition (4.10) is also satisfied because

$$\text{rank}\begin{bmatrix} A & B \\ C & F \end{bmatrix} = \text{rank}\begin{bmatrix} -0.112299 & 1.264706 & 0 & 0 & 0 \\ -1 & 0 & 1 & 0 & 0 \\ 0 & -0.223113 & -0.200472 & 0.020377 & 0 \\ 0 & 0 & -8640 & -2 & 200 \\ 1 & 0 & 0 & 0 & 0 \end{bmatrix} = 5. \tag{4.19}$$

Therefore, a controller of the form (4.11), (4.12), (4.13), (4.14) guarantees that the angular velocity of the drill approach the reference angular velocity $\omega_1 \to \omega_{ref}$ as $t \to \infty$, while rejecting the disturbance T_b.

4.3.3 Controller design

The design of controller (4.11), (4.12), (4.13), (4.14) begins by choosing the desired location of the closed-loop system's poles. For the purpose of simulations in this and next section, we consider two specific set of poles. The fist set, denoted by P_1, is chosen as follows:

$$P_1 := [-10 \qquad -2+2i \qquad -2-2i \qquad -4]. \tag{4.20}$$

The set P_1 consists of two real poles and two complex conjugate poles. On the other hand, the set P_2 contains only poles on the real axis, as follows

$$P_2 = [-5.5 \qquad -2 \qquad -4.5 \qquad -1] \tag{4.21}$$

The feedback gain matrix K_1 such that the poles of $A - BK_1$ are located according to P_1 is

$$K1 = [32.24 \qquad 57.45 \qquad -19.41 \qquad 0.0784]. \tag{4.22}$$

The coefficients $\mathcal{G}^*, \mathcal{G}^\dagger$ in (4.11) are calculated according to the formulas (4.12)-(4.14); the results are

$$\mathcal{G}_1^* = 0.123497, \quad \mathcal{G}_1^\dagger = 60.0844 \tag{4.23}$$

On the other hand, the feedback matrix K_2 such that the poles of $A - BK_2$ are located according to P_2 is

$$K_2 = [-5.167 \qquad 16.943 \qquad -30.62 \qquad 0.0534] \tag{4.24}$$

The corresponding coefficients $\mathcal{G}_2^*, \mathcal{G}_2^\dagger$ are

$$\mathcal{G}_2^* = 0.037286 \quad \mathcal{G}_2^\dagger = 9.603682. \tag{4.25}$$

The above control gains will be used in the simulations below.

4.4 Simulation Results

4.4.1 Stabilization of the angular velocity of the drilling

In this subsection, we will focus only on the stabilization of the rotational dynamics of drillstring. Specifically, the controller (4.6), (4.11)-(4.14) is been implemented to guarantee that the angular velocity of the drill bits $\omega_1(t)$ converges to a desired rotational velocity ω_{1ref}, while the value of the vertical velocity V_{out} is kept fixed. In the simulations below, the initial conditions of the system (4.7) are chosen as follows:

$$x(0) := \begin{bmatrix} \omega_1(0) \\ \phi(0) \\ \omega_2(0) \\ I(0) \end{bmatrix} = \begin{bmatrix} 2 \\ 0 \\ 2 \\ 0 \end{bmatrix}. \tag{4.26}$$

The simulation is conducted in MATLAB. The results of simulations are shown in Figures 4.2-4.9. Specifically, we consider four different values of reference angular velocities equal to $\omega_{1ref} = 10\,rad/s$, $\omega_{1ref} = 20\,rad/s$, $\omega_{1ref} = 30\,rad/s$, and $\omega_{1ref} = 40\,rad/s$, respectively. The results of simulations for $\omega_{1ref} = 10\,rad/s$ are shown in Figures 4.2, 4.3. Specifically, Figure (4.2) shows the output rotational velocity of drillbit $\omega_1(t)$ and the rotary table velocity ω_2, while Figure 4.3 demonstrates the behavior of the depth of cut $d(t)$ and the torque on bit $T_b(t)$. The gain matrix is equal to K_1.

Figures 4.4 and 4.5 correspond to $\omega_{1ref} = 20\,rad/s$ and the gain matrix $K = K_1$. Figures 4.6 and 4.7 demonstrate the response of the system for $\omega_{1ref} = 30\,rad/s$ and the gain matrix $K = K_2$. Finally, Figures 4.8 and 4.9 shows the response for $\omega_{1ref} = 40\,rad/s$ and the gain matrix $K = K_2$. Overall, these simulation results demonstrate that, in all cases, the designed controller guarantees convergence $\omega_1(t) \to \omega_{1ref}$ for different values of ω_{1ref} and different control gains K, while suppressing the disturbance signal T_b.

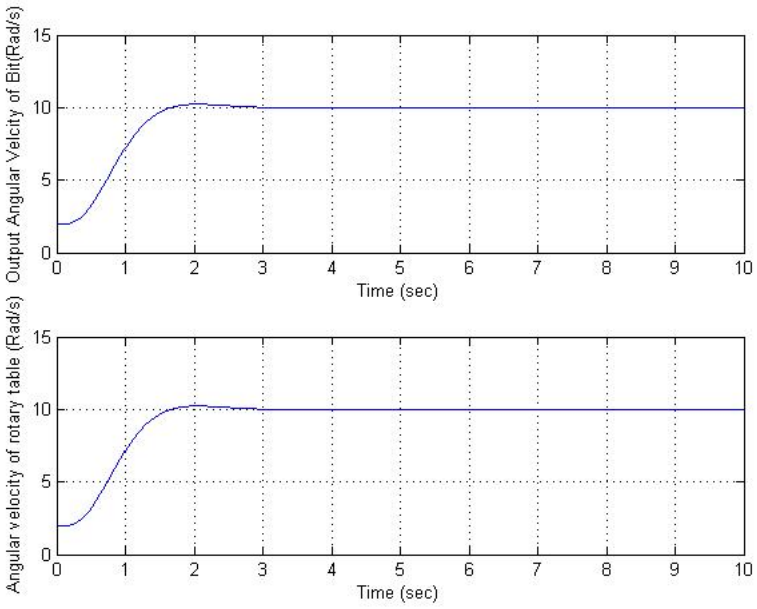

Figure 4.2: Response of the output angular velocity $\omega_1(t)$ (top) and rotary table velocity $\omega_2(t)$ (bottom) for the desired velocity $\omega_{1ref} = 10$ rad/s and $K = K_1$

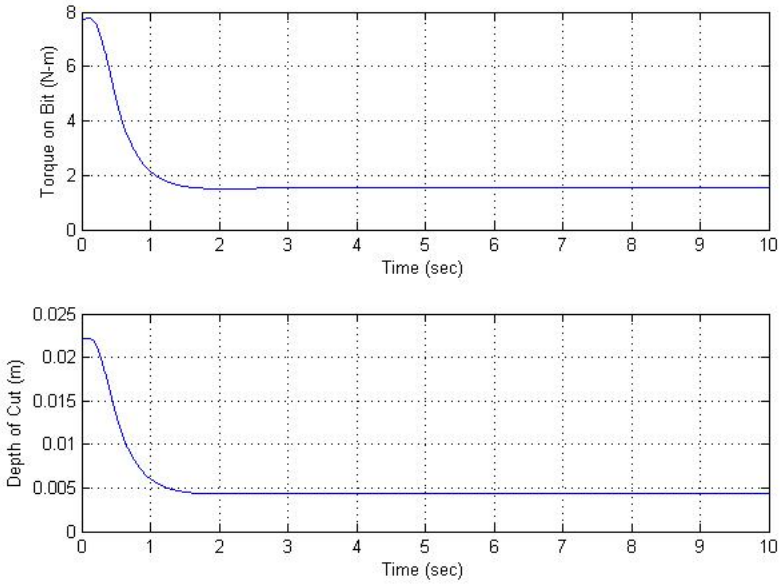

Figure 4.3: Torque on bit $T_b(t)$ (top) and the depth of cut $d(t)$ (bottom) for $\omega_{1ref} = 10$ rad/s and $K = K_1$

4.4.2 Stabilization of the vertical velocity of the drilling process

In this subsection, we present the results of simulations that deal with stabilization of the vertical (penetration) velocity of the drilling process. The vertical motion of the drilling system is described by equation (3.36), and it is interconnected with the rotational dynamics (3.35) through nonlinear equation (3.40). Specific values of the parameters appearing in these equations are given in Table 4.1. For a given reference velocity of the vertical penetration $v_{ref} > 0$, the corresponding reference rotational velocity ω_{ref} is calculated according to the formula (4.6). The control system described above guarantees that the rotational velocity $\omega_1(t)$ tracks ω_{ref}, which in turn stabilizes the vertical penetration velocity $v(t)$ converges to v_{ref}.

It is worth to notice that the equation (4.6) depends on the parameter $\epsilon > 0$ which is the intrinsic specific energy that is required to cut a unit volume of rock with perfectly sharp bit. This parameter reflects the hardness of the media and is, generally speaking,

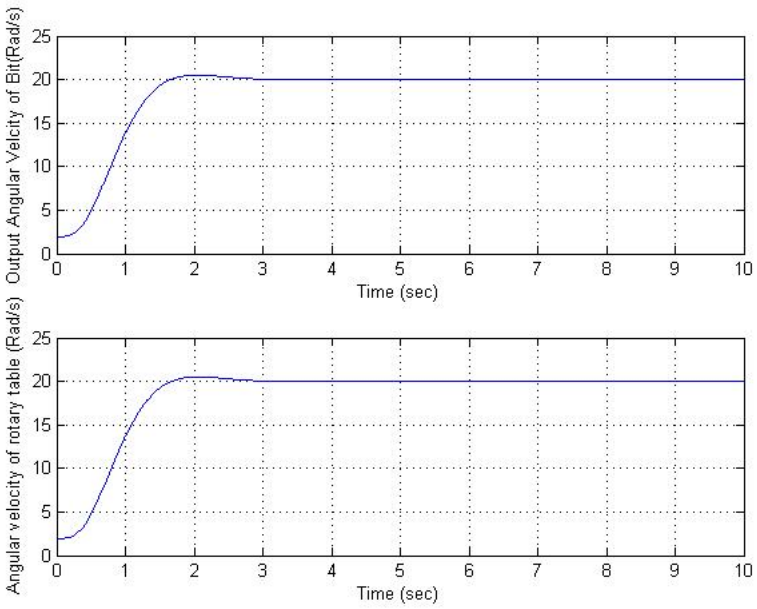

Figure 4.4: Response of the output angular velocity $\omega_1(t)$ (top) and rotary table velocity $\omega_2(t)$ (bottom) for $\omega_{1ref} = 20$ rad/s and $K = K_1$

unknown beforehand. However, in this section, it is assumed that $\epsilon > 0$ is known. The case of unknown ϵ will be addressed below in Chapter 5 of this Thesis, where the parameter estimation algorithm will be implemented.

Below, the simulation results are presented for the following three values of the reference vertical velocity v_{ref}: 0.03 m/s, 0.05 m/s, and 0.08 m/s. Similarly to the simulations presented above, two different set of feedback gains $K = K_1$ and $K = K_2$ are used which are defined by (4.22), (4.24). We also use two different values of the weight applied on the drillbit from the top $W_0 := W_s - H_0$, which are 100 N and 1000 N. The initial value of the vertical velocity $v(t)$ in all the simulations is $v(0) = 0.02$ m/s.

Figures 4.10 and 4.11 demonstrate the trajectories of the system for $v_{ref} = 0.03$ m/s, the feedback gains $K = K_1$, and the applied weight $W_0 := W_s - H_0 = 100$ N. Specifically, Figure 4.10 shows the trajectories of the vertical velocity $v(t)$ and the rotational velocity $\omega_1(t)$. One can see that both $v(t)$ and $\omega_1(t)$ converge to their reference values, although the rotational velocity converges faster. In Figure 4.10, on the other hand, the responses of

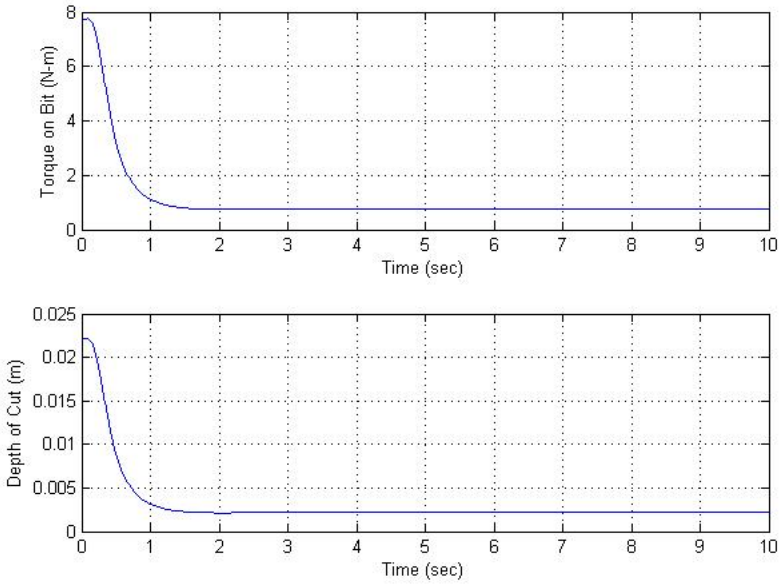

Figure 4.5: Torque on bit $T_b(t)$ (top) and the depth of cut $d(t)$ (bottom) for $\omega_{1ref} = 20$ rad/s and $K = K_1$

torque-on-bit $T_b(t)$ and depth of cut $d_{cut}(t)$ are shown. Figure 4.12 and 4.13 presents the same processes for the case of $v_{ref} = 0.05$ m/s, while in Figures 4.14 and 4.15, the same processes are shown for $v_{ref} = 0.08$ m/s and $K = K_2$.

In Figures 4.16, 4.17, the responses of $v(t)$, $\omega_1(t)$, $T_b(t)$ and $d_{cut}(t)$ are presented for the case where $v_{ref} = 0.03$ m/s and $K = K_1$, however, the applied downward weight is increase to $W_0 = W_s - H_0 = 1000$ N. This increase in weight results in much faster convergence of $v(t)$ to v_{ref}. Figures 4.18 and 4.19 depict analogous response of the four mentioned variables for the case $v_{ref} = 0.05(m/s)$. Again, a faster response time for $v(t)$ is displayed. Finally, Figures 4.20 and 4.21 presents the case where $W_0 = 1000$ N, $v_{ref} = 0.08$ m/s and gains are $K = K_2$. Overall, the simulation results confirm the validity of the proposed method.

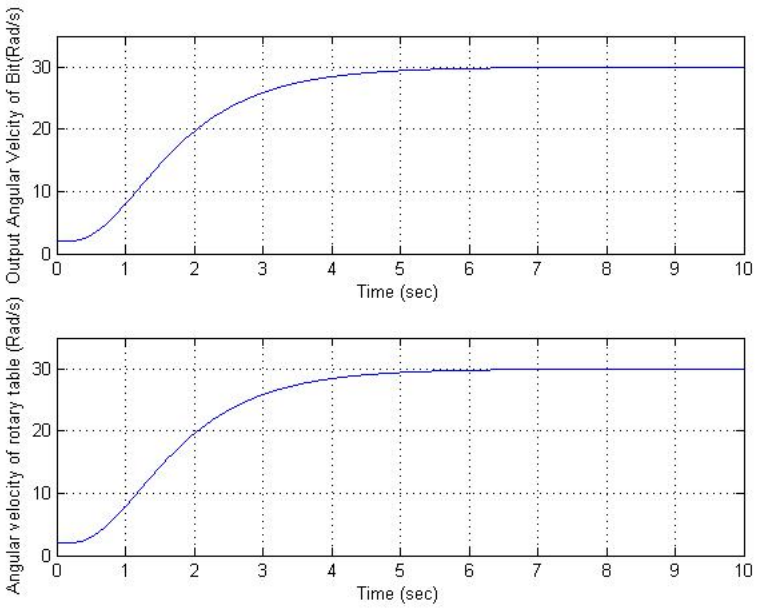

Figure 4.6: Response of the output angular velocity $\omega_1(t)$ (top) and rotary table velocity $\omega_2(t)$ (bottom) for $\omega_{1ref} = 30$ rad/s and $K = K_2$

4.5 Conclusions

In this Chapter, the controller design for drilling system is presented. The proposed controller has a cascaded structure, where the velocity of the vertical penetration is controlled indirectly by stabilizing the rotational velocity while rejecting the disturbances in the form of torque-on-bit. In particular, the controller presented assumes exact knowledge of all parameters, including the value of intrinsic specific energy ϵ. In the next Chapter, this requirement is removed by designing an on-line parameter estimation algorithm for ϵ.

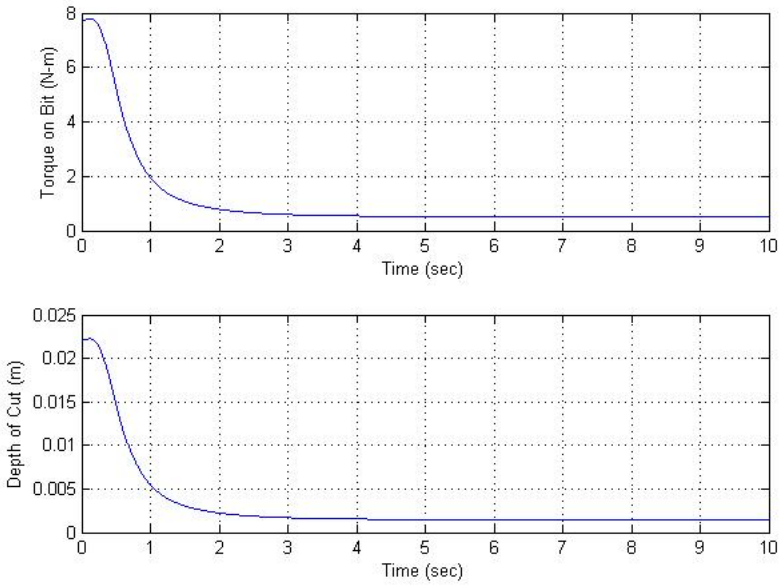

Figure 4.7: Torque on bit $T_b(t)$ (top) and the depth of cut $d(t)$ (bottom) for $\omega_{1ref} = 30$ rad/s and $K = K_2$

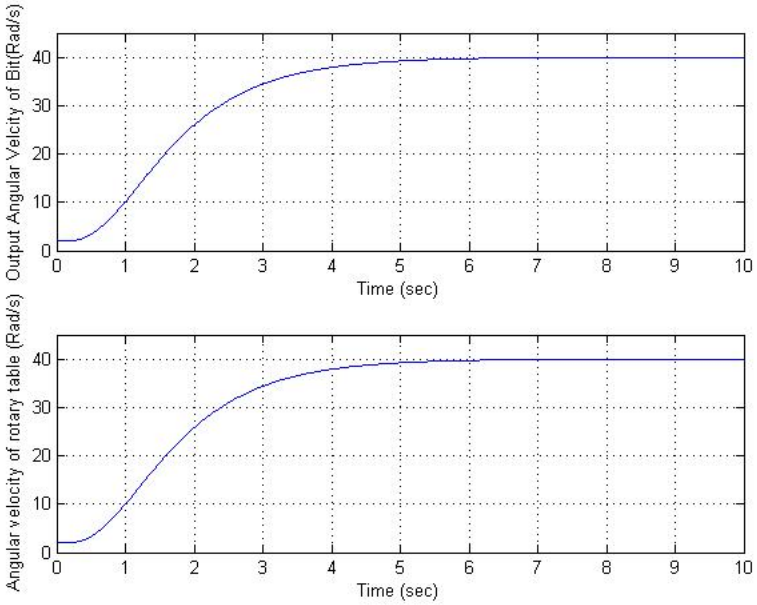

Figure 4.8: Response of the output angular velocity $\omega_1(t)$ (top) and rotary table velocity $\omega_2(t)$ (bottom) for $\omega_{1ref} = 40$ rad/s and $K = K_2$

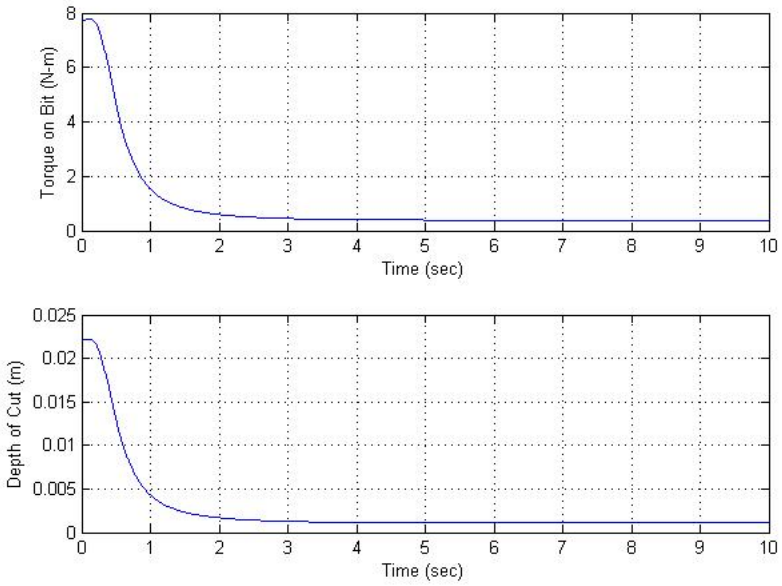

Figure 4.9: Torque on bit $T_b(t)$ (top) and the depth of cut $d(t)$ (bottom) for $\omega_{1ref} = 40$ rad/s and $K = K_2$

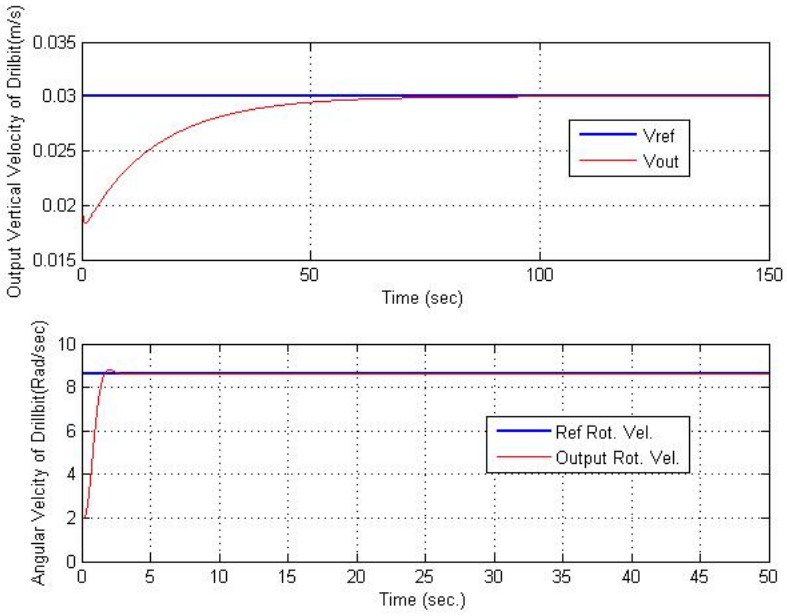

Figure 4.10: Response of output vertical velocity $v(t)$ (top) and output angular velocity $\omega_1(t)$ (bottom) when $v_{ref} = 0.03\,m/s$, gain $K = K_1$ and applied weight $W_0 = 100$ N

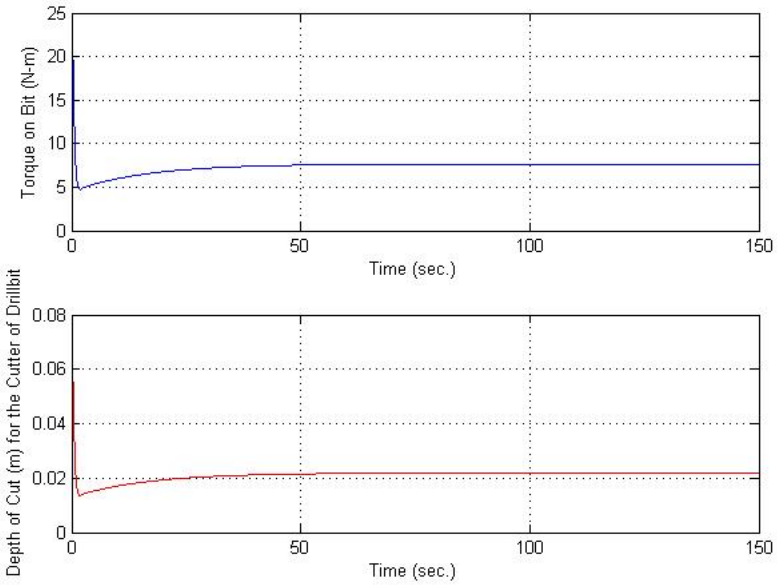

Figure 4.11: Torque on bit $T_b(t)$ (top) and depth of cut $d(t)$ (bottom) when $v_{ref} = 0.03\,m/s$, gain $K = K_1$ and applied weight $W_0 = 100$ N

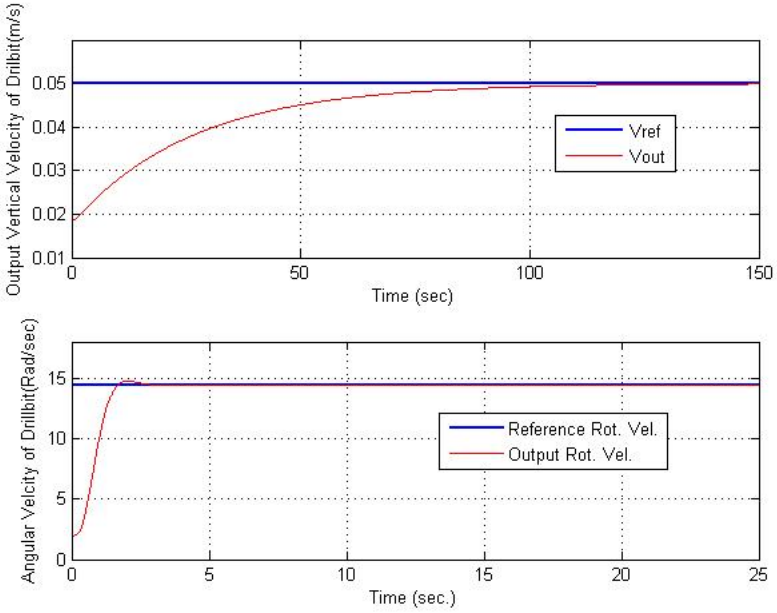

Figure 4.12: Response of output vertical velocity $v(t)$ (top) and output angular velocity $\omega_1(t)$ (bottom) when $v_{ref} = 0.05\,m/s$, gain $K = K_1$ and applied weight $W_0 = 100$ N

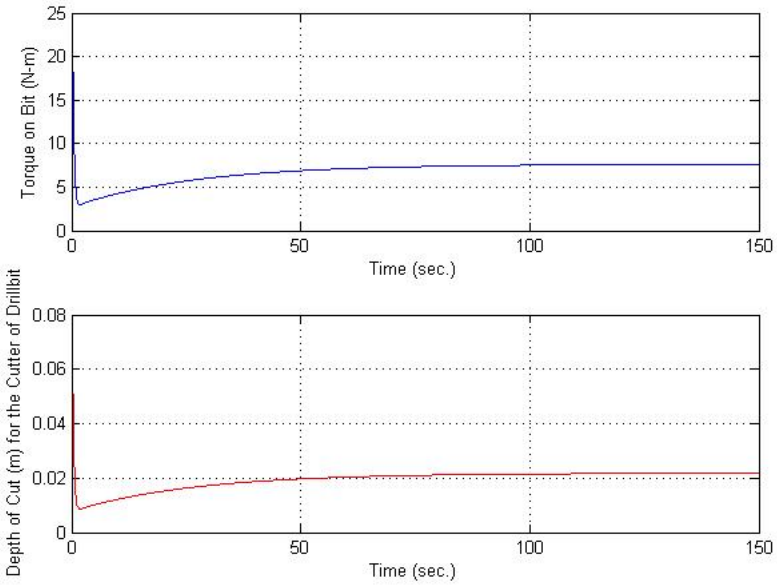

Figure 4.13: Torque on bit $T_b(t)$ (top) and depth of cut $d(t)$ (bottom) when $v_{ref} = 0.05\,m/s$, gain $K = K_1$ and applied weight $W_0 = 100$ N

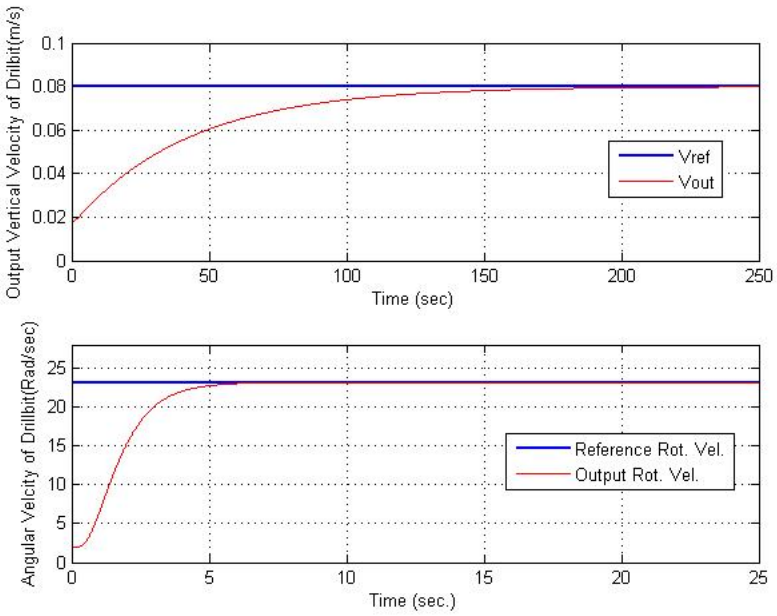

Figure 4.14: Response of output vertical velocity $v(t)$ (top) and output angular velocity $\omega_1(t)$ (bottom) when $V_{ref} = 0.08\,m/s$, gain $K = K_2$ and applied weight $W_0 = 100$ N

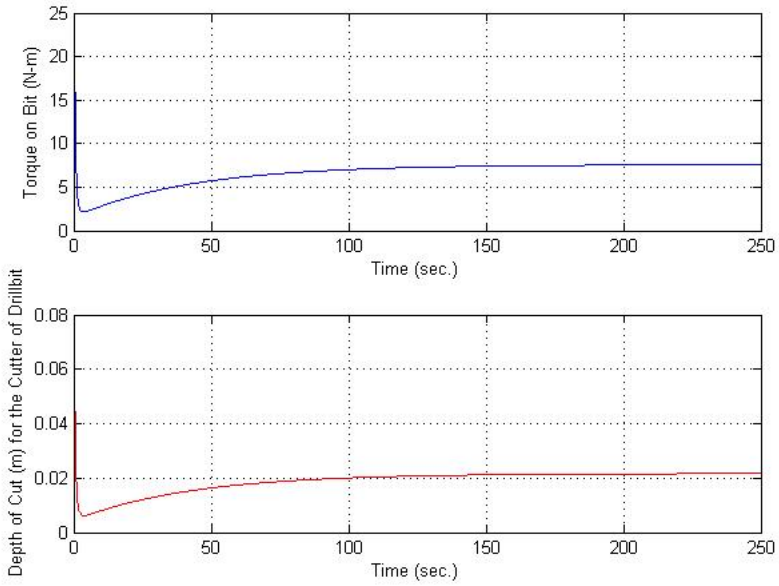

Figure 4.15: Torque on bit $T_b(t)$ (top) and depth of cut $d(t)$ (bottom) when $v_{ref} = 0.08\,m/s$, gain $K = K_2$ and applied weight $W_0 = 100$ N

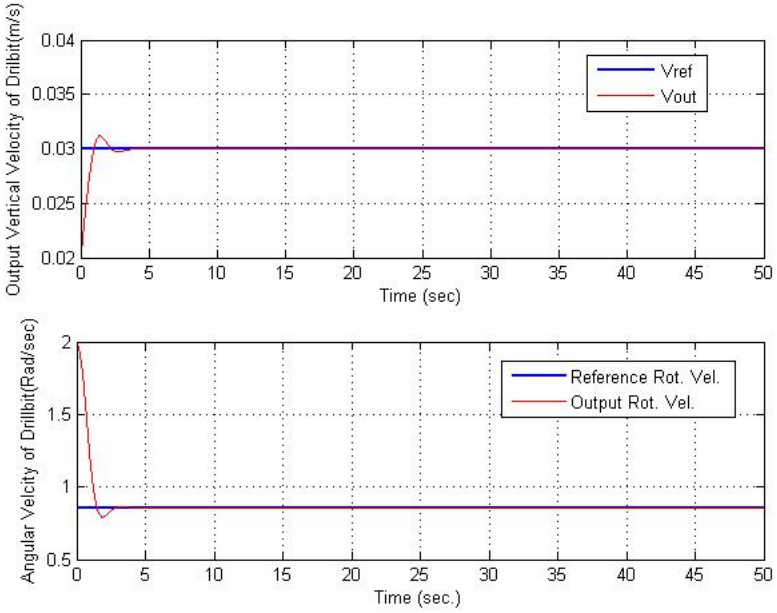

Figure 4.16: Response of output vertical velocity $v(t)$ (top) and output angular velocity $\omega_1(t)$ (bottom) when $v_{ref} = 0.03\,m/s$, gain $K = K_1$ and applied weight $W_0 = 1000$ N

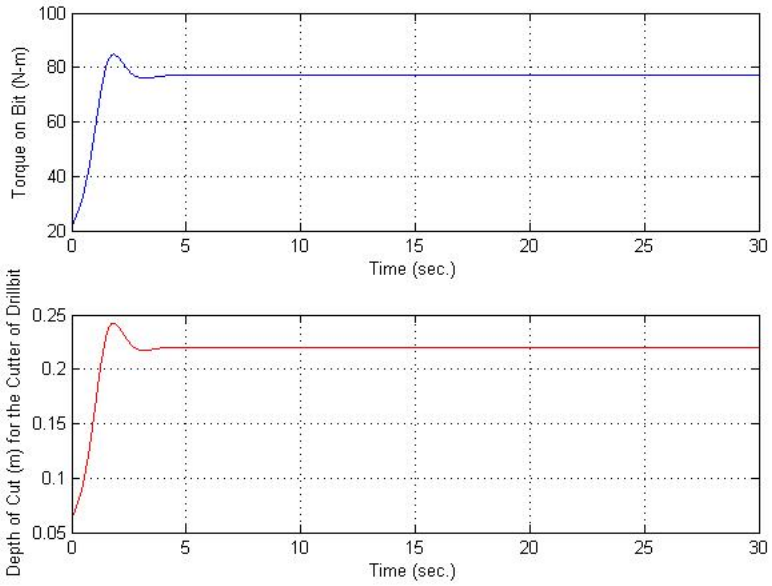

Figure 4.17: Torque on bit $T_b(t)$ (top) and depth of cut $d(t)$ (bottom) when $v_{ref} = 0.03\,m/s$, gain $K = K_1$ and applied weight $W_0 = 1000$ N

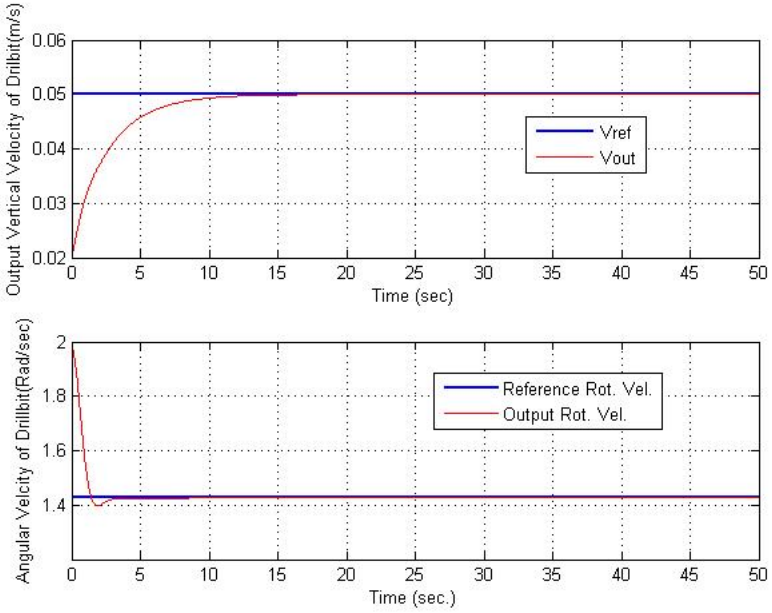

Figure 4.18: Response of output vertical velocity $v(t)$ (top) and output angular velocity $\omega_1(t)$ (bottom) when $v_{ref} = 0.05\,m/s$, gain $K = K_1$ and applied weight $W_0 = 1000$ N

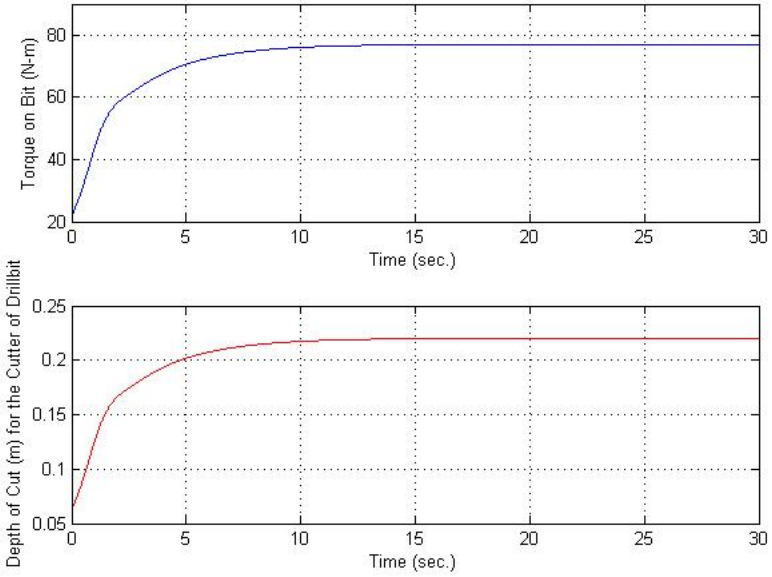

Figure 4.19: Torque on bit $T_b(t)$ (top) and depth of cut $d(t)$ (bottom) when $v_{ref} = 0.05\,m/s$, gain $K = K_1$ and applied weight $W_0 = 1000$ N

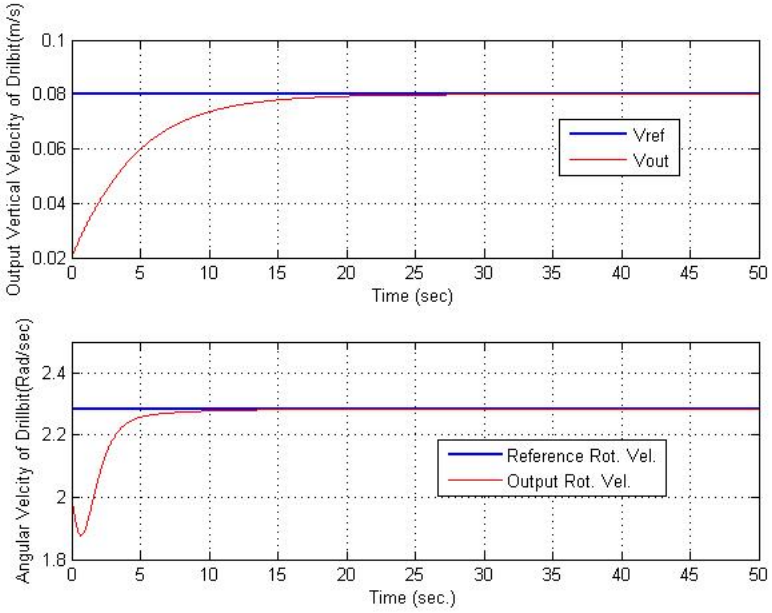

Figure 4.20: Response of output vertical velocity $v(t)$ (top) and output angular velocity $\omega_1(t)$ (bottom) when $v_{ref} = 0.08\,m/s$, gain $K = K_2$ and applied weight $W_0 = 1000$ N

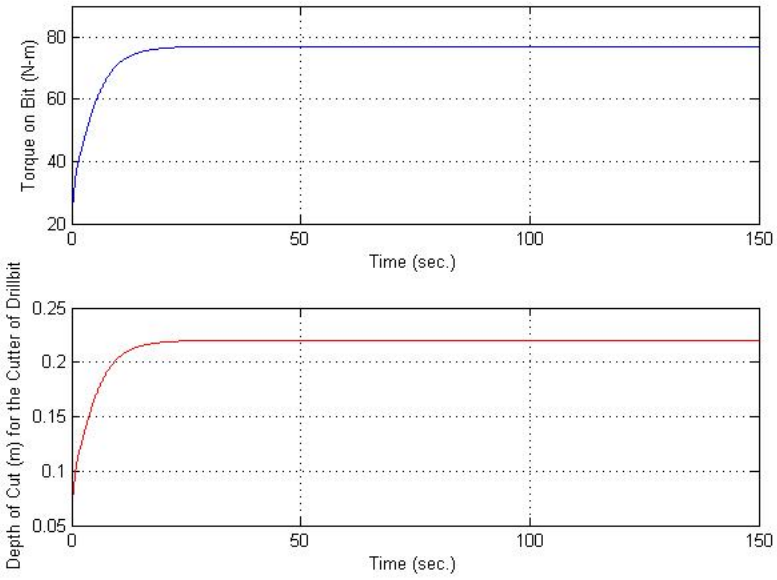

Figure 4.21: Torque on bit $T_b(t)$ (top) and depth of cut $d(t)$ (bottom) when $v_{ref} = 0.08\,m/s$, gain $K = K_2$ and applied weight $W_0 = 1000$ N

Chapter 5

Rock Stiffness Estimation and the Design of Adaptive Controller

In the controller design for drilling system presented in Chapter 4, it was assumed that the "hardness" of the rock, represented by the intrinsic specific energy ϵ, is constant and exactly known. This knowledge of ϵ was used explicitly in the controller design, in particular, in formula (4.6). In practical geological drilling, however, the hardness of different layers of rock lying underneath the surface can be different and usually is not exactly known beforehand. More specifically, different characteristics of the rock, such as hardness, density and porosity, typically remain constant through each layer, but differs from layer to layer. This geological phenomenon of multiple rock layers, also called rock strata, with various hardness and other characteristics, has some significant consequences for drilling. In particular, when the drilling tool encounters the variation in the stiffness of the rock, it may result in change of the penetration rate as well as slip-stick oscillations. In practice, the drilling crew at the rig monitors such changes in the penetration rate. Once the change is detected, the crew, with the support of geologists, who approximately determine the strength of the layer at the contact, either increases or decreases the rotational velocity of the drill bit in order to maintain the desired rate of drilling.

On the other hand, control engineers and scientists frequently deal with the problem

of designing a controller without *a priori* knowledge of the exact values of one or more parameters involved in the process. Often, the processes can be robustly controlled without the actual knowledge of some of the parameters. In other cases, the unknown parameters can be identified using specially designed estimators. In this Chapter, a simple on-line estimator of the rock intrinsic specific energy ϵ is designed, and the resulting estimate is then used in the controller for for drilling system.

The structure of this Chapter is as follows. The design principles of simple on-line parameter estimators are reviewed in Section 5.1. In Section 5.2, an on-line parameter estimator for the intrinsic specific energy ϵ is designed. Simulation results of an adaptive control system, where the actual value of ϵ is substituted by its on-line estimate, are presented in Section 5.3. Finally, some brief conclusions are given in Section 5.4.

5.1 Online Parameter Estimator: Design Principles

If the structure of the plant's model is known, then with the help of model parameters the output of the plant can be obtained. However as it is discussed in the start of the chapter that not always the parameters of the plant are present. Hence the designers of control systems rely upon the outputs and inputs of model to evaluate the unknown parameters. If the missing parameters are constant with time then they could be easily evaluated with time and frequency domain techniques and the process is called off-line parameter estimation. If however the unknown plant parameters are changing with respect to time, then frequent values of inputs and outputs are monitored to constantly update the unknown plant parameter. This process or scheme for observing and updating the unknown parameter for the plant model is called on-line parameter estimation [25].

Consider a plant with a single unknown parameter θ^* which is described by a simple algebraic expression of the form

$$y(t) = \theta^* u(t), \tag{5.1}$$

where the input $u(t)$ and the output $y(t)$ are assumed to be measured [25]. Our goal is to

obtain an estimate $\theta(t)$ which would converge to θ^*. For this purpose, we first generate a predicted value of the output $\hat{y}(t)$, according to the formula

$$\hat{y}(t) = \theta(t)u(t), \tag{5.2}$$

where $\theta(t)$ is the current value of the estimate. The error between the estimated output and actual plant output

$$\epsilon_1(t) := y(t) - \hat{y}(t) = y(t) - \theta(t)u(t) \tag{5.3}$$

is called the estimation error or prediction error [25]. By rearranging the above equation and considering the fact that ϵ_1 is dependent on the parameter estimation error $\tilde{\theta} = \theta - \theta^*$, we get

$$\epsilon_1 = \theta^* u - \theta u = -\tilde{\theta} u \tag{5.4}$$

Now, the differential equation that gives an estimate of θ^* can be obtained by minimizing a given cost functional with respect to $\theta(t)$. In one of the simplest cases, such a functional has a form

$$J(\theta) = \frac{\epsilon_1^2}{2} = \frac{(y - \theta u)^2}{2}. \tag{5.5}$$

Minimization of the above functional with respect to θ can be achieved using the gradient or Newton's method. Application of the gradient method to minimization of the cost functional $J(\theta)$ leads to the following differential equation

$$\dot{\theta} = -\gamma \bigtriangledown J(\theta) = \gamma(y - \theta u)u = \gamma \epsilon_1 u, \qquad \theta(0) = \theta_0, \tag{5.6}$$

where $\gamma > 0$ is the estimator gain. It can be shown [25] that the above parameter adjustment law (5.6) guarantees that $\theta(t) \to \theta^*$ as $t \to +\infty$ if $u(u)$ is *persistently exciting* which is to say that there exist $\alpha_0 > 0$, $T_0 > 0$ such that the inequality

$$\int_t^{t+T_0} u^2(\tau) d\tau \geq \alpha_0 T_0 \tag{5.7}$$

holds for all t. In particular, $u(t)$ is persistently exciting if $u^2(t) \geq \alpha_0$ for all t.

In the next Section, the above described method will be applied to the design of an estimator for the intrinsic specific energy ϵ.

5.2 Online Parameter Estimation for the Intrinsic Specific Energy ϵ

During the cutting process, the torque-on-bit T_b is produced by bit rock interaction, according to the formula

$$T = \frac{1}{2}a^2\epsilon d, \tag{5.8}$$

where a is the radius of drill bit, d is the depth of cut, and $\epsilon > 0$ is the intrinsic specific energy. The intrinsic specific energy $\epsilon > 0$ depends on the properties of the media and typically unknown beforehand. However, since the torque on bit $T_b(t)$ can typically be measured with advanced transducers located in the bottom hole assembly [26], $a > 0$ is constant and known, and $d(t)$ can be calculated according to the formula (3.40), one can use the method described in the previous section to design an on-line estimation scheme for ϵ. Specifically, considering $\frac{1}{2}a^2d(t)$ as the input and torque-on-bit T_b as the measured output, one can follow the procedure described in the previous section to design an estimator for an unknown parameter ϵ. The predicted torque-on-bit $\hat{T}_b$ is defined according to the formula

$$\hat{T}_b(t) := \frac{1}{2}a^2\hat{\epsilon}d(t), \tag{5.9}$$

where $\hat{\epsilon}(t)$ is the current estimate of actual rock strength ϵ. The algorithm for online estimation of the intrinsic specific energy ϵ has a form

$$\dot{\hat{\epsilon}} = \gamma_0(T_b - \hat{T}_b)\frac{1}{2}a^2d, \tag{5.10}$$

where $\gamma_0 > 0$ is an arbitrary gain.

A natural question regarding the algorithm (5.10) is does it guarantee the convergence of the parameter estimate to the true value of the parameter ϵ; mathematically, is $\hat{\epsilon}(t) \to \epsilon$ as $t \to +\infty$. As described in the above Section 5.1, the convergence can be guaranteed if the "input" signal $\frac{1}{2}a^2d(t)$ is persistently exciting. Since $d(t)$ is the depth of cut, we see that, during normal cutting process, $d(t) \geq d_0 > 0$, which results in persistent excitation of the input $\frac{1}{2}a^2d(t)$. The parameter convergence $\hat{\epsilon}(t) \to \epsilon$, therefore, is guaranteed during

normal cutting process. This is also confirmed by the simulation results presented below. It is also worth noting that drilling is a slow process, and the stiffness of the rock strata do not change instantly. Usually while drilling, the operators encounter hundreds of feet of rock bed with same stiffness. Therefore, ϵ can be consider as approximately constant during cutting process, which makes the above described method for parameter estimation applicable in this case.

The obtained estimate of the rock strength $\hat{\epsilon}$ is then used in the control algorithm. Specifically, in the original formulation of the control algorithm, for a given reference vertical velocity v_{ref}, the reference rotational velocity ω_{ref} is calculated according to the formula (4.6), which depends on the parameter ϵ. In case ϵ is unknown, it is substituted by its estimate $\hat{\epsilon}(t)$ obtained above. The new formula for ω_{ref} has the form

$$\omega_{ref} := \frac{2\pi a \zeta \hat{\epsilon}}{\left(\frac{(W_s - H_0)}{v_{ref}}\right) - K_f}. \tag{5.11}$$

The rest of the controller in this case remains unchanged. The obtained estimate of the rock stiffness $\hat{\epsilon}$ will also be used to update the stiffness of the virtual spring in the haptic teleoperator drilling system described below in Chapter 6.

5.3 Simulation Results

In this section, the results of simulations of the drilling control system with intrinsic specific energy estimator are presented. The simulations are carried out using MATLAB, where the simulation program is similar to the one developed for tracking of the reference vertical velocity v_{ref} in the previous Section, with the difference that the algorithm for the intrinsic specific energy estimation (5.10) is added, and the estimate $\hat{\epsilon}$ is used in the calculation of the reference angular velocity according to the formula (5.11).

In these simulations, the performance of the system was evaluated for different values of actual intrinsic specific energy ϵ, different gains γ_0 and different values of applied weight $W_0 := W_s - H_0$. In all the simulations presented below, the initial condition for vertical

velocity is $v(0) = 0.001$ m/s. The integration step for each simulation is equal to 0.005 s. The feedback gain matrix is chosen $K = K_1$, where K_1 is defined by (4.22). All other initial conditions and parameter values are same as those used in Chapter 4.

Figures 5.1 and 5.2 show the response of the vertical penetration velocity $v(t)$, the intrinsic specific energy estimate $\hat{\epsilon}$, the torque-on-bit $T_b(t)$, the predicted value of the torque-on-bit $\hat{T}_b(t)$, and the rotational velocity $\omega_1(t)$ for the case where the applied weight on bit $W_0 = 5000$ N, intrinsic specific energy ϵ or rock stiffness $\epsilon = 20$ MPa, and and the desired vertical velocity v_{ref} is set to 0.005 m/s. The estimator gain for the estimator is set to $\gamma_0 = 5 \cdot 10^9$. The plots shows that $v(t)$ converges to v_{ref} in less than 8 sec whereas the the estimate $\hat{\epsilon}$ converges to the actual value of ϵ in less than 4 sec. Similarly, the convergence of $\hat{T}_b(t)$ to $T_b(t)$, along with the response of $\omega_1(t)$ and $d(t)$ is displayed in Figure 5.2.

Figures 5.3 and 5.4 show the output responses of described parameters where $W_0 = 2500$ N and the desired vertical velocity v_{ref} is set to 0.01 m/s. It can be clearly seen that by reducing the applied weight on drill string W_0, the output value of $v(t)$ and $\hat{\epsilon}$ approaches their reference values in about 12 sec. Reducing W_0 results in that ω_{1ref} increases, the steady-state value of $T_b(t)$ drops to around 200 N, and the steady-state value of $d(t)$ is also dropped to less than 2 mm. On the other hand, Figures 5.5 and 5.8 demonstrate the response of the system with the same parameters except the intrinsic specific energy ϵ is reduced to 5 MPa. This results in decreased convergence time for $v(t)$ and $\hat{\epsilon}(t)$. The steady state value of rotational velocity $\omega_1(t)$ is also decreased to under 10 rad/s, and steady state value of the depth of cut $d(t)$ is increased to 6.5 mm. The steady-state value of $T_b(t)$ remains unchanged.

Figures 5.7 and 5.8 present the output response for the case where the estimator gain is dropped 10 times to $\gamma_0 = 5 \cdot 10^8$. The rest of the parameters are the same as in the last simulation except the intrinsic specific energy is set to $\epsilon = 10$ MPa. The resulting response is predictably characterized by much slower convergence, which takes about 25 sec for $v(t)$ and $\hat{\epsilon}(t)$ to approach their steady-state values.

Figures 5.9, 5.10, 5.11, and 5.12 correspond to two sets of simulations where the applied weight on the drillbit is increased to $W_0 = 5000$ N. In Figures 5.9 and 5.10, the parameters

are $\epsilon = 60$ MPa and $\gamma_0 = 5 \cdot 10^9$. Figures 5.11 and 5.12 correspond to the case where $\epsilon = 20$ MPa and $\gamma_0 = 1 \cdot 10^8$.

Overall, simulation results presented show that the control system with intrinsic specific energy estimation demonstrate good stability and performance characteristics for a wide range of the parameters. In particular, in every case considered, the vertical velocity converges to the desired value, and the estimate of the intrinsic specific energy $\hat{\epsilon}(t)$ converges to an actual value of ϵ.

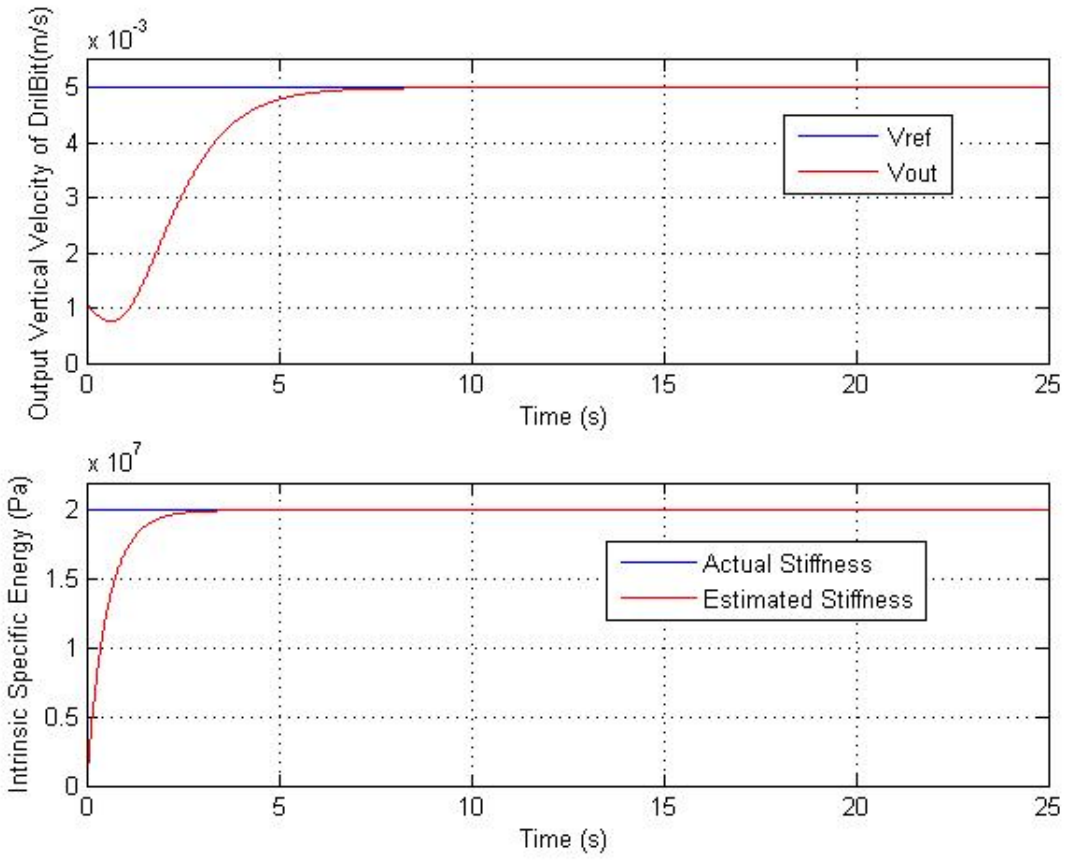

Figure 5.1: Response of the vertical velocity $v(t)$ (top) and the intrinsic specific energy estimate $\hat{\epsilon}(t)$ (bottom) for $W_0 = 5000$ N, $\epsilon = 20$ MPa, and $\gamma_0 = 5 \cdot 10^9$.

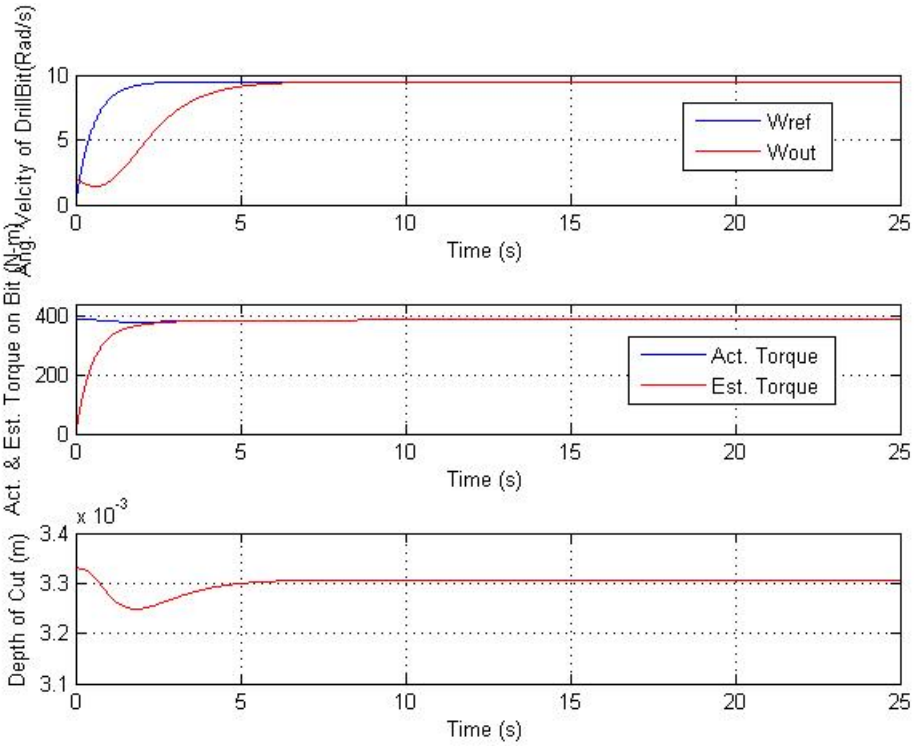

Figure 5.2: Response of rotational velocity $\omega_1(t)$ (top), torque-on-bit $T_b(t)$ vs. estimated torque-on-bit $\hat{T}_b(t)$ (middle), and the depth of cut $d(t)$ (bottom) for $W_0 = 5000$ N, $\epsilon = 20$ MPa, and $\gamma_0 = 5 \cdot 10^9$.

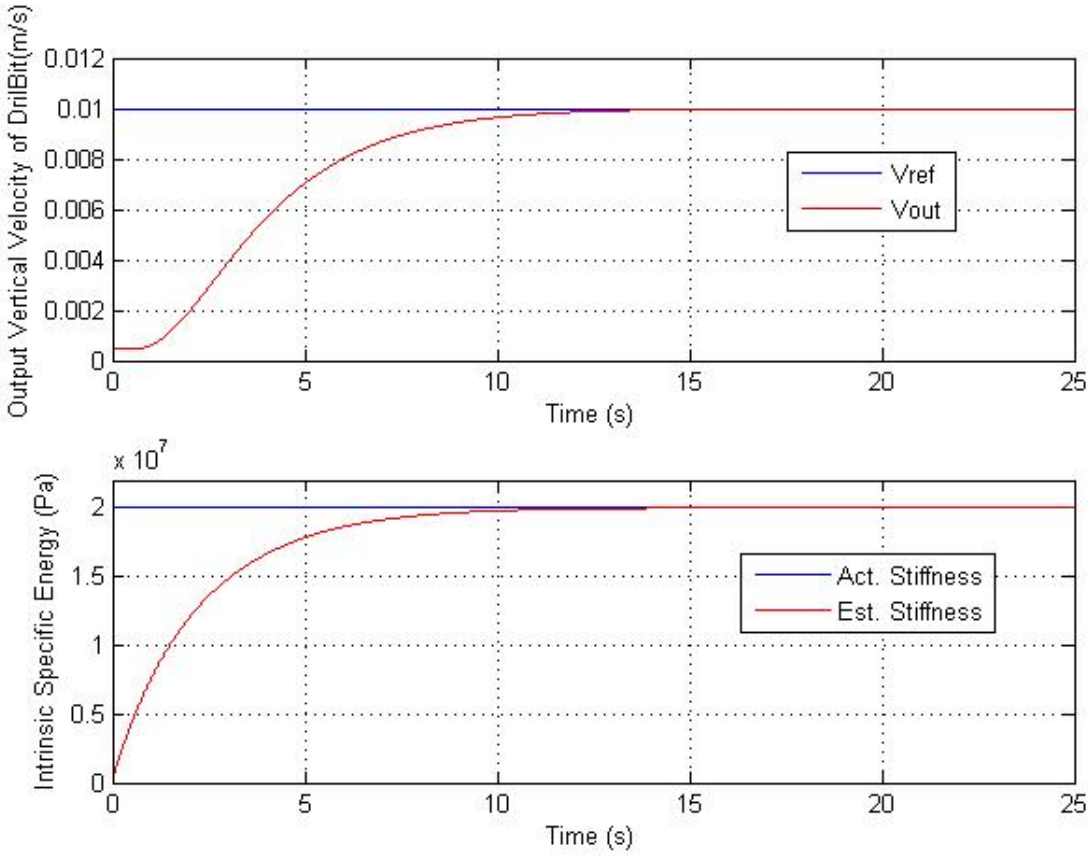

Figure 5.3: Response of the vertical velocity $v(t)$ (top) and the intrinsic specific energy estimate $\hat{\epsilon}(t)$ (bottom) for $W_0 = 2500$ N, $\epsilon = 20$ MPa, and $\gamma_0 = 5 \cdot 10^9$.

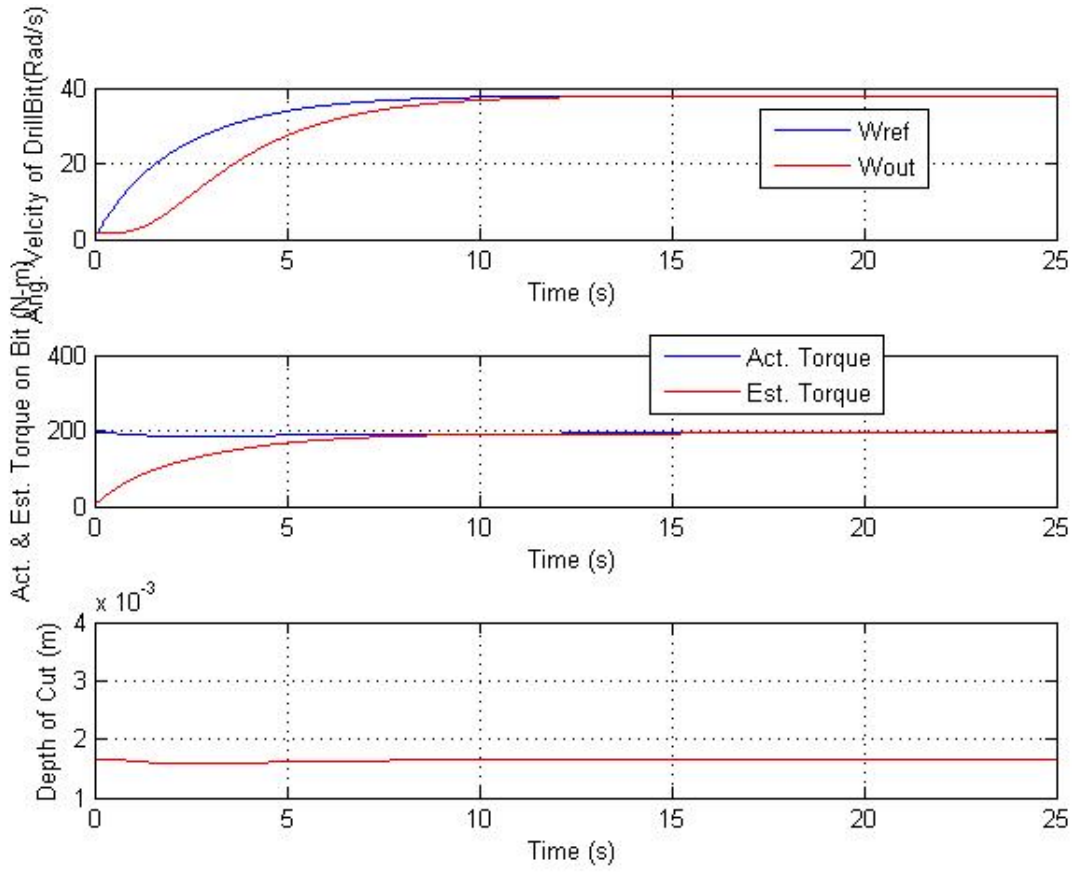

Figure 5.4: Response of rotational velocity $\omega_1(t)$ (top), torque-on-bit $T_b(t)$ vs. estimated torque-on-bit $\hat{T}_b(t)$ (middle), and the depth of cut $d(t)$ (bottom) for $W_0 = 2500$ N, $\epsilon = 20$ MPa, and $\gamma_0 = 5 \cdot 10^9$

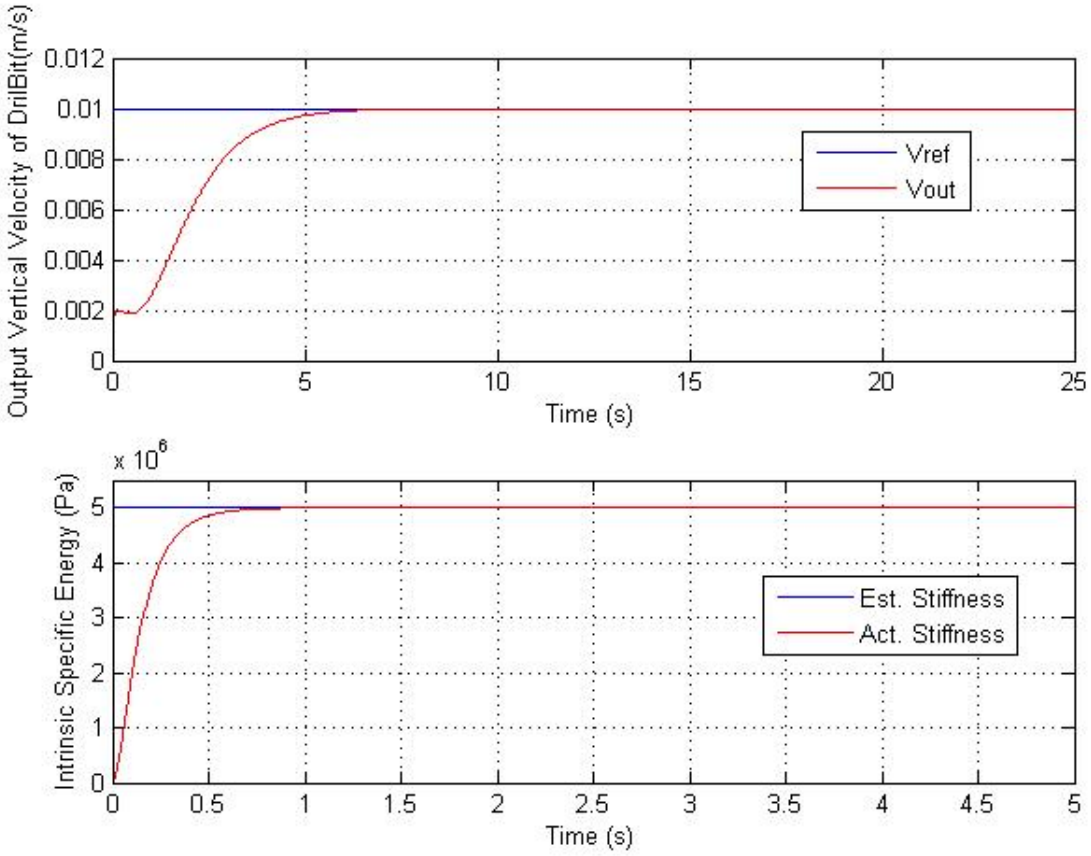

Figure 5.5: Response of the vertical velocity $v(t)$ (top) and the intrinsic specific energy estimate $\hat{\epsilon}(t)$ (bottom) for $W_0 = 2500$ N, $\epsilon = 5$ MPa, and $\gamma_0 = 5 \cdot 10^9$.

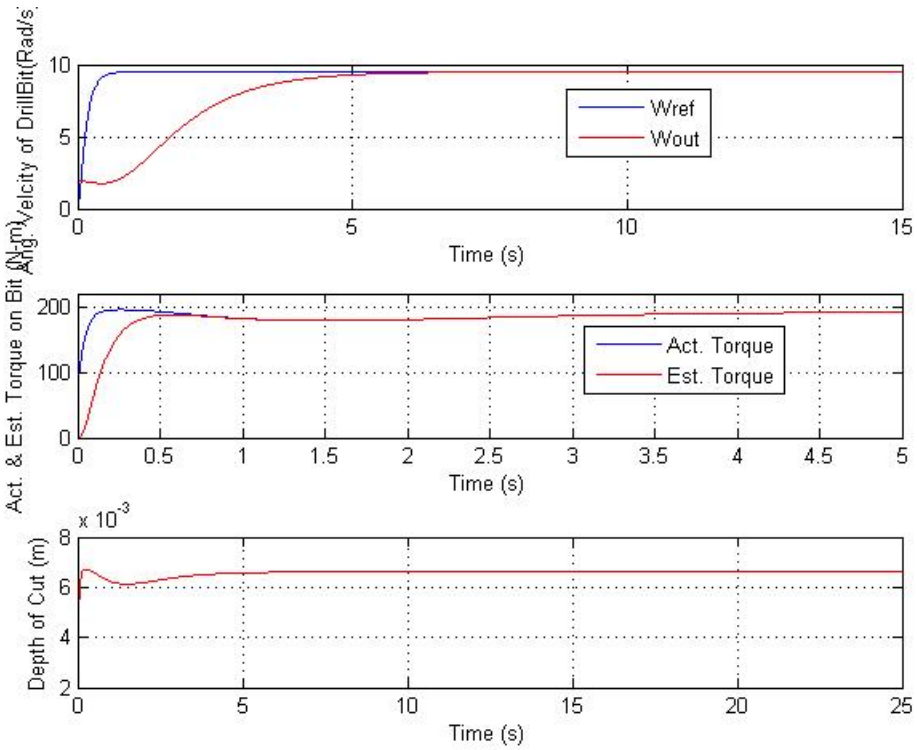

Figure 5.6: Response of rotational velocity $\omega_1(t)$ (top), torque-on-bit $T_b(t)$ vs. estimated torque-on-bit $\hat{T}_b(t)$ (middle), and the depth of cut $d(t)$ (bottom) for $W_0 = 2500$ N, $\epsilon = 5$ MPa, and $\gamma_0 = 5 \cdot 10^9$

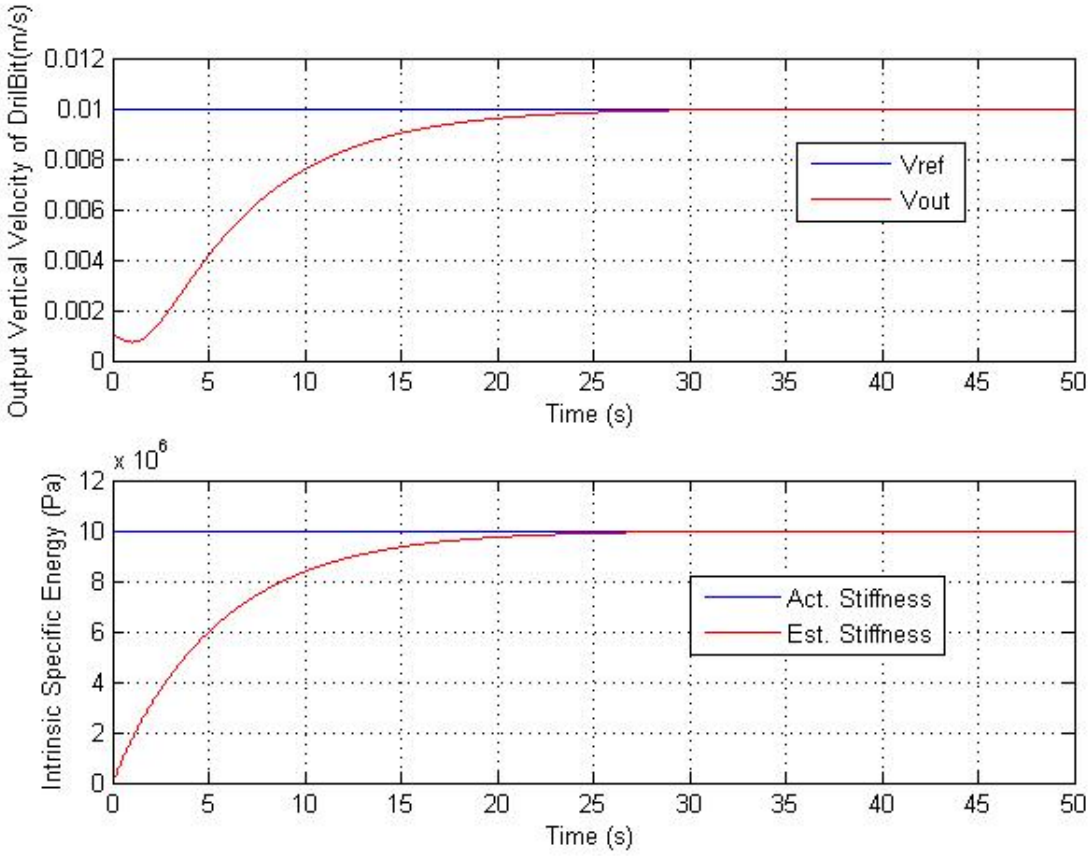

Figure 5.7: Response of the vertical velocity $v(t)$ (top) and the intrinsic specific energy estimate $\hat{\epsilon}(t)$ (bottom) for $W_0 = 2500$ N, $\epsilon = 10$ MPa, and $\gamma_0 = 5 \cdot 10^8$.

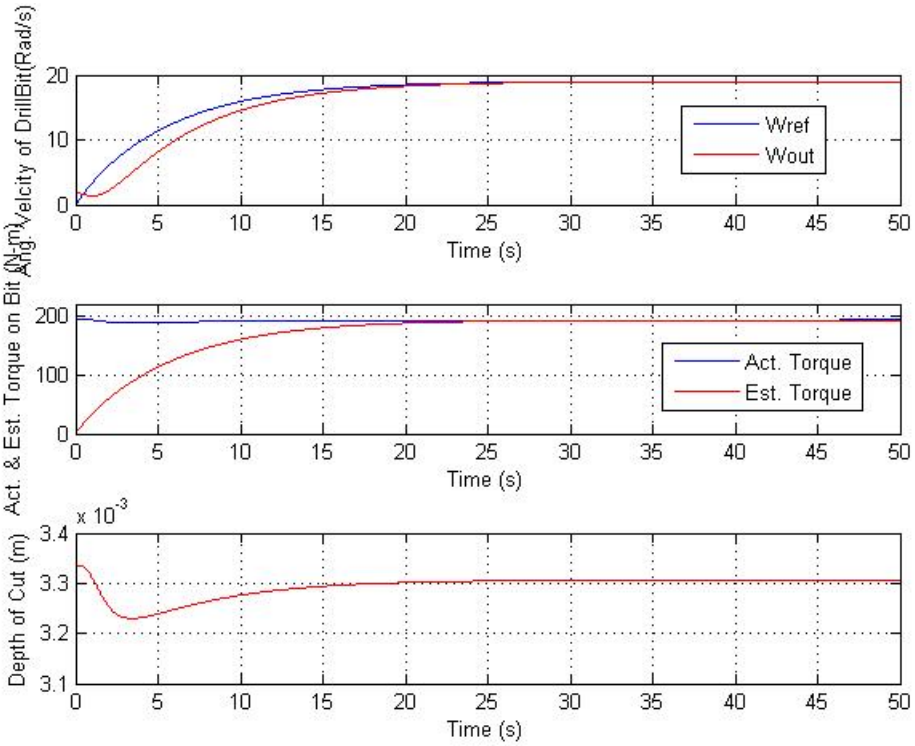

Figure 5.8: Response of rotational velocity $\omega_1(t)$ (top), torque-on-bit $T_b(t)$ vs. estimated torque-on-bit $\hat{T}_b(t)$ (middle), and the depth of cut $d(t)$ (bottom) for $W_0 = 2500$ N,, $\epsilon = 10$ MPa, and $\gamma_0 = 5 \cdot 10^8$

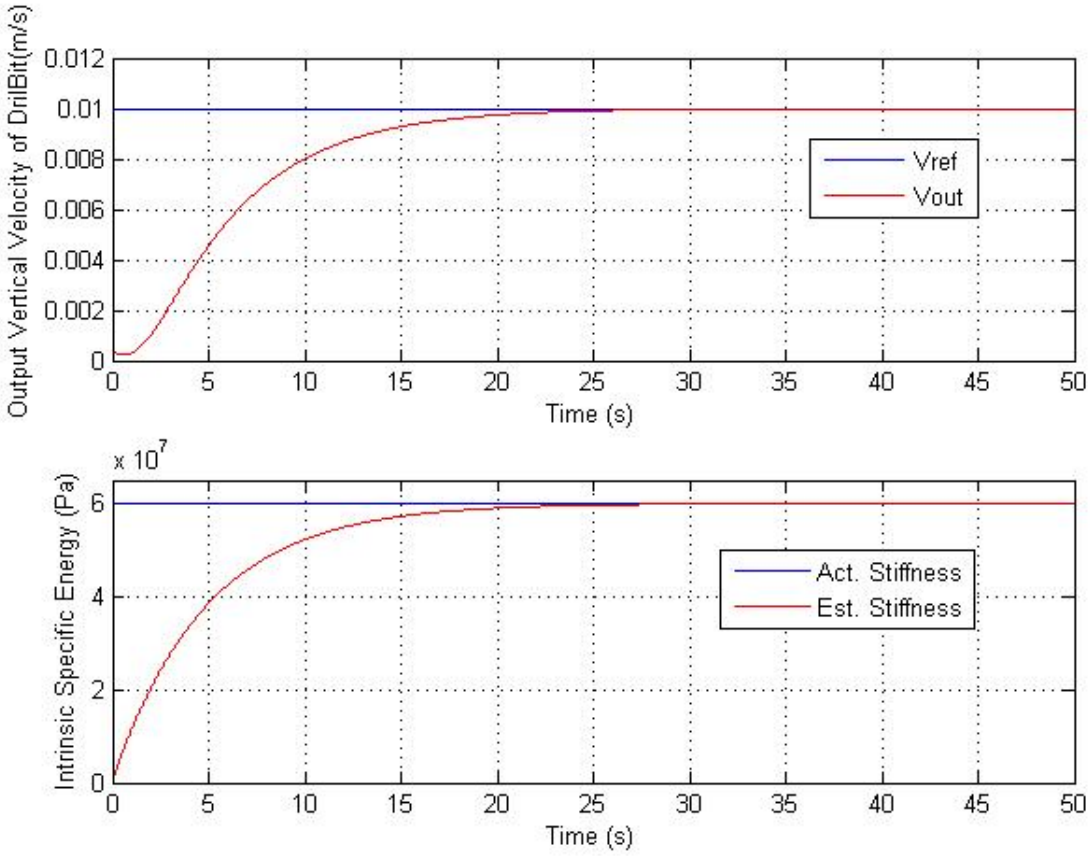

Figure 5.9: Response of the vertical velocity $v(t)$ (top) and the intrinsic specific energy estimate $\hat{\epsilon}(t)$ (bottom) for $W_0 = 2500$ N, $\epsilon = 60$ MPa, and $\gamma_0 = 5 \cdot 10^9$

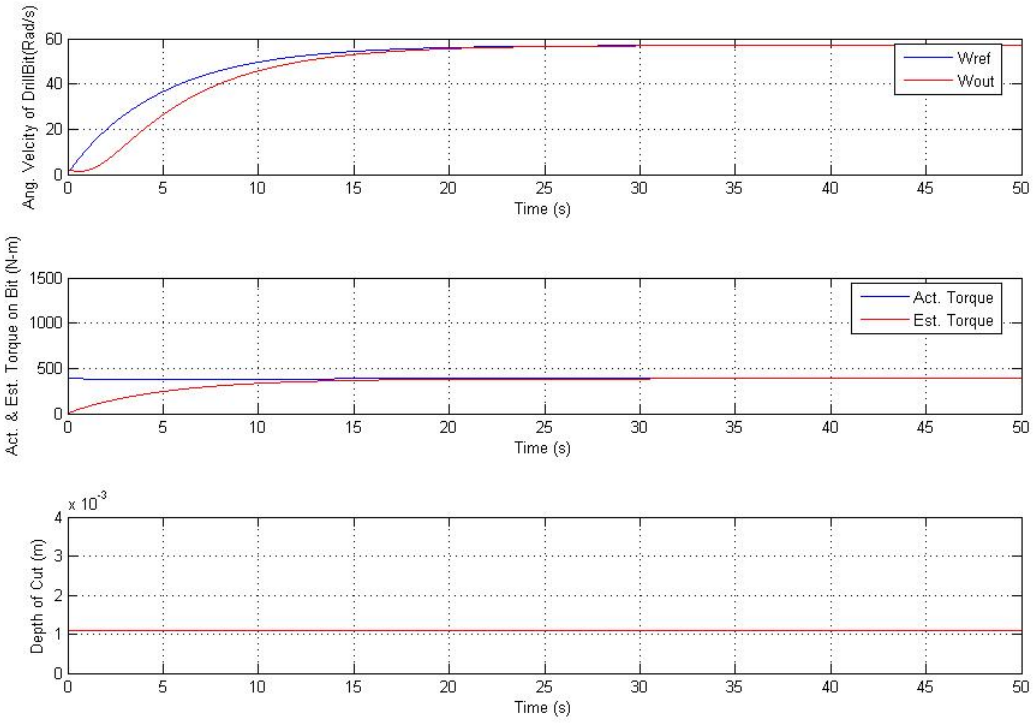

Figure 5.10: Response of rotational velocity $\omega_1(t)$ (top), torque-on-bit $T_b(t)$ vs. estimated torque-on-bit $\hat{T}_b(t)$ (middle), and the depth of cut $d(t)$ (bottom) for $W_0 = 2500$ N, $\epsilon = 60$ MPa, and $\gamma_0 = 5 \cdot 10^9$

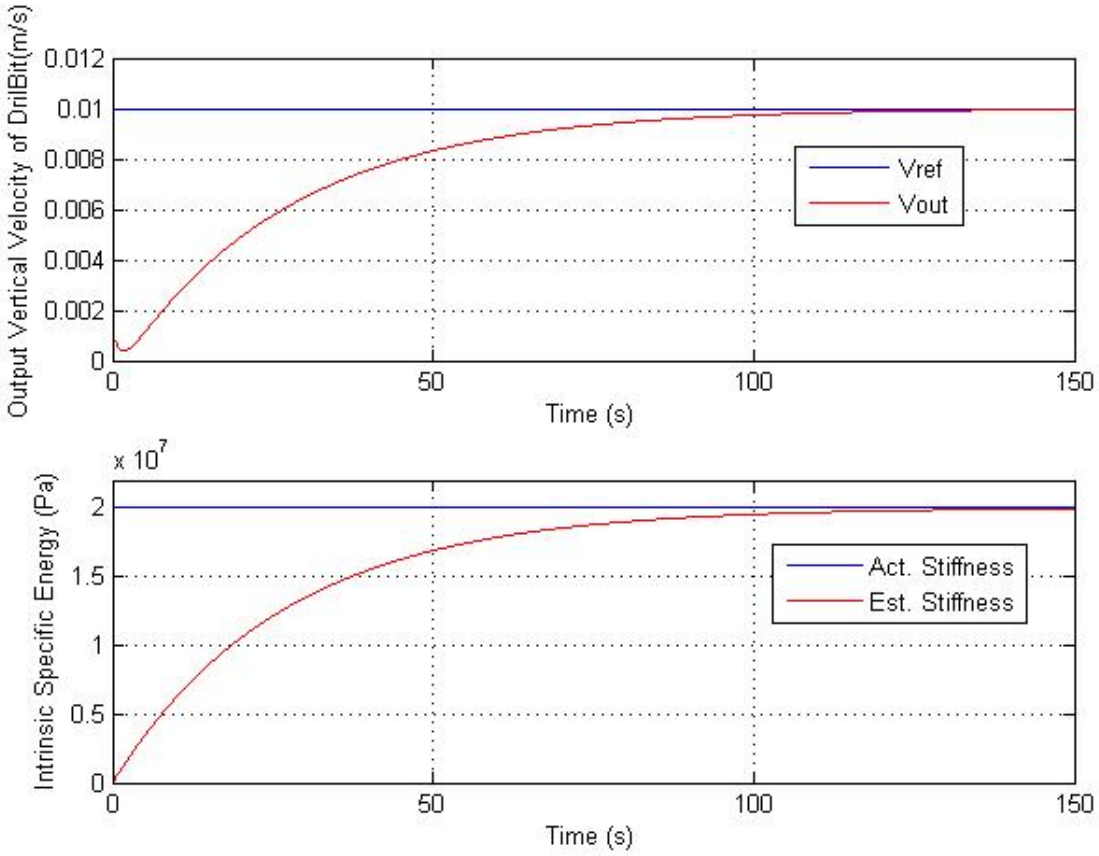

Figure 5.11: Response of the vertical velocity $v(t)$ (top) and the intrinsic specific energy estimate $\hat{\epsilon}(t)$ (bottom) for $W_0 = 2500$ N, $\epsilon = 20$ MPa, and $\gamma_0 = 10^8$

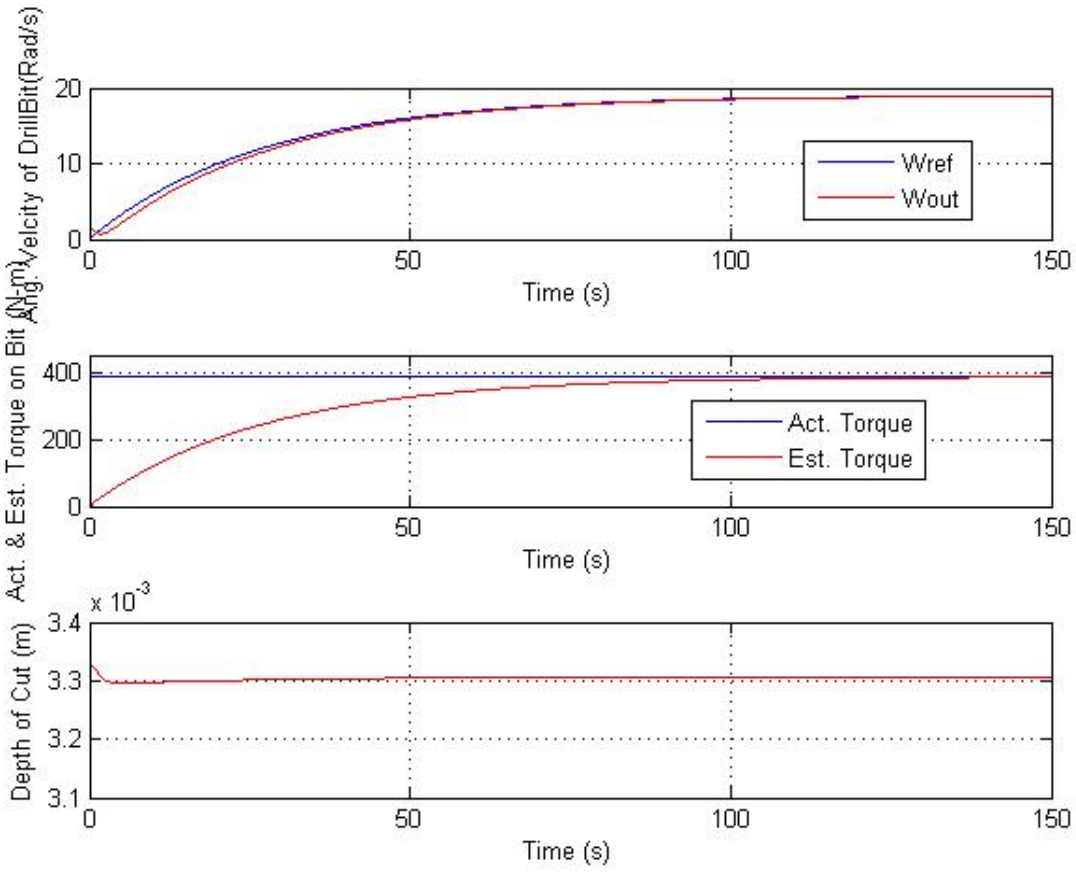

Figure 5.12: Response of rotational velocity $\omega_1(t)$ (top), torque-on-bit $T_b(t)$ vs. estimated torque-on-bit $\hat{T}_b(t)$ (middle), and the depth of cut $d(t)$ (bottom) for $W_0 = 2500$ N, $\epsilon = 20$ MPa, and $\gamma_0 = 10^8$

5.4 Conclusions

In this Chapter, a simple on-line algorithm for estimation of the intrinsic specific energy ϵ is designed. The estimate $\hat{\epsilon}(t)$ of ϵ is then substituted into the control algorithm designed in the previous Chapter, and the resulting adaptive control system is evaluated through simulations. The estimate $\hat{\epsilon}(t)$ will be used below to update the stiffness of the virtual environment, thus providing the human operator with haptic feedback that reflects the stiffness of the rock cut.

Chapter 6

Telerobotic Drilling System with Haptic Feedback

The goal of this Chapter is to design and experimentally test a telerobotic drilling system with haptic feedback. This Chapter is organized as follows. Definitions of haptics and a haptic device are given in Section 6.1. The general structure of the telerobotic drilling system with haptic feedback is presented in Section 6.2. In Section 6.3, the experimental setup is described, while the experimental results are presented in Section 6.4. Conclusions are given in Section 6.5.

6.1 Haptics and Haptic Devices

Haptics can be defined as the physical or virtual interaction through touch sensation for the purpose of perception and manipulation of objects [27]. The interactions can be between human hand and real object; or robot end-effector and real object; and either human hand or robot end-effector with virtual object [27]. In particular, haptics is used to create virtual interactions with virtual reality environments, where they can simulate real or imaginary scenes with which an operator can interact and perceive the effects of their actions in real time [28, 27]. Consequently, haptics provides kinaesthetic clues of the physical features

of virtual or real remote environment.

A haptic device is a system that generates an output which could be perceived haptically [29]. A haptic device, which is also referred as a haptic interface, typically exhibits the properties of a small robot that exchanges mechanical energy with a user [27]. In this Thesis, the experiments are conducted using PHANTOM Omni haptic device, a product from SensAble Technologies Inc., which is shown in Figure 6.1. The PHANTOM Omni is equipped with pen-like handle for positioning in three dimensional space. The device has 6 degrees-of-freedom position sensing and provides 3 degrees-of-freedom force feedback.

Figure 6.1: The PHANTOM Omni haptic device (from http://www.sensable.com/)

6.2 Structure of the Telerobotic Drilling System with Haptic Feedback

The structure of a telerobotic drilling system with haptic feedback is shown in Figure 6.2. In this system, the human operator controls the drilling process using a haptic device. Specifically, the position of an end-effector of the haptic device defines the reference vertical velocity of the drilling. The reference vertical velocity is then transmitted to the drilling control system, designed in Chapters 4 and 5, which stabilizes the actual vertical penetration velocity to the level equal to the reference vertical velocity. On the other hand, an

estimate of the intrinsic specific energy $\epsilon(t)$, which is generated on-line by an estimator described in Chapter 5, is sent back to the haptic device. The end-effector of the haptic device interacts with a virtual spring of variable stiffness; the stiffness of this virtual spring is updated in real time proportionally to the current estimate of the intrinsic specific energy $\epsilon(t)$. Thus, the telerobotic drilling system provides haptic feedback to the human operator which creates an intuitive feeling of the hardness of the remotely drilled material.

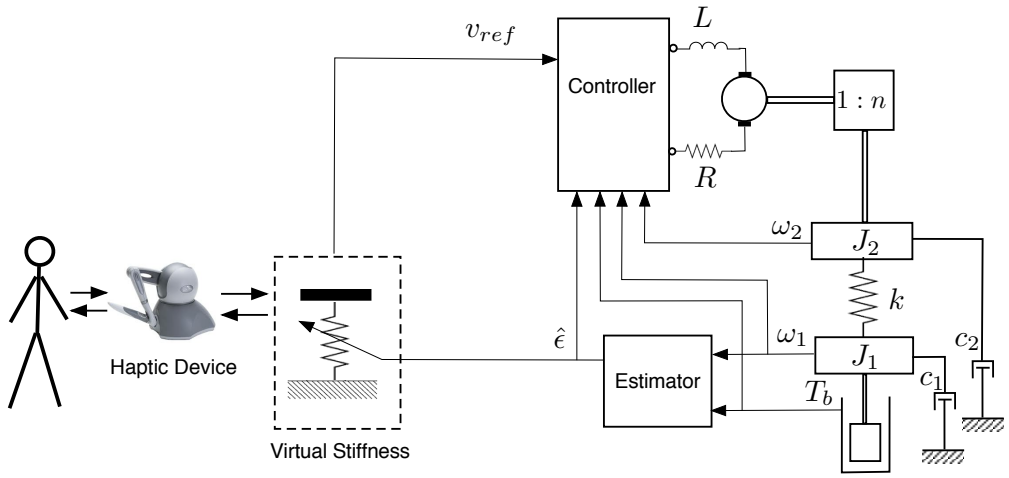

Figure 6.2: The structure of a telerobotic drilling system

6.3 Experimental Setup

In this Section, the implementation of a complete algorithm for telerobotic drilling with haptic feedback is described. The algorithm is implemented using the PHANTOM Omni Haptic device. The PHANTOM Omni Haptic device is designed for kinematic interaction with the virtual or real environment while providing the kinesthetic feedback to the operator. In this project, the drilling process is simulated in real time using Microsoft Visual C++. Hence, a virtual environment is designed that, in particular, simulates the bit-rock interaction as the drill bit penetrates through the rock. PHANTOM Omni Haptic device is used here to generate a desired rate of vertical penetration for the drilling system and also

to reflect back the haptic information that exhibits the intrinsic specific energy or stiffness of the rock that is drilled.

The experimental setup consists of PC based on Intel Pentium 4 processor with operational frequency of 1GHz and RAM of 1GB, and a PHANTOM Omni Haptic device manufactured by Sensable Technologies Inc. The PHANTOM Omni Haptic device is connected with the PC through Firewire port. The device has six degrees of freedom and is equipped with a pen-based stylus. The workspace of PHANTOM Omni Haptic device has dimensions of $160\,mm \times 120\,mm \times 70\,mm$ in x, y, and z directions respectively. In order to interact with the real-time software simulations, the PHANTOM device uses the OpenHaptics Toolkit, which is implemented using Microsoft Visual C++. The human operator uses the haptic device to i) generate a desired vertical velocity $v_{ref}(t)$ which is used as an input to the drilling control system, and ii) to haptically perceive the stiffness ϵ of the rock layers. The control objective is to maintain the desired velocity of the vertical penetration regardless of the stiffness of the rock.

Since the conventional oil well drilling is conducted in the vertical (normal to the ground) direction, it is natural for the human operator to assign the desired velocity $v_{ref}(t)$ by controlling the position of the end-effector of the PHANTOM device along its y-axis. More specifically, a specific distal range along y-axis is assigned to each desired vertical velocity. The number of levels designated to y-axis for stylus is determined by the number of different reference vertical velocities that are adopted in the program. In our experiments, the boundaries of these levels are chosen as follows,

$$y_s := [0, \quad 80, \quad 0];$$

$$y_1 := [0, \quad 60, \quad 0];$$

$$y_2 := [0, \quad 40, \quad 0];$$

$$y_3 := [0, \quad 25, \quad 0];$$

$$y_4 := [0, \quad 10, \quad 0];$$

$$y_e := [0, \quad 1, \quad 0].$$

Once the boundary positions for each distal range on $y - axiz$ of stylus are determined, the corresponding desired vertical velocities $v_{ref}(t)$ for each level are defined below:

$v_{ref}(t)$ = 0.001 m/s when the position of stylus $y_n(t)$ is $\geq y_s$.

$v_{ref}(t)$ = 0.003 m/s when the position of stylus $y_n(t)$ is $\leq y_s$ and $\geq y_1$.

$v_{ref}(t)$ = 0.005 m/s when the position of stylus $y_n(t)$ is $\leq y_1$ and $\geq y_2$.

$v_{ref}(t)$ = 0.008 m/s when the position of stylus $y_n(t)$ is $\leq y_2$ and $\geq y_3$.

$v_{ref}(t)$ = 0.01 m/s when the position of stylus $y_n(t)$ is $\leq y_3$ and $\geq y_4$.

$v_{ref}(t)$ = 0.015 m/s when the position of stylus $y_n(t)$ is $\leq y_4$ and $\geq y_e$.

$v_{ref}(t)$ = 0.018 m/s when the position of stylus $y_n(t)$ is $\leq y_e$.

As it can be seen from the above chart, the first level is activated once the device is initialized and the program starts to run. Therefore, in our experiments, the minimum desired vertical velocity is equal to 0.001 m/s. This velocity is enforced until the stylus is moved down to the next level (distal range) on the y-axis. The desired reference velocity increases or decreases as the stylus is vertically pulled up and down, crossing from one distal range to another.

Another important function of the haptic device is to allow the human operator to feel the stiffness of the rocks. As explained above, this is achieved by updating the stiffness of the virtual spring proportionally to the current estimate of the rock stiffness (intrinsic specific energy $\hat{\epsilon}(t)$). Since it is not possible to project and feel directly the large range of magnitudes of the intrinsic specific energy, the value of the intrinsic specific energy is

scaled down before updating the stiffness of the virtual spring. Specifically, the coefficient of proportionality between the estimate of the intrinsic specific energy (with units of Pascals) and the stiffness of the virtual spring (with units of is N/m) is set in our experiments equal to 10^{-7}. The feedback force $F_{est}(t)$ due to the virtual spring is therefore calculated according to the formula

$$F_{est}(t) = 10^{-7} \cdot \hat{\epsilon}(t) \cdot y_n(t), \tag{6.1}$$

where $y_n(t)$ is the vertical position of the stylus, and $\hat{\epsilon}(t)$ is the current estimate of the intrinsic specific energy.

6.4 Experimental Results

In this Section, the experimental results are presented. The experiments are performed in order to confirm the applicability of the system designed, as well as to evaluate the performance of the robust servo controller, the online parameter estimator, and the force feedback displayed by the haptic device. Five different experiments have been conducted where the drill bit velocity is been controlled through the haptic device. In all experiments presented here, the applied weight $W_0 = 5000$ N, and the rest of the parameters are same as those used in Chapter 5.

In our experiments, we have attempted to simulate a real drilling case scenario. The composition, characteristics, and types (which all contribute to the intrinsic specific energy or stiffness (strength)) of various rock strata vary at different geographical locations. Similarly, these characteristics vary at different depths during drilling. In our experiments, we have have used multiple values for $\epsilon(t)$ ranging from 4 MPa to 60 MPa. The runtime for each experiment is about 100 sec.

Six graphs are plotted for each experiment. The first graph shows the values of the intrinsic specific energy $\epsilon(t)$ and its estimate $\hat{\epsilon}(t)$. The changes in the magnitude of the intrinsic specific energy occur during the course of program when the drill bit crosses certain depth levels. The plot of the force $F_{est}(t)$ felt by the human operator is shown in second

graph. Third plot shows the vertical penetration velocity $v_{out}(t)$ together with its reference $v_{ref}(t)$. Fourth graph shows the output rotational velocity $\omega_1(t)$ and the reference rotational velocity $\omega_{1d}(t)$ of the drill bit. The torque-on-bit $T_b(t)$ and its estimated (predicted) value $\hat{T}_b(t)$ are shown in the fifth plot. Finally, sixth plot shows the depth of cut $d_{cut}(t)$ response.

In every experiment, three layers of rocks with different intrinsic specific energy ϵ are simulated. In the first experiment, the top layer has the stiffness of 5 MPa and its thickness is 20 cm from the surface. The second layer has a stiffness value of 12 MPa and lies between 20 cm and 30 cm from the surface (total thickness is 10 cm). The third layer starts at the depth of 30 cm and continues downward. It has a stiffness value of 20 MPa. The experiment is performed with the estimator gain $\gamma_0 = 10^9$. Figure 6.3 shows the actual and the estimated intrinsic specific energies (rock stiffness) $\epsilon(t)$ and its estimate $\hat{\epsilon}(t)$ on the top graph, and the reflected force $F_{est}(t)$ on the bottom graph. Due to high gain value for estimator, $\hat{\epsilon}(t)$ quickly tracks $\epsilon(t)$ for all three layers as the drill bit progressed cutting through these layers. Figure 6.4 shows the vertical velocity $v_{out}(t)$ and the reference vertical velocity $v_{ref}(t)$ on the top graph, and the reference rotational velocity $\omega_{1d}(t)$ and the actual drill bit rotational velocity $\omega_1(t)$ at the bottom graph. Lastly, Figure 6.5 shows the behaviour of the actual torque-on-bit $T_b(t)$ and the estimated torque $\hat{T}_b(t)$, along with depth of cut $d_{cut}(t)$. These plots shows that the system is stable and demonstrates good performance; in particular, all the output variables track their desired (reference) trajectories.

The results of the second experiment are displayed by Figures 6.6, 6.7, and 6.8. In this experiment, the boundaries of rock layers are kept same as in the first experiment but the values of the intrinsic specific energy for these rock layers have been modified. Starting from the ground, the first layer has the stiffness $\epsilon = 12$ MPa. The second layer has high stiffness value equal to 20 MPa, however, the stiffness of the third layer is decreased to 5 MPa. This increment and decrement in stiffness of the corresponding rock layers is been tracked by the estimated stiffness $\hat{\epsilon}(t)$; the corresponding plot are shown in Figure 6.6 along with the reflected force $F_{est}(t)$. Figure 6.7 shows the graph of output velocity $v_{out}(t)$ that tracks reference vertical velocity $v_{ref}(t)$, along with the rotational velocities $\omega_{1d}(t)$ and

$\omega_1(t)$. Figure 6.8 shows the response of the actual and the estimated torques-on-bit, as all as the depth of cut $d_{cut}(t)$. All figures demonstrates stability and good performance of the drilling control system; in particular, zero steady state errors are achieved for all tracking variables.

In the third experiment, the estimator gain is increased to $\gamma_0 = 5 \cdot 10^9$. To monitor and validate the performance of the on-line stiffness parameter estimator and the robust servo controller when $v_{ref}(t)$ is varied using haptic device, the depth of the rock layers and their corresponding stiffness values have been altered in this experiment. For the first rock layer, ϵ is set to 20 MPa. It is increased to 40 MPa for the second layer, which now lies between 20 cm and 40 cm from the surface. Finally, for the third layer, ϵ is increased to 60 MPa. Figure 6.9 shows the graphs of $\epsilon(t)$, $\hat{\epsilon}(t)$ and $F_{est}(t)$. Figure 6.10 shows the response of $v_{ref}(t)$ and $v_{out}(t)$ on the top graph, and the responses of $\omega_{1d}(t)$ and $\omega_1(t)$ on the bottom graph, respectively. The response of $\hat{T}_b(t)$ and $T_b(t)$ along with $d_{cut}(t)$ are shown in Figure 6.11.

In the fourth experiment, the estimator gain γ_0 is significantly reduced to $5 \cdot 10^8$. For simplicity, the depths of the three rock layers are kept similar to the ones defined in the third experiment, however, the stiffness values for these layers have been altered. The first layer now has stiffness equal to 4 MPa, it increases to 10 MPa for the second layer, and is further elevated to 18 MPa for the third layer. It can be seen from Figure 6.12 that, because of the lower estimator gain γ_0, the convergence of the estimated stiffness $\hat{\epsilon}(t)$ to its actual value $\epsilon(t)$ becomes slower. The corresponding response of $F_{est}(t)$ is also displayed in this figure. Figure 6.13 shows the response of $v_{ref}(t)$ and $v_{out}(t)$ on the top graph, and $\omega_{1d}(t)$ and $\omega_1(t)$ on the bottom graph, respectively. Similarly, the response of $\hat{T}_b(t)$ and $T_b(t)$ along with $d_{cut}(t)$ are portrayed in Figure 6.14.

Finally, Figures 6.15, 6.16, and 6.17 demonstrate the output plots for experiment number five. Here, the estimator gain γ_0 is set equal to $8 \cdot 10^8$. The stiffness of the top rock layer ϵ is 4 MPa for distance equal to 30 cm from the surface. Then it is raised to 20 MPa for the second layer which is located between 30 cm and 50 cm from the surface. Finally,

for the third rock layer, ϵ is decreased to 8 MPa. when the drill bit crosses 50 cm beneath the surface. All the responses are shown in Figures 6.15, 6.16, and 6.17.

Overall, the above described experiments demonstrate stability and good performance of the designed telerobotic drilling system with haptic feedback, for a range of parameters and control gains. The description of the experimental results can be concluded with a few observations. First, the response of the on-line stiffness estimator depends strongly upon the gain γ_0. It is observed that higher γ_0 corresponds to faster estimator response resulting in better tracking of $v_{ref}(t)$ by $v_{out}(t)$. Second, the torque-on-bit $T_b(t)$ is maintained at the value of about 400 N·m. This could be because of the type and the design characteristics of the drill bit. Third, the depth of cut $d_{cut}(t)$ typically depends upon the rock stiffness ϵ. The higher the rock stiffness, the lower is the magnitude of $d_{cut}(t)$.

6.5 Conclusions

In this Chapter, the structure of telerobotic drilling system with haptic feedback is described. Next, the experimental setup for this research is discussed in detail. Experimental results are presented in form of graphs, and relevant description is provided along with some conclusions.

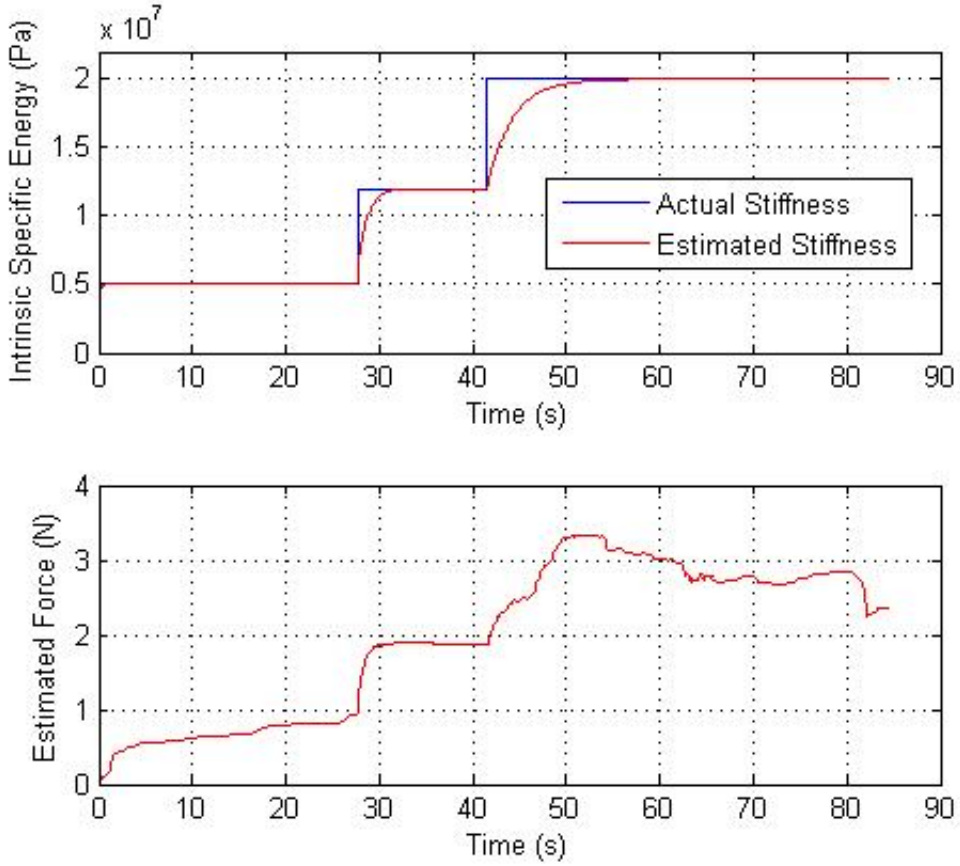

Figure 6.3: Experiment 1: Actual stiffness $\epsilon(t)$ vs. the estimated stiffness $\hat{\epsilon}(t)$ (top); the reflected force $F_{est}(t)$ (bottom)

.

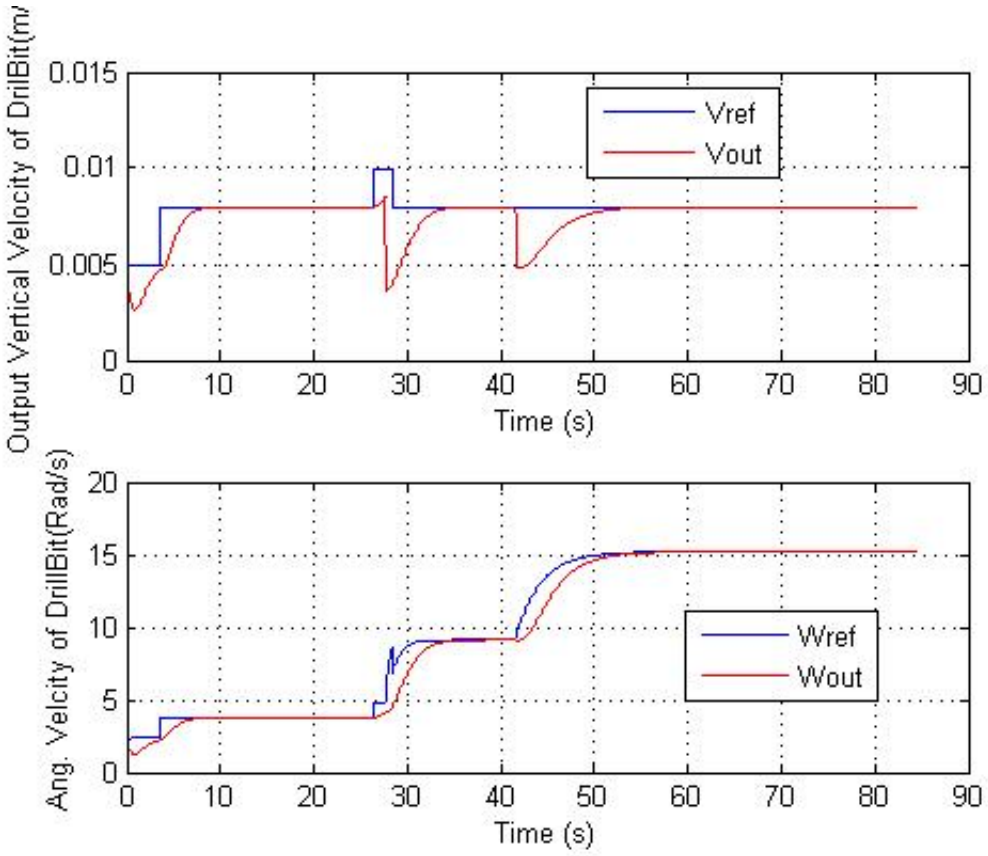

Figure 6.4: Experiment 1: Output vertical velocity $v_{out}(t)$ vs. reference vertical velocity $v_{ref}(t)$ (top); output rotational velocity of the drill bit $\omega_1(t)$ vs. reference rotational velocity $\omega_{1d}(t)$ (bottom)

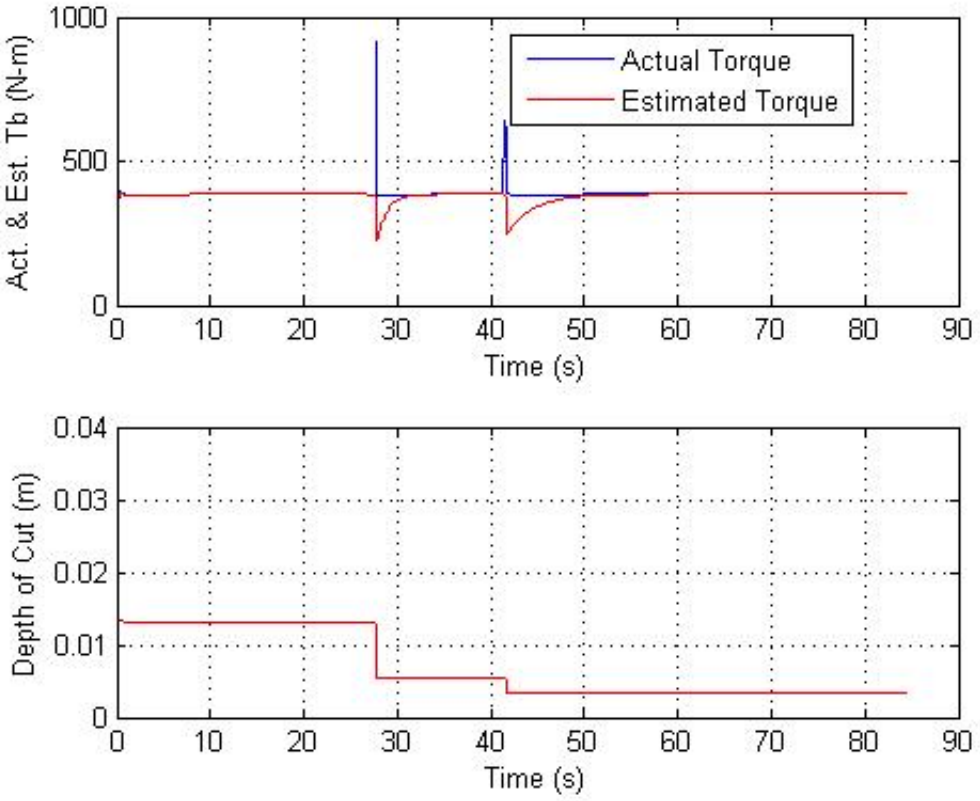

Figure 6.5: Experiment 1: Torque-on-bit $T_b(t)$ vs. estimated torque-on-bit $\hat{T}_b(t)$ (top graph); depth of cut $d_{cut}(t)$ (bottom graph)

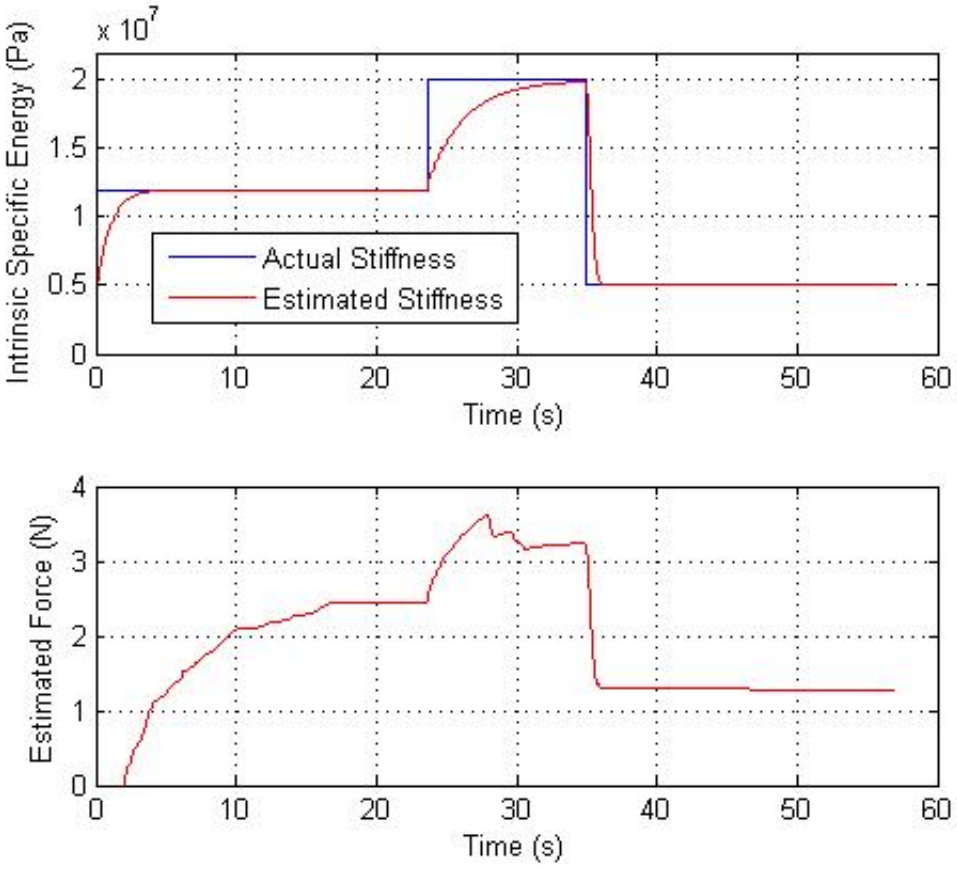

Figure 6.6: Experiment 2: Actual stiffness $\epsilon(t)$ vs. estimated stiffness $\hat{\epsilon}(t)$ (top); reflected force $F_{est}(t)$ (bottom)

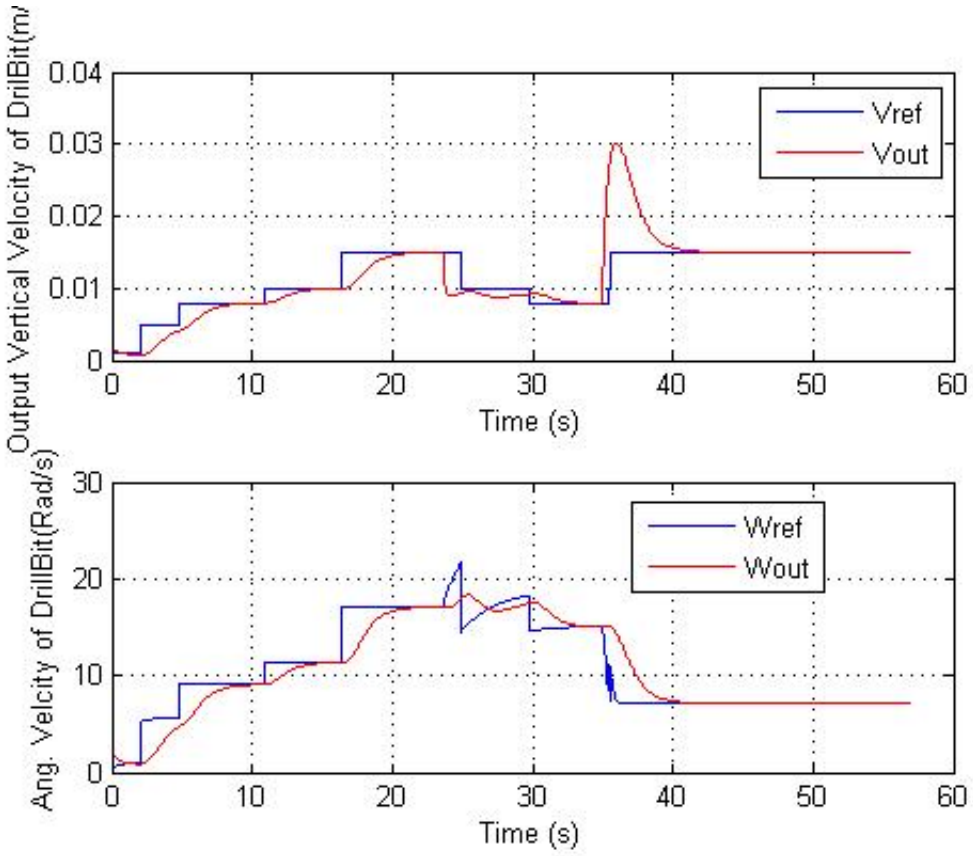

Figure 6.7: Experiment 2: Output vertical velocity $v_{out}(t)$ vs. reference vertical velocity $v_{ref}(t)$ (top); output rotational velocity of the drill bit $\omega_1(t)$ vs. reference rotational velocity $\omega_{1d}(t)$ (bottom)

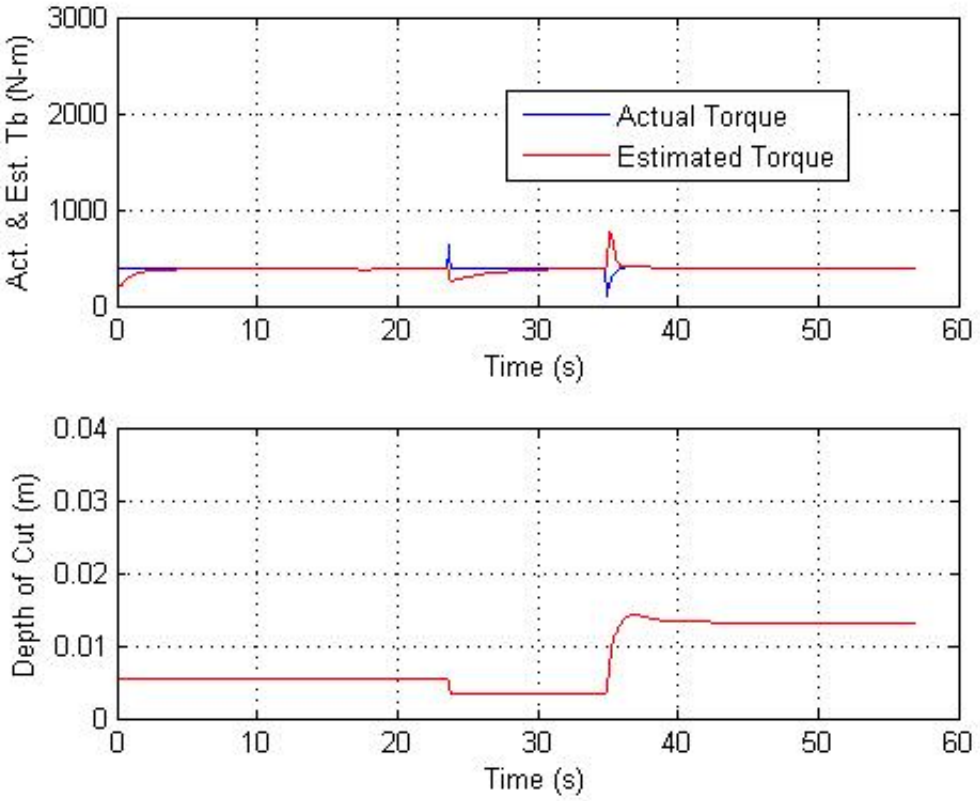

Figure 6.8: Experiment 2: Torque-on-bit $T_b(t)$ vs. estimated torque-on-bit $\hat{T}_b(t)$ (top); depth of cut $d_{cut}(t)$ (bottom)

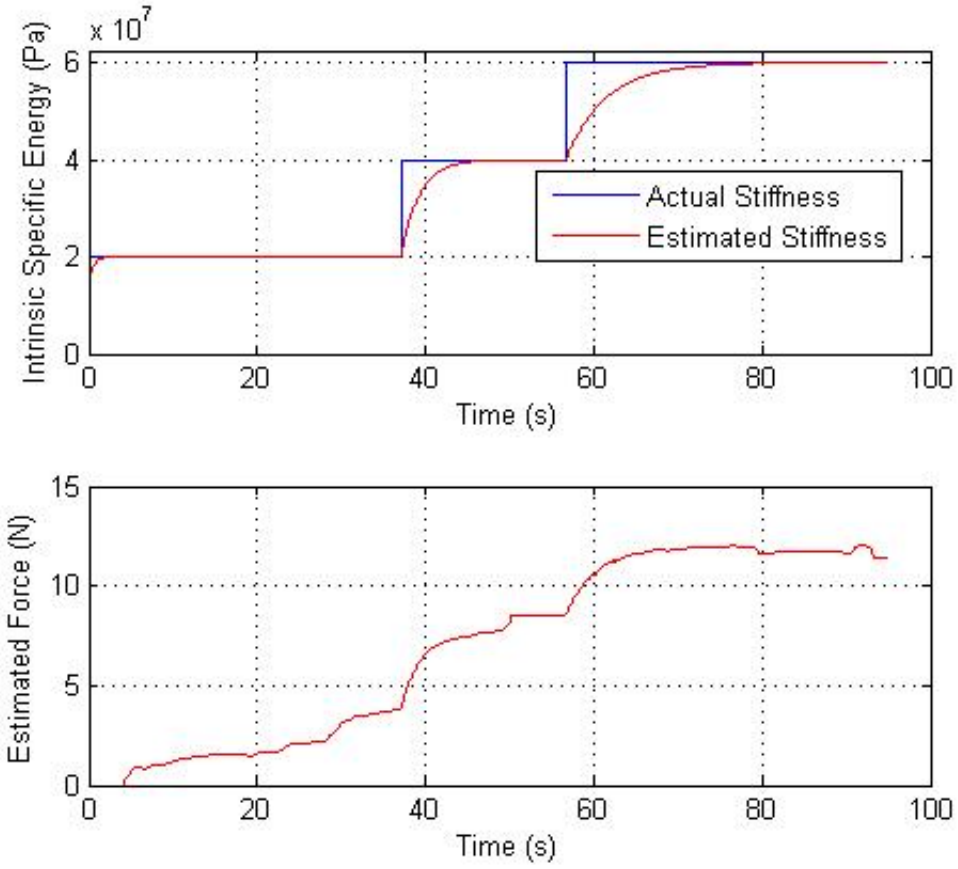

Figure 6.9: Experiment 3: Actual stiffness $\epsilon(t)$ vs. estimated stiffness $\hat{\epsilon}(t)$ (top); reflected force $F_{est}(t)$ (bottom)

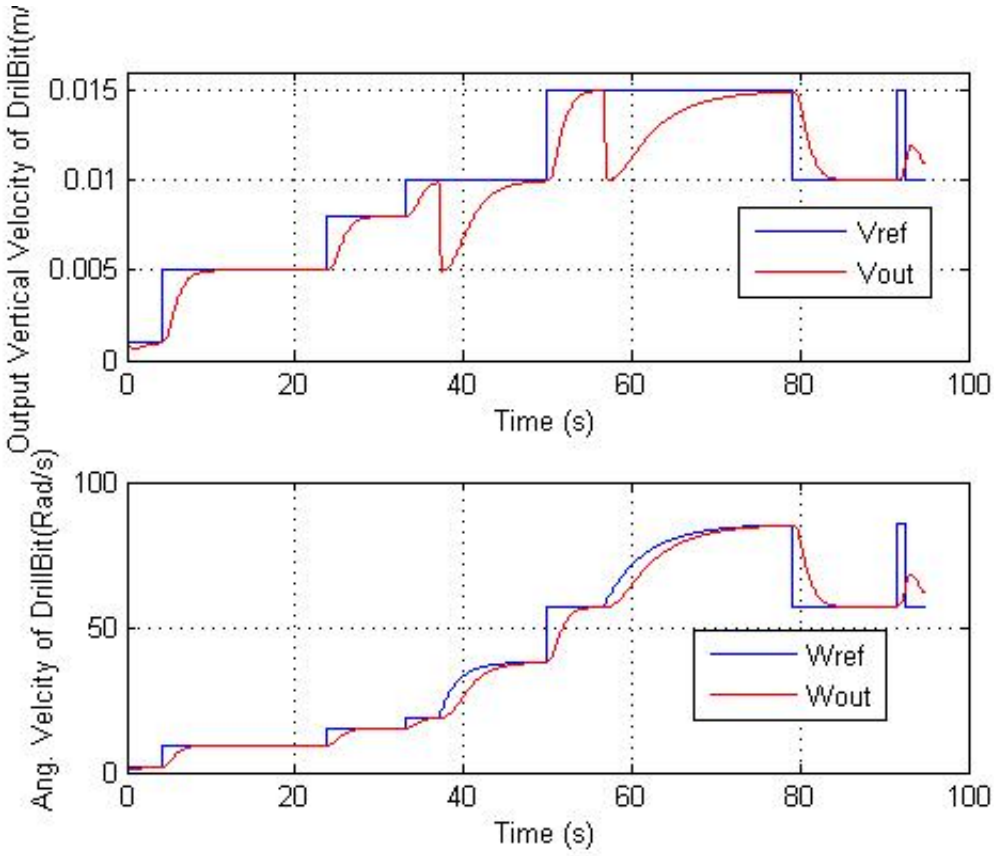

Figure 6.10: Experiment 3:Output vertical velocity $v_{out}(t)$ vs. reference vertical velocity $v_{ref}(t)$ (top); output rotational velocity of the drill bit $\omega_1(t)$ vs. reference rotational velocity $\omega_{1d}(t)$ (bottom)

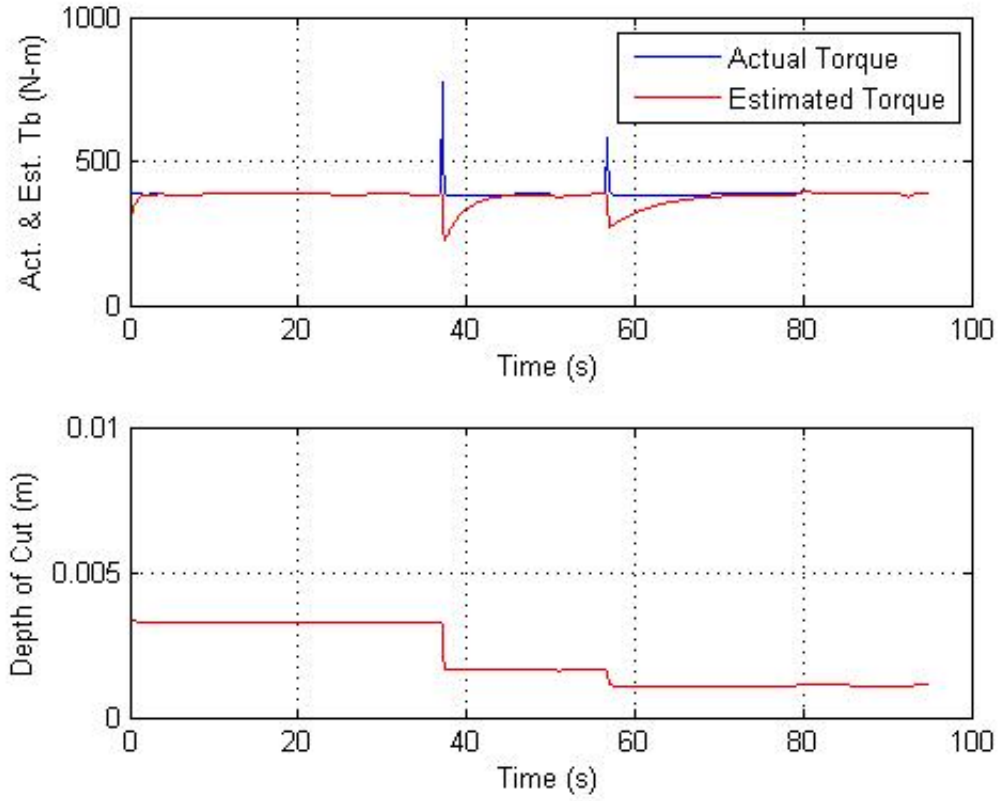

Figure 6.11: Experiment 3: Torque-on-bit $T_b(t)$ vs. estimated torque-on-bit $\hat{T}_b(t)$ (top); depth of cut $d_{cut}(t)$ (bottom)

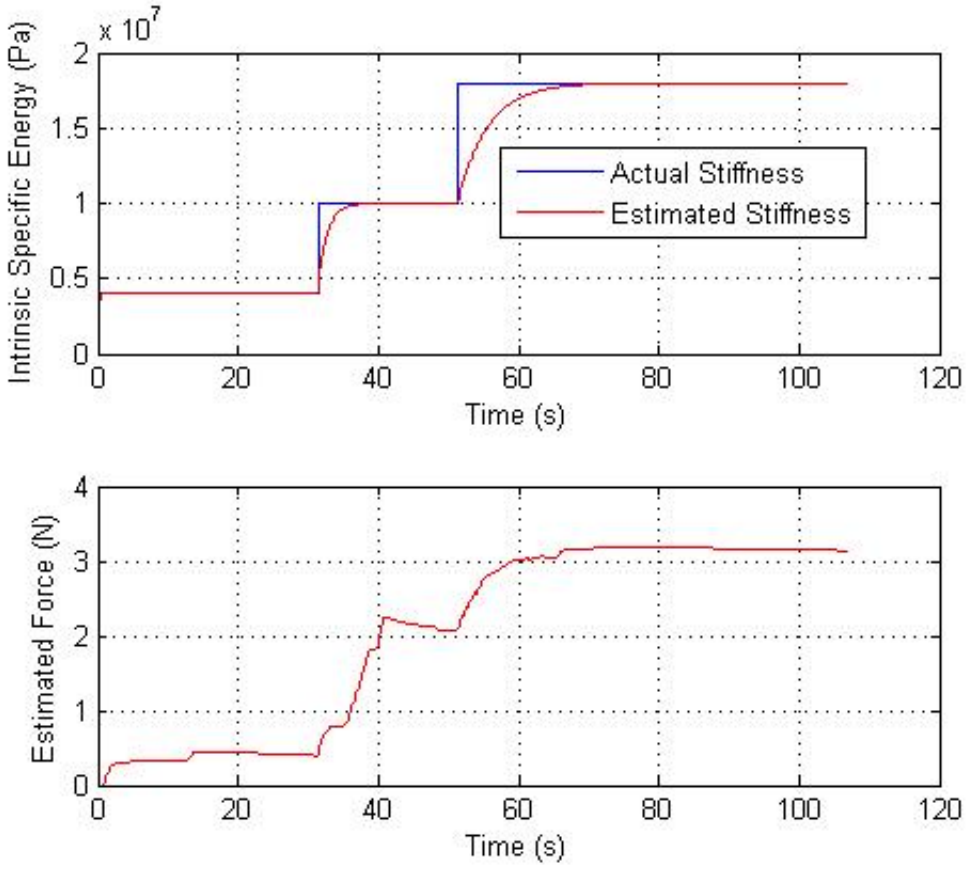

Figure 6.12: Experiment 4: Actual stiffness $\epsilon(t)$ vs. estimated stiffness $\hat{\epsilon}(t)$ (top); reflected force $F_{est}(t)$ (bottom)

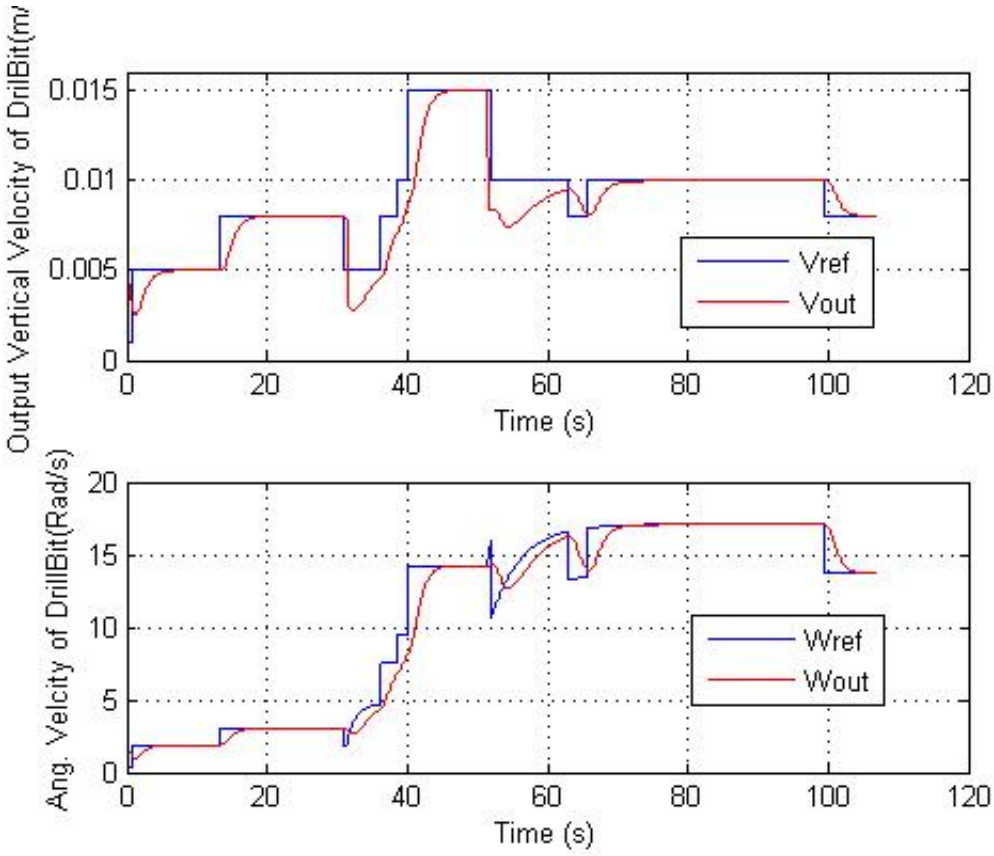

Figure 6.13: Experiment 4: Output vertical velocity $v_{out}(t)$ vs. reference vertical velocity $v_{ref}(t)$ (top); output rotational velocity of the drill bit $\omega_1(t)$ vs. reference rotational velocity $\omega_{1d}(t)$ (bottom)

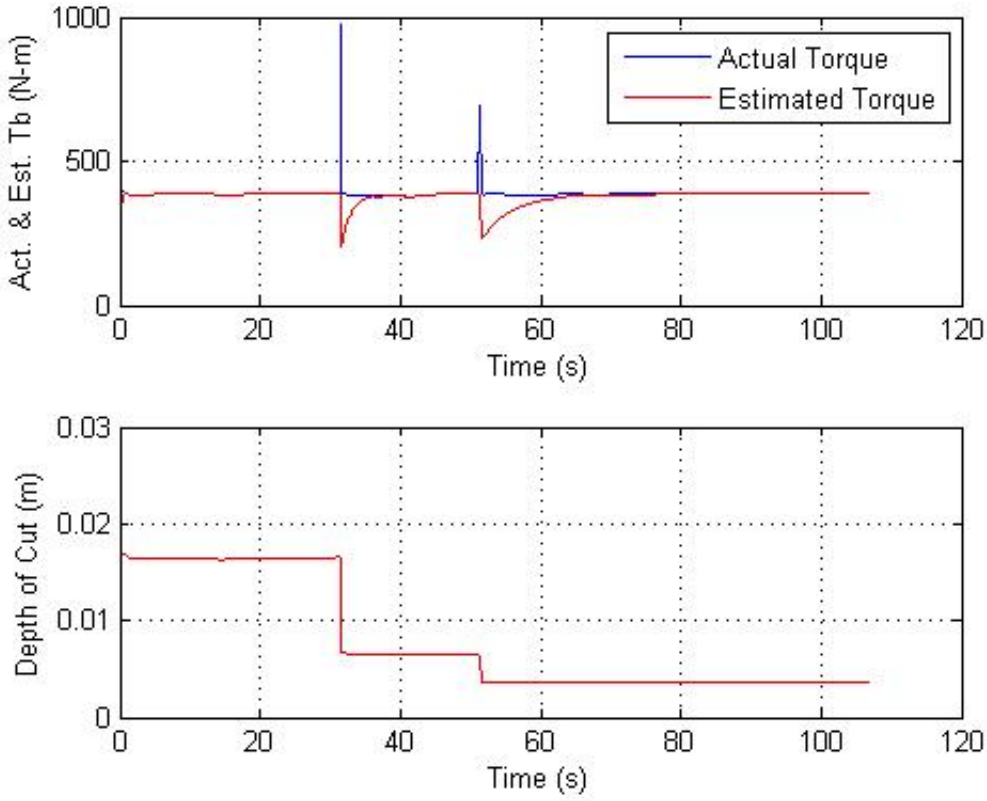

Figure 6.14: Experiment 4: Torque-on-bit $T_b(t)$ vs. estimated torque-on-bit $\hat{T}_b(t)$ (top); depth of cut $d_{cut}(t)$ (bottom)

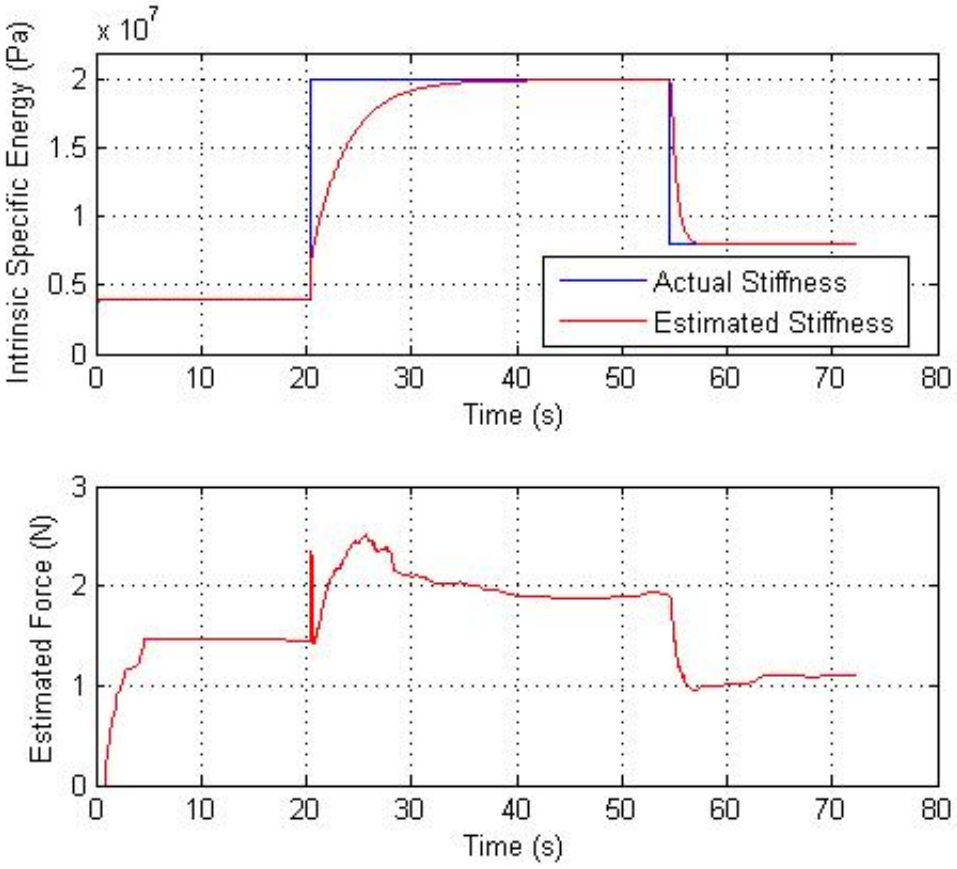

Figure 6.15: Experiment 5: Actual stiffness $\epsilon(t)$ vs. estimated stiffness $\hat{\epsilon}(t)$ (top); reflected force $F_{est}(t)$ (bottom)

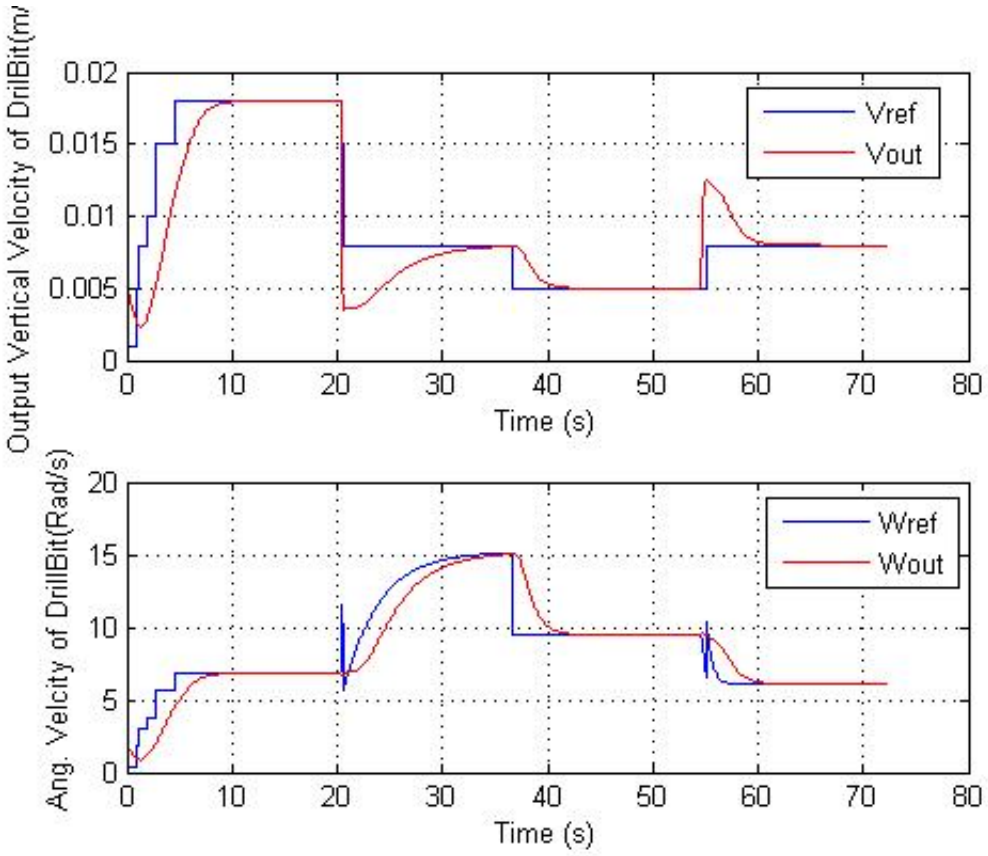

Figure 6.16: Experiment 5: Output vertical velocity $v_{out}(t)$ vs. reference vertical velocity $v_{ref}(t)$ (top); output rotational velocity of the drill bit $\omega_1(t)$ vs. reference rotational velocity $\omega_{1d}(t)$ (bottom)

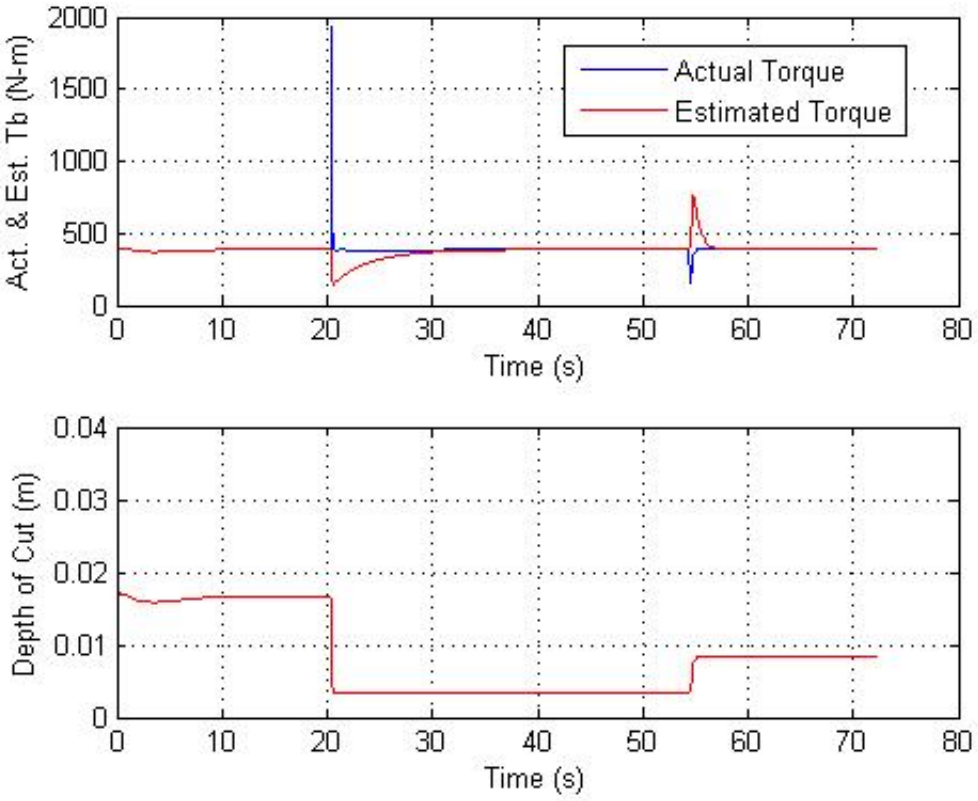

Figure 6.17: Experiment 5: Torque-on-bit $T_b(t)$ vs. estimated torque-on-bit $\hat{T}_b(t)$ (top); depth of cut $d_{cut}(t)$ (bottom)

Chapter 7

Conclusions

7.1 Thesis Overview

The research presented in this Thesis deals with application of some concepts of telerobotics to a conventional oil well drilling process. After considering mathematical models of the drilling process, a control algorithm was designed that guarantee the convergence of the vertical penetration velocity to an arbitrary reference value. The control algorithm has a cascaded structure, where the velocity of vertical penetration is controlled indirectly through stabilization of the rotational motion of the drill bit. In order to guarantee the convergence of the angular velocity to a desired value in the presence of disturbances in the form of torque-on-bit, a robust servo controller was designed. However, the design of such controller depends on the parameter of environment called the intrinsic specific energy, which is generally unknown beforehand. To solve this issue, an on-line parameter estimator was designed that provides an estimate of the intrinsic specific energy. This estimate is substituted for the actual value of the parameter in the control algorithm, and the corresponding adaptive control system is evaluated through simulations. Finally, a telerobotic drilling system with haptic feedback is designed and verified through experiments. The haptic feedback for the human operator is provided by creating a virtual spring that interacts with the haptic device; the stiffness of the spring is adjusted in real time depending

on the current estimate of the intrinsic specific energy. Experiments are conducted using PHANTOM Omni Haptic device, where the drilling process model is implemented in C++ environment, and the haptic feedback is provided to the human operator.

Below, the most significant results of this Thesis are outlined.

- The design of robust controller that guarantees asymptotic tracking of a reference rotational velocity $\omega_{ref}(t)$ by the output rotational velocity of the drill bit $\omega_1(t)$ while rejecting the measured disturbances $T_b(t)$ is presented in Section 4.3. Simulation results are presented that confirm the stability and performance of the designed controller. In particular, Figures 4.2, 4.4, 4.6 and 4.8 demonstrate stability and performance of the designed controller for different values of the gains K and constant desired velocity ω_{ref}.

- Based on the robust servo control algorithm described above, the controller for vertical velocity stabilization is designed that guarantees the convergence of the vertical drillbit velocity $v_{out}(t)$ to its desired value v_{ref}. The design of this controller is described in Section 4.2. Section 4.4 presents results of simulations that demonstrate stability and performance of the designed algorithm for different values of the reference velocity v_{ref}, different gains K, and different values of the applied weight-on-bit W_0.

- In Chapter 5, an on-line parameter estimator for the intrinsic specific energy parameter ϵ is designed. This estimate is then used in the above described robust controller, and the stability and performance of the resulting adaptive control system is demonstrated through simulations. The corresponding simulation results are presented in Section 5.3. In particular, Figures 5.1, 5.3, 5.5, 5.7, 5.9 and 5.11 demonstrate how the response of the output vertical velocity of drill bit depends upon the estimate of the intrinsic specific energy.

- Based on the controllers described above, a telerobotic control system for remote drilling is designed that provides haptic feedback to the user. The structure of the

telerobotic system is described in Section 6.2. Extensive experimental results are presented in Section 6.4, that demonstrate stability and good performance of the designed system in different drilling scenarios.

7.2 Future Work

Some possible directions for future research are as follows.

- A telerobotic drilling system includes a communication link between master and slave. However, this research does not address the issue of communication delay while performing the experiments. Thus, it is reasonable to include fixed or variable communication delay between the virtual and remote models of drilling when conducting experiments.

- The model used in this thesis corresponds to the vertical drilling rig. In recent years, horizontal drilling is developed, which is a new method of drilling where the drill bit makes an angular bore hole rather than the straight conventional well bore. Thus, the control of angular or semi-horizontal drilling could be addressed.

- This research deals with the remote cutting (drilling) action of rocks and vertical penetration of drill bit. The same ideas can potentially be applied to seafloor drilling, as well as other applications. In these cases, the control design can be modified depending upon the model of the mechanical cutter and the environment.

Bibliography

[1] F. Poletto and F. Miranda, *Seismic While Drilling: Fundamentals of Drill-bit Seismic for Exploration*, ser. Handbook of Geophysical Exploration: Seismic Exploration. Elsevier, 2004, vol. 35.

[2] N. J. Hyne, *Nontechnical Guide to Petroleum Geology, Exploration, Drilling, and Production*. Penn Well Corporation, 2001.

[3] E. Detournay and P. Defourny, "A phenomenological model for the drilling action of drag bits," *International Journal of Rock Mechanics, Mining Sciences & Geomechanics*, vol. 29, no. 1, pp. 13–23, 1992.

[4] E. Detournay, T. Richard, and M. Shepherd, "Drilling response of drag bits: Theory and experiment," *International Journal of Rock Mechanics & Mining Sciences*, vol. 45, pp. 1347–1360, 2008.

[5] T. Richard, C. Germay, and E. Detournay, "Self excited stick-slip oscillations of drill bits," *Comptes Rendus Mecanique (Journal of Mechanics)*, vol. 332, no. 8, pp. 619–626, Aug. 2004.

[6] M. Zamanian, S. E. Khadem, and M. R. Ghazavi, "Stick-slip oscillations of drag bits by considering damping of drilling mud and active damping system," *Journal of Petroleum Science and Engineering*, vol. 59, pp. 289–299, Apr. 2007.

[7] L. V. D. S. J.D.Jansen, "Active damping of self-excited torsional vibrations in oil well drillstrings," *Journal of Sound and Vibrations*, vol. 179(4), pp. 647–668, 1995.

[8] P. F. Hokayem and M. W. Spong, "Bilateral teleoperation: A historical survey," *Automatica*, vol. 42, no. 12, pp. 2035–2057, 2006.

[9] P. Arcara and C. Melchiorri, "Control schemes for teleoperation with time delay: a comparative study," *Robotics and Autonomous Systems*, vol. 38, no. 1, pp. 49–64, Jan. 2002.

[10] P. Corke, J. Roberts, J. Cunningham, and D. Hainsworth, "Mining robots," in *Springer Handbook of Robotics*, 1st ed. Springer, 2007, pp. 1127–1150.

[11] E. Jackson and D. Clarke, "Subsea excavation of seafloor massive sulphides," in *IEEE Oceans Conference*, Vancouver, BC, Sep. 2007.

[12] N. Ridley, S. Graham, and S. Kapusniak, "Seafloor production tools for the resources of the future," in *Offshore Technology Conference*, Houston, TX, May 2011.

[13] M. N. Wendt and G. A. Einicke, "Development of a water-hydraulic self-propelled robotic drill for underground mining," in *Field and Service Robotics*. Springer, 2006, vol. 25, pp. 355–366.

[14] G. Baiden, "Telerobotic lunar habitat construction and mining: A miner's perspective," in *9th International Symposium on Artificial Intelligence, Robotics and Automation for Space (i-SAIRAS 2008)*, 2008.

[15] F. Lee, I. Hwang, K. Kim, S. Choi, W. Chung, and Y. Kim, "Cooperative robotic assistant with drill-by-wire end-effector for spinal fusion surgery," *Industrial Robot: An International Journal*, vol. 36, no. 1, pp. 60–72, 2009.

[16] B. Glass, H. Cannon, S. Hanagud, and J. Frank, "Telerobotic lunar habitat construction and mining: A miner's perspective," in *8th International Symposium on Artificial Intelligence, Robotics and Automation for Space (i-SAIRAS 2005), Munich, Germany*, 2008.

[17] D. Glowka, "Development of a method for predicting the performance and wear of PDC drill bits," 1987, Sandia National Laboratories, Albuquerque, NM, USA.

[18] ——, "Use of singe-cutter data in the analysis of pdc bit designs: Part 1 - development of PDC cutting force model," *Journal of Petroleum Technology*, vol. 41, no. 8, pp. 797–799, 844–849, Aug. 1989.

[19] ——, "Use of singe-cutter data in the analysis of pdc bit designs: Part 2 - development and use of PDC WEAR computer code," *Journal of Petroleum Technology*, vol. 41, no. 8, pp. 850–859, Aug. 1989.

[20] A. P. C. T.M. Warren, A. Sinor, "Drag bit performance modeling," *SPE Drilling Engineering*, vol. 4, no. 2, pp. 119–127, June 1989.

[21] L. W. Fairhurst C, "Some principles and developments hard rock drilling techniques," in *6th Annual Drilling and Blasting Symposium, University of Minnesota*, October 1956, pp. 15–25.

[22] T. Richard, C. Germay, and E. Detournay, "A simplified model to explore the root cause of stick-slip vibrations in driling systems with drag bits," *Journal of Sound and Vibration*, vol. 305, no. 3, pp. 432–456, 2007.

[23] E. J. Davison, "The feedforward control of linear multivariable time-invariant systems," *Automatica*, vol. 9, pp. 561–573, 1973.

[24] ——, "Multivariable tuning regulators: The feedforward and robust control of a general servomechanism problem," *IEEE Transactions on Automatic Control*, vol. 21, no. 1, pp. 35 – 47, 1976.

[25] P. A. Ioannou and J. Sun, *Robust Adaptive Control*. PTR Prentice-Hall, 1996.

[26] B. P. Peltier, "Drilling monitor with downhole torque and axial load transducers," US Patent 4 695 957, Sep 22, 1987.

[27] K. Salisbury, F. Conti, and F. Barbagli, "Haptic rendering: Introductory concepts," *IEEE Computer Graphics and Applications*, vol. 24, no. 2, pp. 24–32, 2004.

[28] T. H. Massie and J. K. Salisbury, "The PHANTOM haptic interface: A device for probing virtual objects," in *ASME Winter Annual Meeting, Symposium on Haptic Interfaces for Virtual Environment and Teleoperator Systems*, Chicago, IL, Nov. 1994.

[29] T. A. Kern, *Engineering Haptic Devices: A Beginner's Guide for Engineers*, 1st ed. Springer Berlin Heidelberg, 2009.

Curriculum Vitae

Name:	Faraz Shah
Post-Secondary Education and Degrees:	Mehran University of Engineering and Technology Jamshoro, Pakistan 2003 - 2008 B.Eng.
Related Work Experience:	Teaching Assistant The University of Western Ontario 2011 - 2012